ORKUSTOFNUN

Deep geothermal prospecting. Phase I,model calculations. Final report

Knútur Árnason

Greinargerð KÁ-2000/03

ORKUSTOFNUN

Greinargerð
KÁ-2000/3

2000-07-13

DEEP GEOTHERMAL PROSPECTING
Phase I, model calculations
Final report

1. Introduction

The aim of the Deep Geothermal Prospecting (DGP) project is to develop and test resistivity methods for deep geothermal prospecting and mapping of deep (1-5 km) geothermal resources, outside known shallow geothermal systems. The project is a multi national cooperation but initiated by Orkustofnun Iceland and the University of Akureyri. The non-Icelandic participants are: The international Institute for Geothermal Research in Pisa, Italy; the University of Frankfurt, Germany; Uppsala University, Sweden; the University of Edinburgh, Scotland and recently the University of Cologne, Germany, has joined in on the project.

The project contains three phases, scheduled for three years. The first phase, which, according to the work plan, is scheduled from July 1999 to June 2000 and comprises numerical model studies to estimate the resolution of different electrical exploration methods in the depth range of 1-5 km. The second phase is scheduled form April to September 2000. It consists of a test survey where different electrical methods will be tested in a multi-method survey in the volcanic zone of Iceland, on a profile along the road in Þrengsli, west of the Hengill and Skálafell area. The third phase, scheduled for September 2000 to December 2001, consist of data processing and interpretation of the survey data and over all evaluation of the tested methods.

This report contains a description the work performed and the summary of findings in the first phase of the project.

2. MEETINGS

Three official meetings have been held in the framework of the DGP. The first meeting was November 12-14, 1998, where the non-Icelandic partners were invited to Reykjavík to discuss the overall planning of the project. This meeting was financially supported by RANNíS (the Icelandic Science Council). On August 27, 1999, a meeting was held in Reykjavík with the partners from Frankfurt. On June 17-18, 2000, all partners, except from the University of Edinburgh, met in Frankfurt to discuss the findings of the first phase and for detailed planning of the field mission of the second phase. Besides the meetings, a continuous communication has been maintained on the internet by e-mail.

At the meeting on November 12-14, 1998, the scientific content and methodology, the role of individual partners and the work plan was discussed and defined in some details

as well as the budget for the project. It was agreed that, except for direct expenses in connection with the field test in Iceland, each partner should finance its participation. Due to the nature of the project and its strong focus on Iceland, the Icelandic part in the project is relatively big. The Icelandic participation in the project is financed by Orkustofnun and by a substantial support from RANNÍS and the three biggest power companies in Iceland (Reykjavik Energy, Suðurnes District Heating and the National Power Company).

At the meeting on August 27, 1999, the plan and procedures for the numerical model studies in the first phase were discussed in details. The general layout of the test models (which are described in a later section) was decided and specific tasks distributed among the partners. It was decided at the meeting, that it would be necessary to have a preliminary recording of the strength of the natural electro-magnetic signal and man made noise in the test survey area. This is necessary in order to be able to estimate how big the response of geothermal activity at depth has to be in order to be detectable in the ambient noise. It was therefore decided to have scientist form the University in Edinburgh to come to Iceland with recording system (SPAM) to make a few MT-soundings in the test area.

The meeting in Frankfurt on June 17-18 was devoted to the discussion of the results of the model calculations and to a detailed planning of the tests survey.

3. TEST MEASUREMENTS OF THE NATURAL FIELD STRENGTH

The purpose of the test measurements of the natural field strength was twofold. MT soundings that have been performed in Iceland have mainly been in the low frequency range for deep crustal studies. The MT soundings that are planned in the test survey will measure the natural electro-magnetic field signal in broad frequency range, ranging from about 0.001 Hz and up to about 1000 Hz. Little is known about the signal strength above 1 Hz in Iceland and it was considered important to have some idea about which kind of data are to be expected in the test survey.

Secondly, the natural field signal is a noise in the controlled source methods (TEM and CSMT). It is necessary to know the strength of this noise when performing sensitivity analyses of the controlled source methods. In order for them to be able to resolve different resistivity structures, the difference in the response has to be grater than the uncertainty imposed by the ambient noise. In addition the test measurements would give a rough idea about the resistivity structure down to the depth of several kilometres under the test area.

The University of Edinburgh provided an MT recording system (SPAM-system) and an expert in operating the equipment (Grahma Dawes, which actually designed and built the system). The data recoding took place in the planned test area in Þrenglsi and on Hellisheiði from September 28 to October 4, 1999.

The SPAM system records the the five components of the natural electro-magnetic field, i.e. two horizontal orthogonal components of the electric field (NS and EW), the two horizontal components (NS and EW) and the vertical component of the magnetic field.

The field strengths were recorded as time series in two basic overlapping frequency bands: A low frequency band (S-band) from 1/2048 Hz to 128 Hz and a high frequency band (H-band) from 8 Hz and to 2048 Hz. The basic frequency bands are re-sampled and filtered into sub-bands as follows:

H-bands		S-bands	
Band	freq. Hz	Band	freq. Hz
H0	2048 - 256	S0	128 - 8
H1	256 - 32	S1	8 - 1
H2	32 - 8	S2	1 - 1/4
		S3	1/4 - 1/16
		S4	1/16 - 1/64
		S5	1/64 - 1/256
		S6	1/256 - 1/2048

The MT fields were recorded at five stations. The station locations are shown on figure 1 as well as the locations of nearby central loop TEM-soundings. The recorded time series were Fourier transformed and the MT transfer functions (impedance tensors) and induction vectors calculated as functions of frequency, as well as apparent resistivity and phases. Figures 2 and 3 show the Bostic transforms of the apparent resistivity calculated form the off-diagonal elements of the impedance tensor of the low-frequency band (Bostic transform transforms apparent resistivity as a function of frequency into apparent resistivity as a function of approximate depth) for stations 9901, and 9902 (for location see figure 1). The figures show decreasing apparent resistivity to about 10Ωm or lower at the depth of some hundred meters under station 9902 and at the depth of about 1km under stations 9901. In all cases the resistivity increases again below the low-resistivity layer.

The recorded time series were analysed to investigate the field strengths. A frequency analysis of the recorded values was performed for all time series belonging to the above listed sub-bands and at all measuring sites. Examples of such frequency plots are shown on figures 4, 5 and 6 which show the number of recorded values for different field strength in the H1 band at station 9901. Figures 4 and 5 show the distributions for the time derivatives of the vertical and horizontal components of the magnetic field and figure 6 shows frequency of different values for the horizontal electric fields. The figures show that, for the frequency band H1 at station 9901, the distribution of the recorded field values is nearly a normal distribution with zero mean and the standard deviation of about 0.5 nV/m^2 for the time derivative of the magnetic fields and about 0.3 μV/m for the electric fields.

The frequency distributions of recorded values for the other frequency bands, except for the highest frequency band H0, and for all the four stations turned out to be close to normal distribution with zero mean but with varying standard deviations. The distribution for the band H0 seemed to be a superposition of two normal distributions, one with relatively small standard deviation and another one with considerably larger standard

deviation. Figures 7 through 11 show the range and the mean value for the standard deviations of all recorded time series and for all frequency bands, for Ex, Ey, dBx/dt, dBy/dt and dBz/dt, respectively.

The standard deviations are a measure of the signal amplitudes and hence the signal strength. Figures 7 and 8 show a rather typical spectrum for the electric field. The signal strength is lowest around 1 Hz (in the so-called dead band) and increases with decreasing frequency down to about 0.005 Hz, where it seems to decrease a little again. At frequencies higher than 1 Hz, the signal strength increases with increasing frequency. The spectra for the time derivatives of the magnetic fields (figures 9, 10 and 11) show a similar character as the electric fields, when it is taken into account that, in accordance with Maxwell's equations, the time derivative introduces a multiplication with frequency (a slop of one on log-log scale) relative to the spectra for the electric field. One of the main purposes of the test survey was to check the high frequency part of the spectrum and the data clearly show that the signal conditions are favourable for MT-measurements at high frequencies. The quantitative results displayed on figures 7 through 11 will, in a later section, be used as a basis for an estimate, in the case of TEM-measurements, how significantly responses of test models differ when external noise is taken into account.

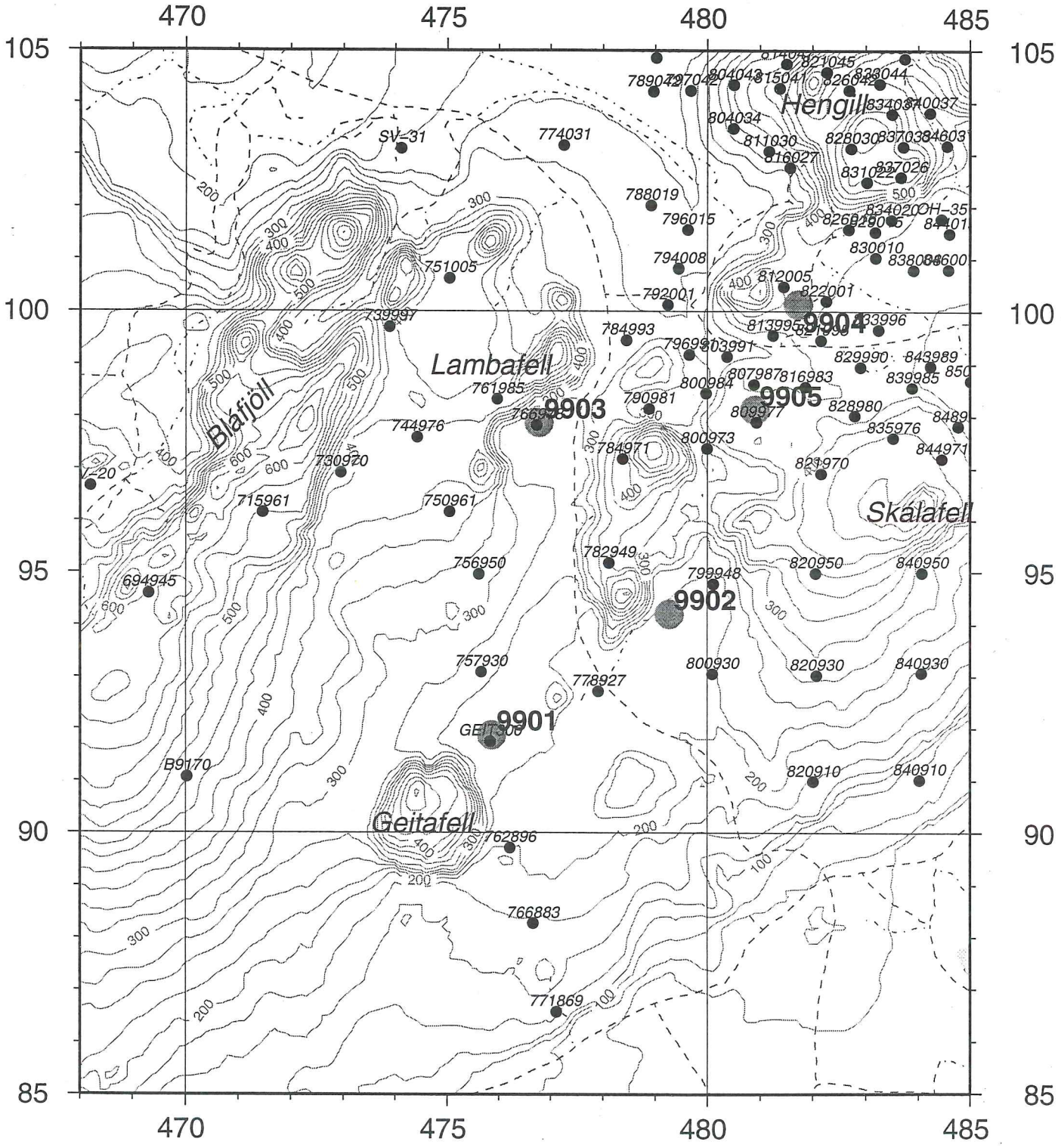

Figure-1. Location of MT-soundings (big gray dots) and TEM-soundings (small black dots).

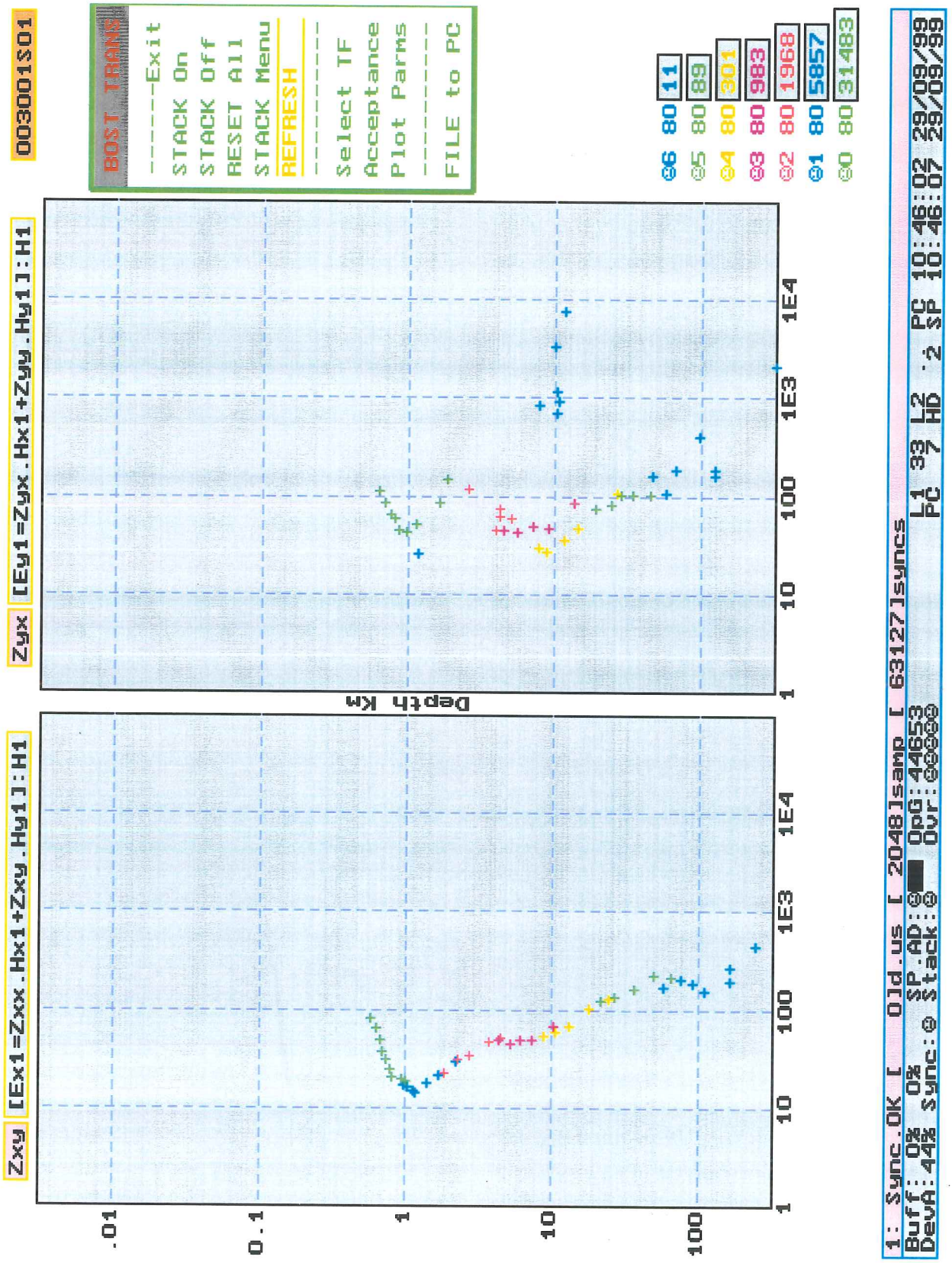

Figure-2. Bostic transform of apparent resistivity for MT-station 9901.

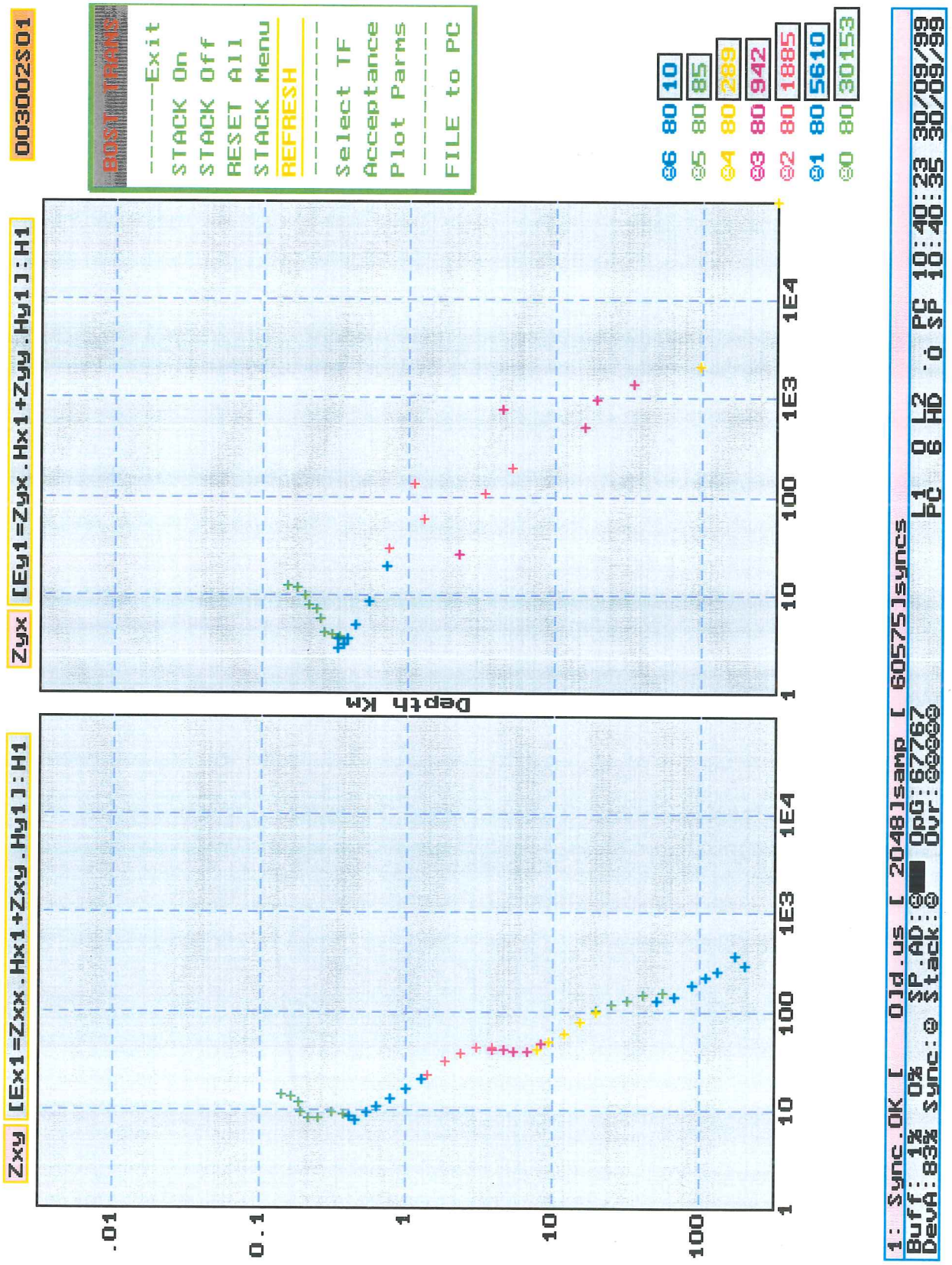

Figure-3. Bostic transform of apparent resistivity for MT-station 9902.

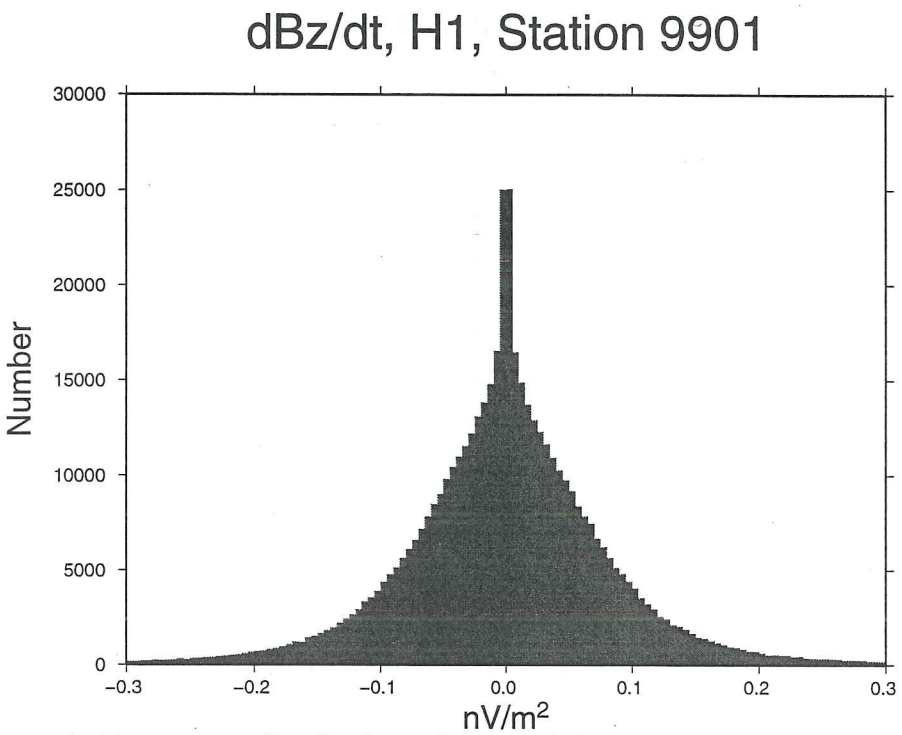

Figure-4. Frequency distribution of vertical induction (dBz/dt) for station 9901 and frequency band H1 (32-256Hz).

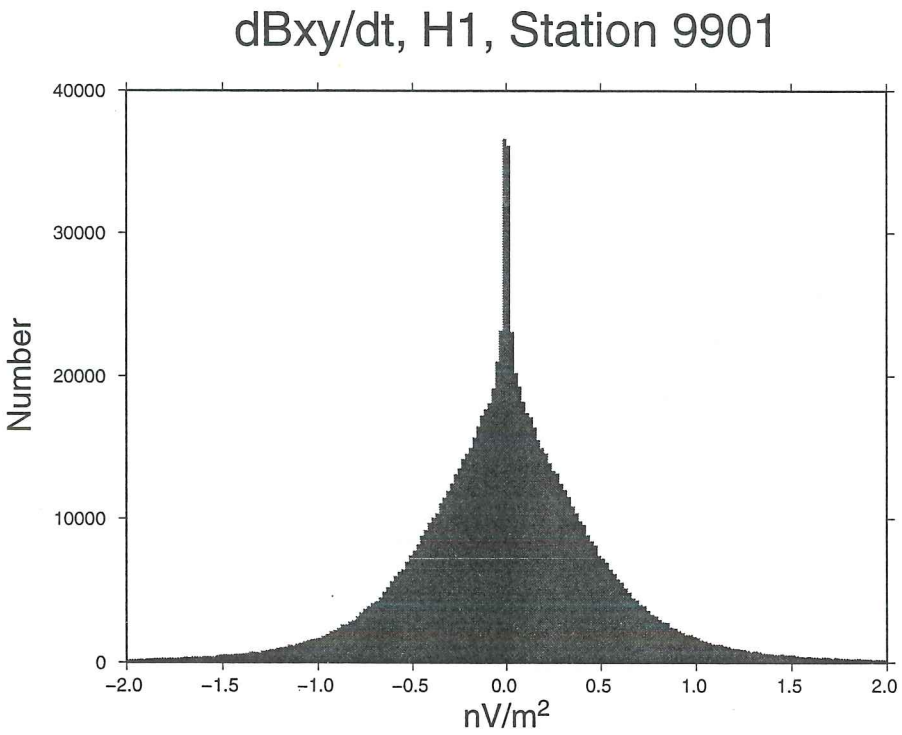

Figure-5. Frequency distribution of horizontal induction (dBxy/dt) for station 9901 and frequency band H1 (32-256Hz).

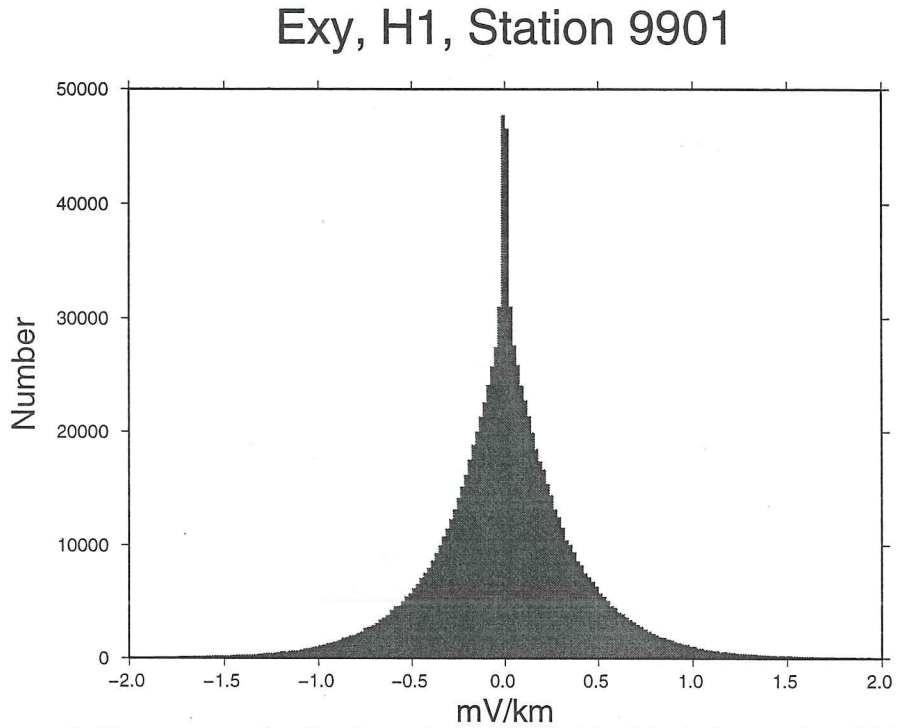

Figure-6. Frequency distribution of electric fields (Exy) for station 9901 and frequency band H1 (32-256Hz).

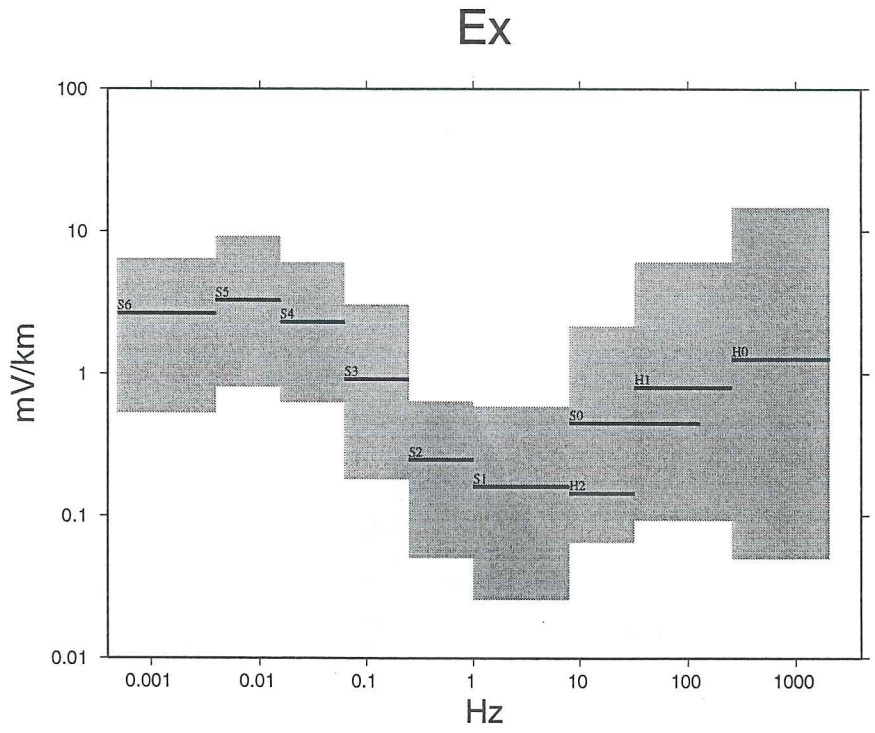

Figure-7. The spans (shaded) and means (solid lines) of standard deviations of Ex for all frequency bands and all MT stations.

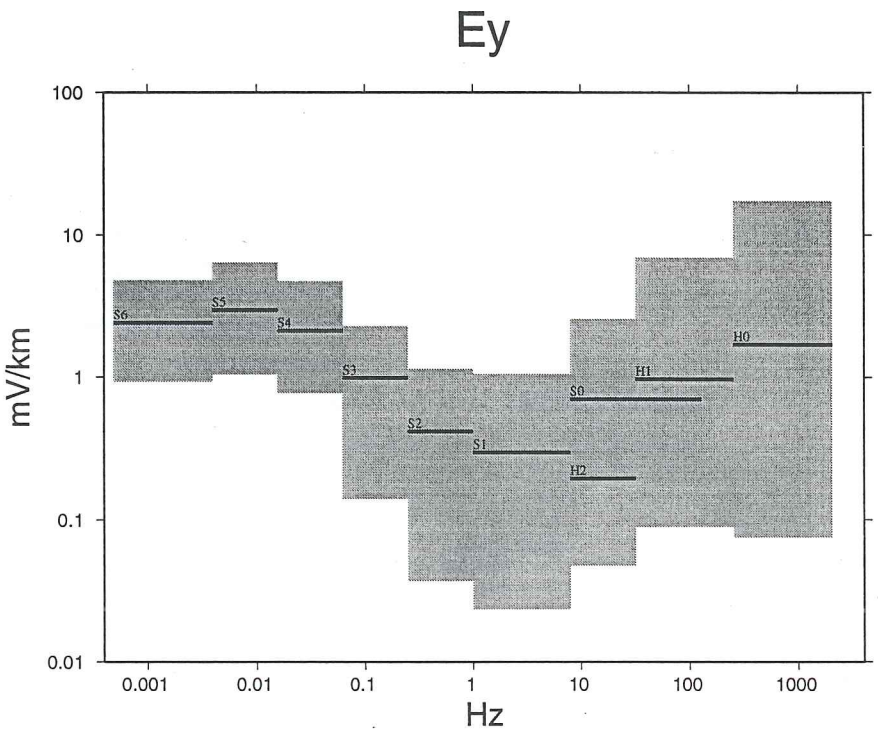

Figure-8. The spans (shaded) and means (solid lines) of standard deviations of Ey for all frequency bands and all MT stations.

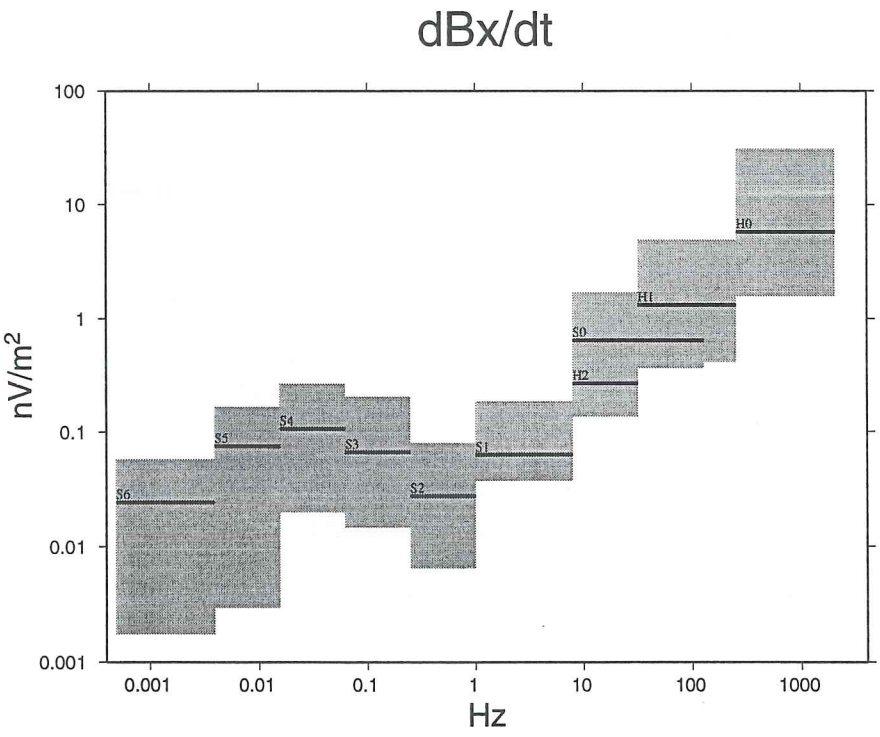

Figure-9. The spans (shaded) and means (solid lines) of standard deviations of dBx/dt for all frequency bands and all MT stations.

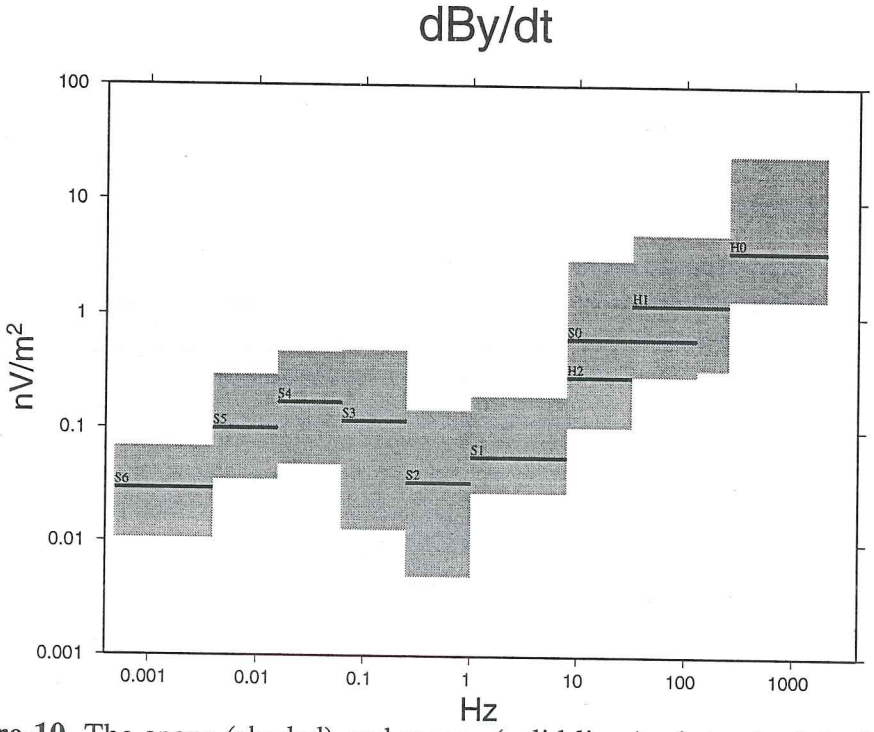

Figure-10. The spans (shaded) and means (solid lines) of standard deviations of dBy/dt for all frequency bands and all MT stations.

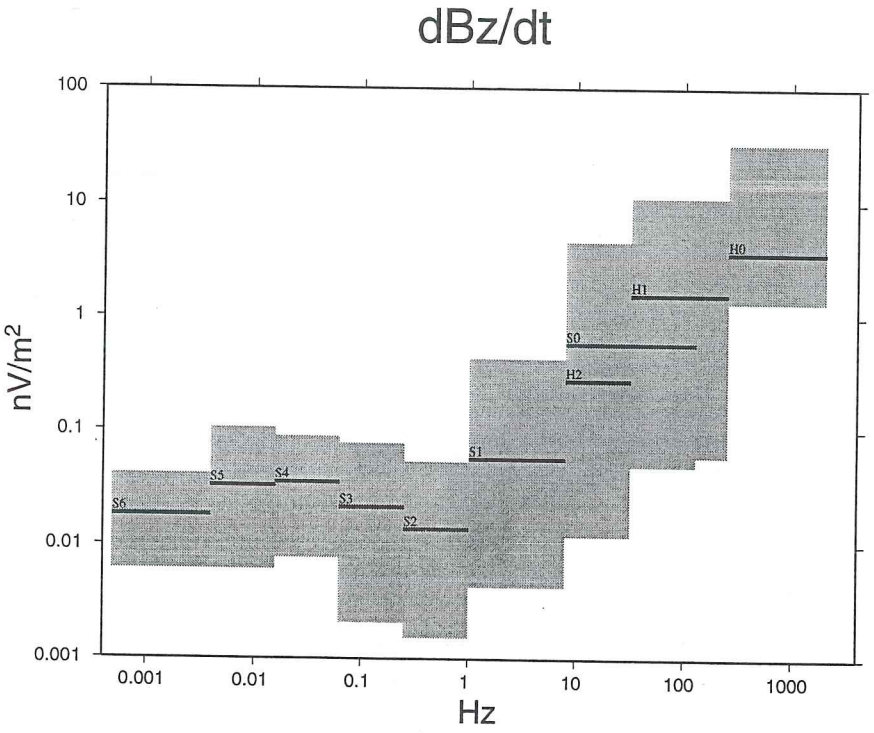

Figure-11. The spans (shaded) and means (solid lines) of standard deviations of dBz/dt for all frequency bands and all MT stations.

4. MODEL CALCULATIONS

The purpose of the numerical model calculations is to investigate the anomalies or signatures observed by different electro-magnetic methods due to different, but likely, resistivity structures caused by deep geothermal activity. The model calculations can be used to estimate the sensitivity of different electro-magnetic methods and different measurement setups. The model calculations are also important because the measured response can, in the case of a 3-dimensional (3D) resistivity structures, be very complicated and it can be difficult to infer the resistivity structure form the measured data. The model calculations can indicate diagnostic features to look for in the measured data and help in developing understanding and intuition which is necessary when dealing with real data.

The original work plan assumed that such a model calculations would be performed for the four different electro-magnetic methods to be tested, that is, Direct Current (DC), the Controlled Source Magneto-Telluric (CSMT), natural source Magneto-Telluric (MT) and Transient Electro-Magnetic (TEM) methods. The modelling turned, however, out to be a very time consuming process and due to limited manpower and time, the main emphasis was put on the MT and TEM methods.

4.1 Definition of test models

The construction of the test models is based on the general resistivity structure of high-temperature geothermal systems in the basaltic crust of Iceland (Árnason et al., 2000). This resistivity structure is characterised by low resistivity cap on the outer margins of the reservoirs, with resistivity lower than 10Ωm, normally in a relatively resistive host rocks. The low resistivity layer is under lain by about an order of magnitude higher resistivity. The resistivity structure turns out to be mainly depicting the alteration mineralogy due to the geothermal activity. If the alteration mineralogy is in equilibrium with the present temperature, the low resistivity cap reflects temperatures in the range of 100-230°C and the more resistive core reflects temperatures higher than 240°C.

High-temperature geothermal systems are found in the volcanic zones of Iceland with approximately 20km intervals. The electro-magnetic exploration methods which have been used up till now can map this resistivity structure in some details down to the depth of about 1km, At the margins of the reservoirs, the low resistivity layer is always seen to dip down below the depth of exploration. The main purpose of the project is to identify methods which are able to trace the low resistivity layer outside and in between the shallow reservoirs in order to investigate if the volcanic zones host much bigger geothermal resources at depth.

The test models contain three main components or building blocks. The first component is a layered back-ground resistivity model, "typical" for the Icelandic crust. The layered structure was composed by going through existing MT-soundings outside volcanic zones and their layered (1D) models. The layered background model consists of a 500m thick layer of 1000Ωm at the surface. Below this layer is a 11.5km thick layer of 100Ωm and a low resistivity basement of 10Ωm at the depth of 12km.

A second building block is a "typical" high-temperature geothermal system in the volcanic zones. It is a conical resistivity anomaly, with the diameter of about 3km closest to the surface, at the depth of 500m. On the outer margins is about 750m thick low resistivity cap of 10Ωm and a more resistive core of 50Ωm underneath. The depth to the low-resistivity layer increases away form the centre of the system (with the slope of about 45°). The depth extension of the anomaly varies in different models, from 4.5km and up to 6km. It is assumed that the permeability is a little higher along the volcanic zone, than perpendicular to it, and hence the anomaly is taken to be a little elongated along the volcanic zone. Figures 12 and 13 show vertical sections through such an anomaly extending to the depth of 6km. Figure 12 shows a section along the volcanic zone and figure 13 perpendicular to it. Figure 14 shows a horizontal cross-section at the depth of 3250m.

The third component is a low-resistivity anomaly ridge along the volcanic zone. It has, like the cone anomaly, about 750m thick low-resistivity cap of 10Ωm with 50Ωm below. The ridge slopes gently away form the axis of the volcanic zone and its thickness is variable (1.5km or 2.5km) in different models. Figure 15 shows a vertical cross section perpendicular to a 2.5km thick ridge at the depth of 4km.

The above described components are put to together to build models which are thought to reflect likely conditions. A typical model is with two shallow geothermal systems, 20km apart, in the volcanic zone. A series of models was constructed where the two systems extend to different depths and are connected or not connected at various depths. Three classes of models where considered where the systems are connected by low-resistivity ridge at different depths along the volcanic zone. In the first class there are two models where the two systems are connected with the top of the ridge at the depth of 2km and extending down to the depth of 2.5km and 3.0km. The second class contains two models with the systems connected at 3km depth and extending down to 4.0km and 4.5km respectively and in the third class there are two models connected at 4km depth and extending down to 5.5 and 6.0km. In all cases the response of a model with the geothermal systems connected is compared to the response when they are not connected.

Figures 16 through 21 show a typical example of connected and non connected models. Figure 16 shows a vertical section along the axis of a volcanic zone with two geothermal systems 20km apart and extending down to the depth of 6km. Figure 17 shows a similar cross-section in the case where the systems are connected at 4km depth and figures 18 through 21 show horizontal sections at the depths of 1750m, 3250m, 4250m and 5250m respectively.

The definition of the test models was a rather complicated and time consuming process and they had to be fitted into appropriate discretization grids for the forward modelling codes used to calculate the response of the models. The discretization grids were kept, as far as possible, the same for the MT and TEM forward modelling codes, in order to avoid differences caused by different dscretization. A special software had to be developed for graphical displaying of the models form the model files, because the visualisation of 3D resistivity models is not a trivial task.

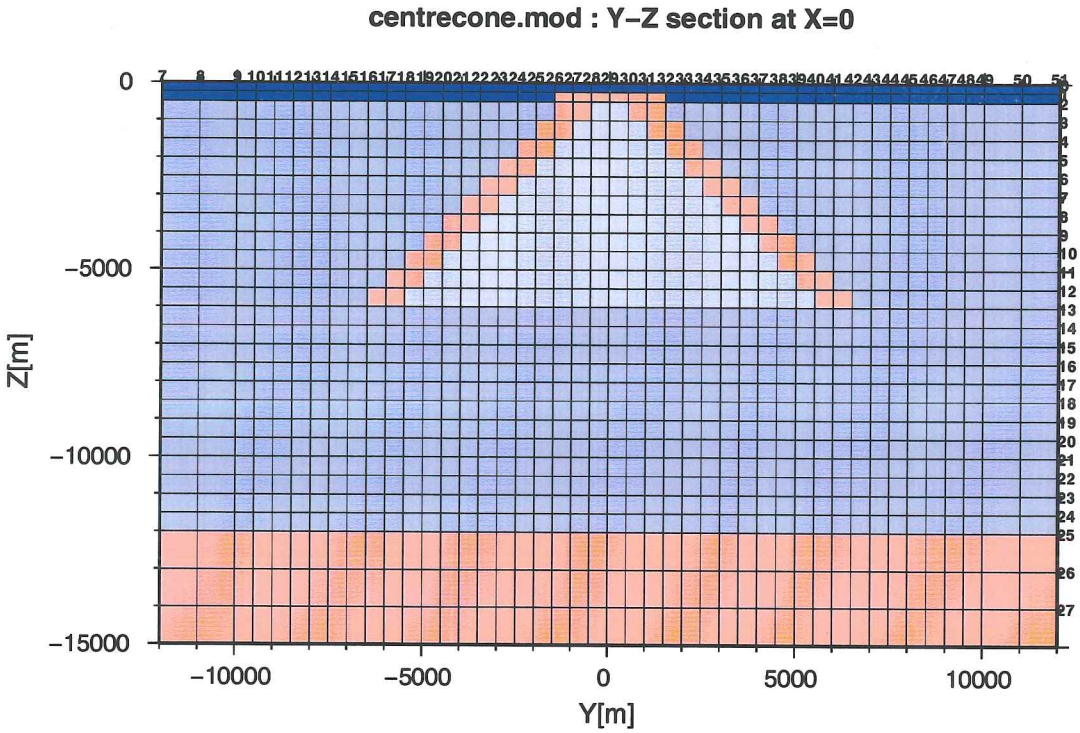

Figure-12. Resistivity model for a "typical" high-temperature geothermal system; vertical section along the volcanic zone. Dark blue is 1000Ωm, middle blue is 100Ωm, light blue is 50Ωm and light red is 10Ωm

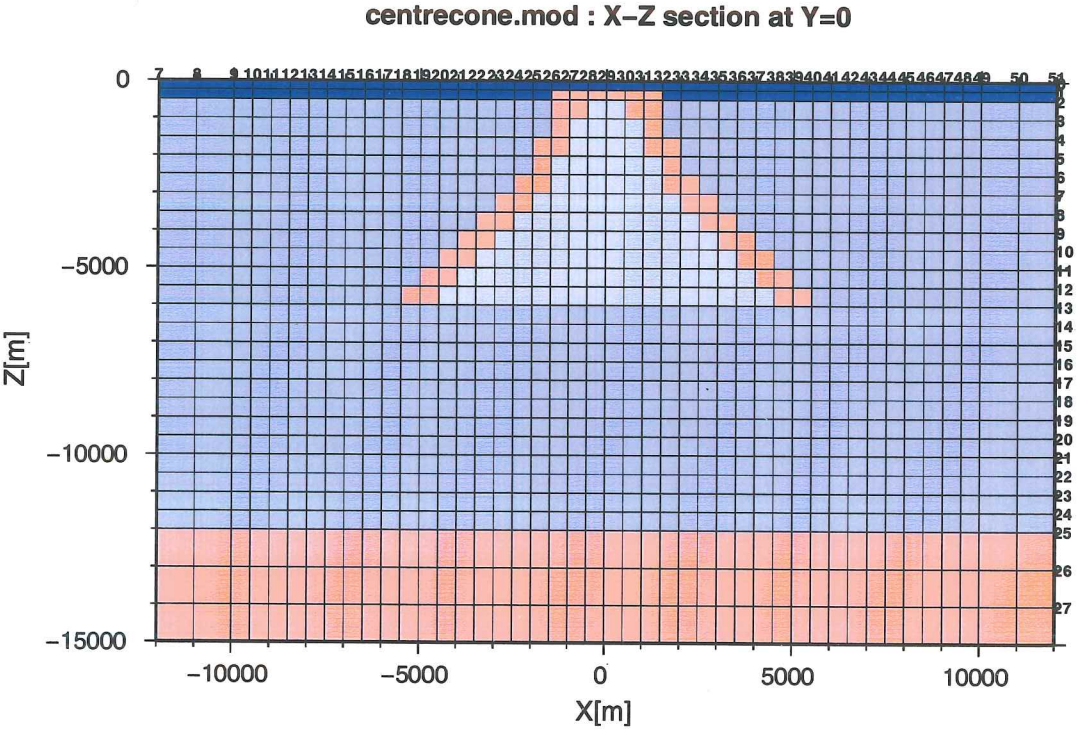

Figure-13. Resistivity model for a "typical" high-temperature geothermal system; vertical section perpendicular to the volcanic zone (color codes the same as in fig.-12).

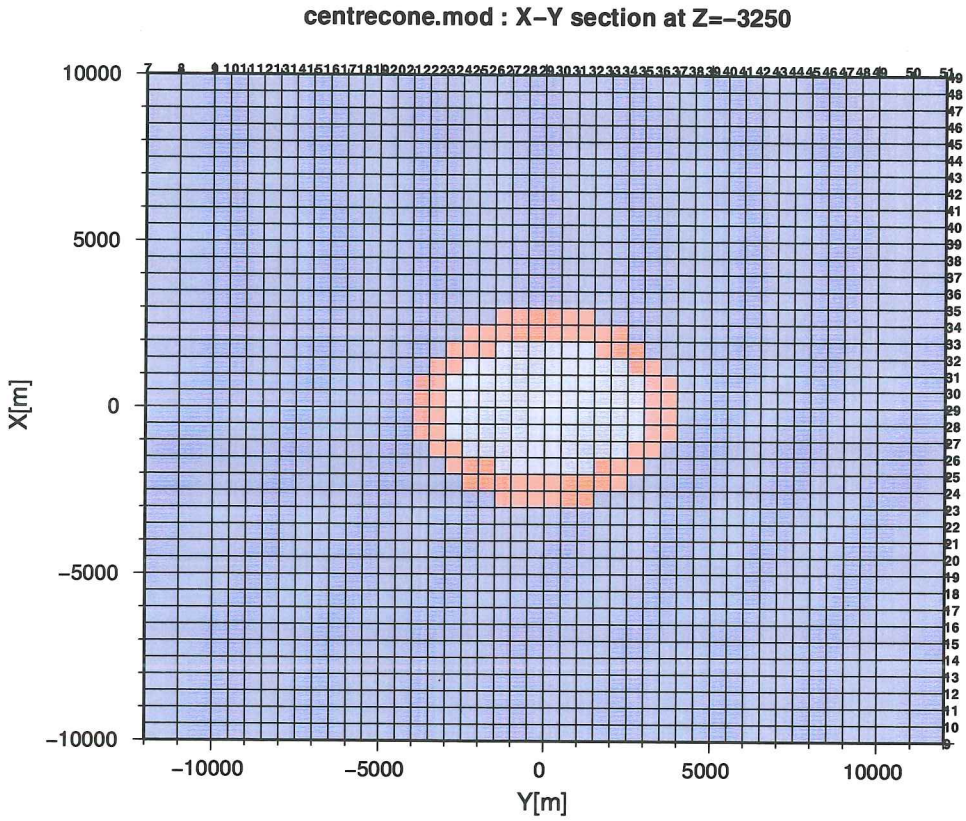

Figure-14. Resistivity model for a "typical" high-temperature geothermal system; horizontal section at 3250m depth. (color codes the same as in fig.-12).

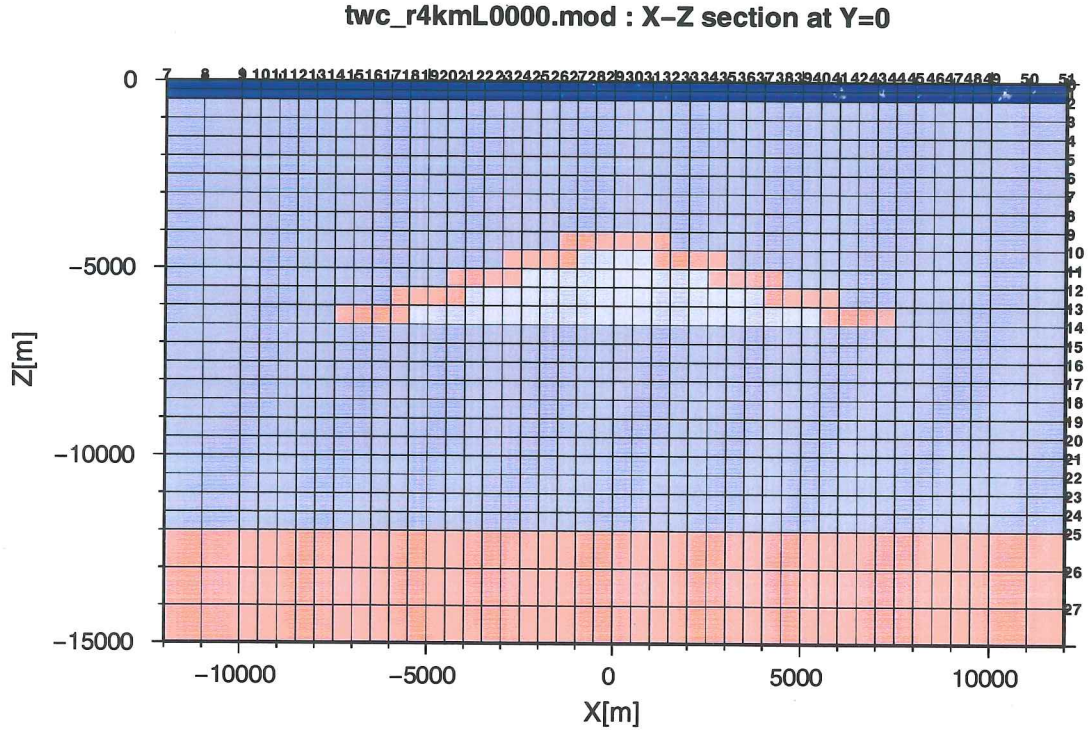

Figure-15. Resistivity model for a ridge connecting two high-temperature geothermal systems; vertical section perpendicular to the volcanic zone (color codes the same as in fig.-12).

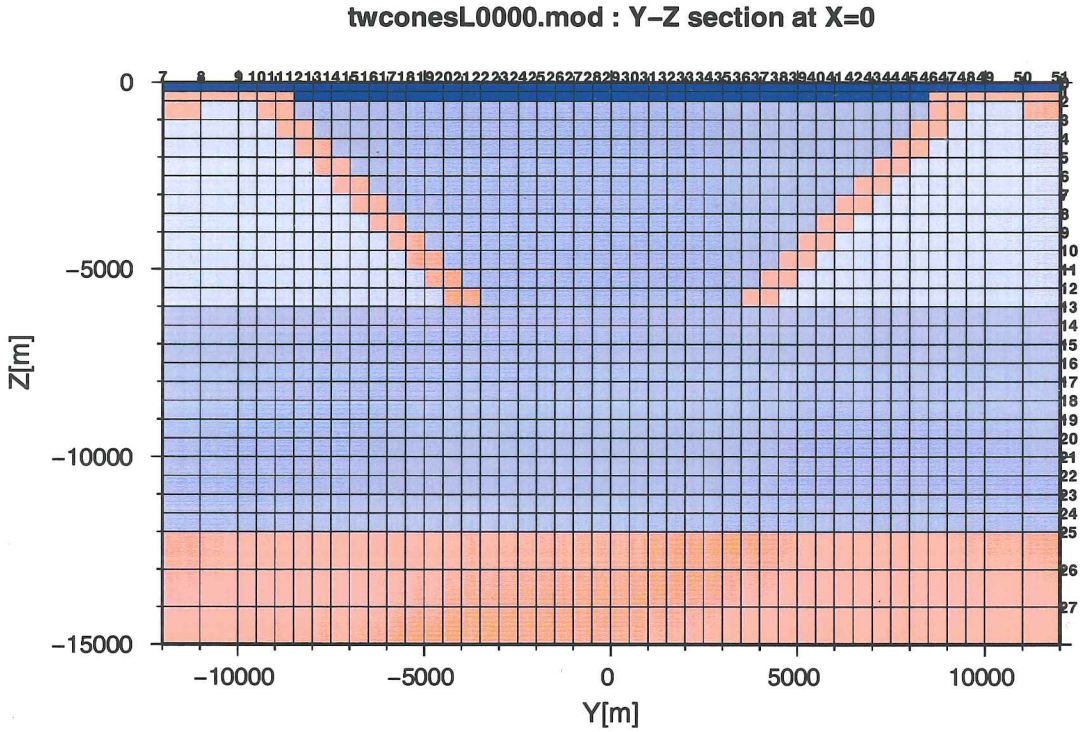

Figure-16. Resistivity model for two non-connected high-temperature geothermal systems 20km apart; vertical section along the volcanic zone (color codes the same as in fig.-12).

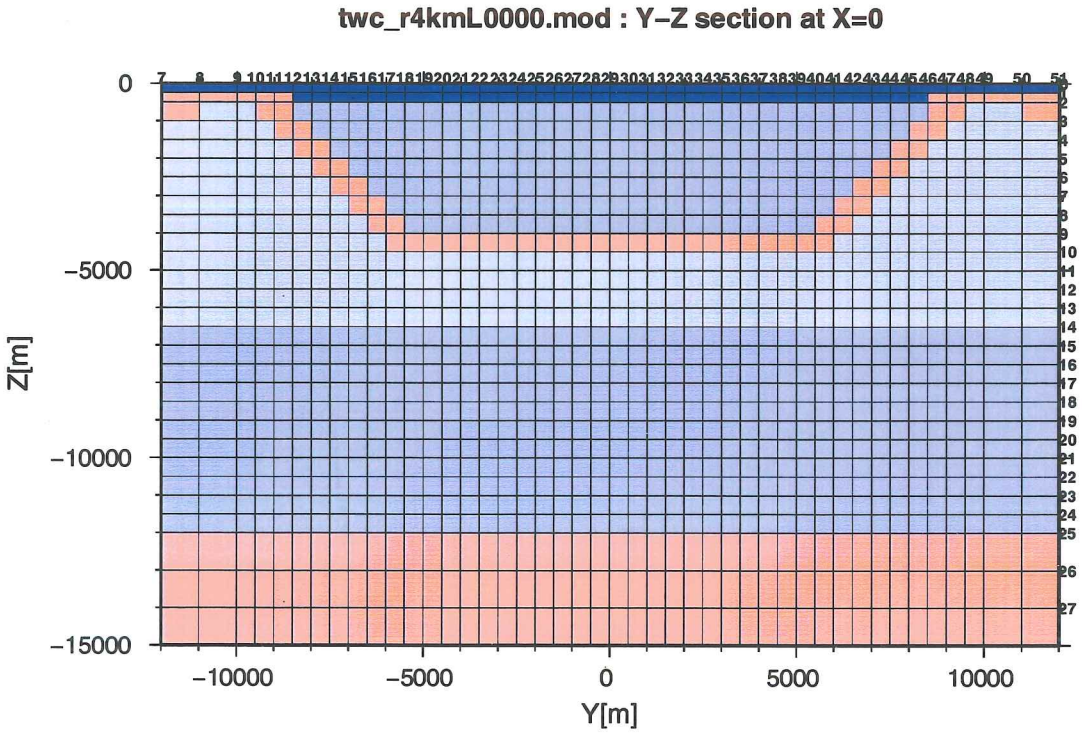

Figure-17. Resistivity model for two connected high-temperature geothermal systems 20km apart; vertical section along the volcanic zone (color codes the same as in fig.-12).

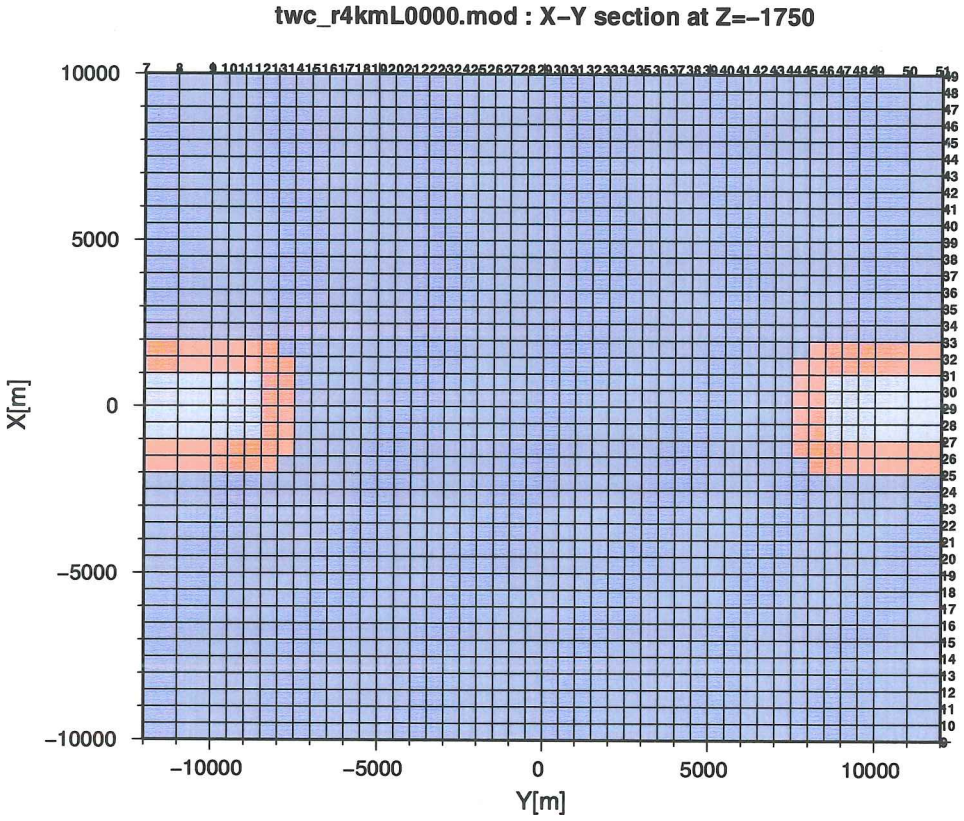

Figure-18. Resistivity model for two high-temperature geothermal systems 20km apart; horizontal section at the the depth of 1750m. (color codes the same as in fig.-12).

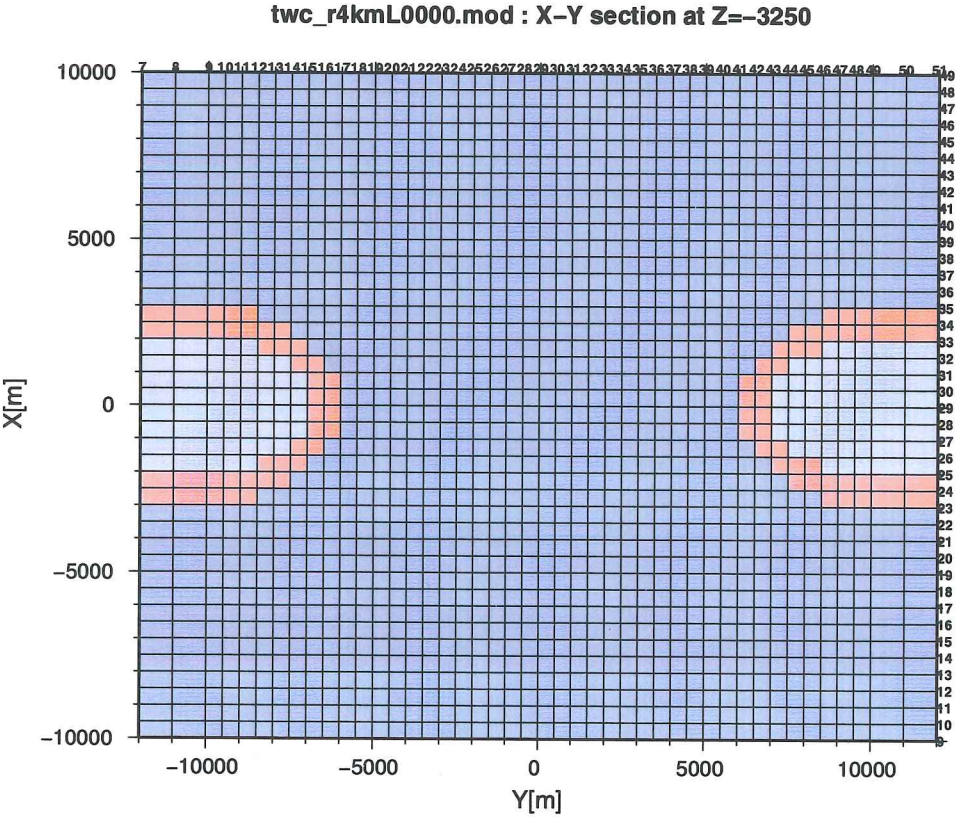

Figure-19. Resistivity model for two high-temperature geothermal systems 20km apart; horizontal section at the the depth of 3250m. (color codes the same as in fig.-12).

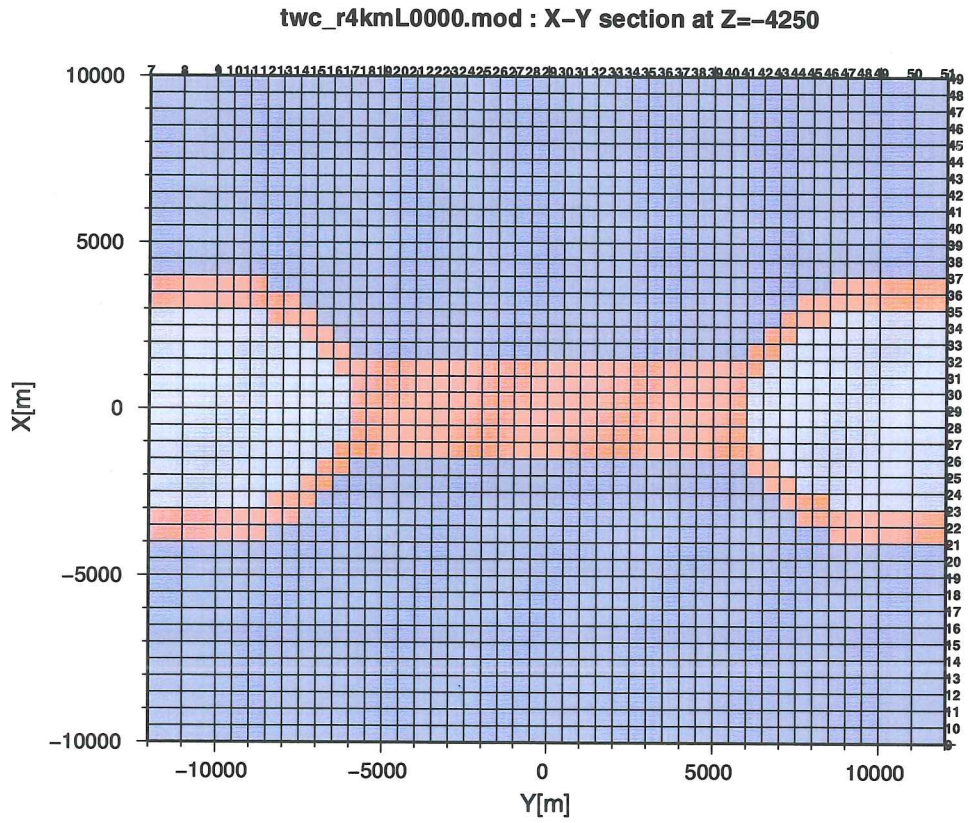

Figure-20. Resistivity model for two connected high-temperature geothermal systems 20km apart; horizontal section at the the depth of 4250m. (color codes as in fig.-12).

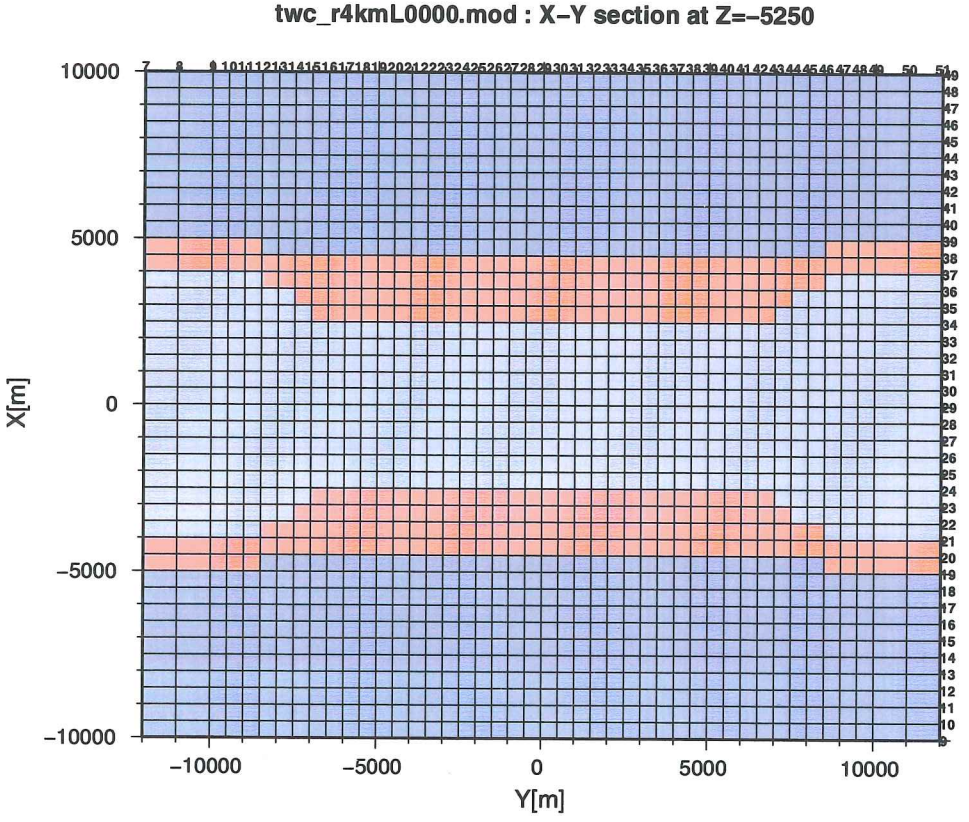

Figure-21. Resistivity model for two connected high-temperature geothermal systems 20km apart; horizontal section at the the depth of 5250m. (color codes as in fig.-12).

4.2 Model calculations for the TEM Method

The sensitivity of a given electro-magnetic method to resistivity variations at different places in the earth is in general highly dependent on the resistivity distribution. The sensitivity to variations around a given model is therefore often specific to the model at hand and can be hard to generalise to other models. There are newer the less often certain features which are common to all models, reflecting what could be called "intrinsic sensitivity" of the method and geometrical configuration of the source and receivers. Even though this is a rather ill-defined concept, it is worth while looking at, because it helps to understand some general properties and can shed light on more model specific results. Before the sensitivity study for the above described models was performed, an attempt was made to study the intrinsic sensitivity of the TEM-method.

The model calculations for the TEM-method were performed by a general 3D modelling code called TEMDDD. The program, which was developed at Orkustofnun (Árnason, 1999), is a finite difference code for calculating the transient electro-magnetic response due to step-function excitation, by a loop or a dipole source, of a half-space with an arbitrary resistivity distribution.

4.2.1 Intrinsic sensitivity of th TEM-method

The following methodology was used to study the intrinsic sensitivity of the TEM-methods. The transient response for the case of a homogeneous half-space of 100Ωm was calculated for different sources (horizontal loop and grounded dipole) and at different receiver locations at the surface. All five components of the measurable electro-magnetic field, i.e. two horizontal components of the electric field, Ex and Ey, and the time derivative of the three components of the magnetic field, dBx/dt, dBy/dt and dBz/dt, where calculated as a function of time after the current in the source is turned off.

The resistivity was then lowered from 100Ωm to 1Ωm in a cube of side length 100m and the response calculated and compared to that of the homogeneous half-space. This was don for cubes at many different locations underneath the measuring devices. Comparison of the perturbed and unperturbed responses gives information on the sensitivity to resistivity variations at different locations in the earth and how it changes with time after the source turn-off. Figures 22 through 33 show examples of results of these calculations.

Figures 22 through 25 show the intrinsic sensitivity in the case where the transmitter is a rectangular loop with the side length of 300m (marked as Tx on the figures) and the receiver is horizontal coil (marked as Rx) measuring dBz/dt at the distance of 1600m from the centre of the transmitter loop. The figures show the sensitivity at different times (0.11ms, 1.1ms, 11ms and 110ms respectively) after the source is turned off, and at different depths in a vertical section through the transmitter and receiver. Iso-value contours in the sections show the logarithm of the fractional difference of the perturbed and unperturbed response, calculated as:

$$s = \log | (v_{pert} - v_{ref})/v_{ref} | \qquad (1)$$

when the resistivity is lowered at different places in the section (the higher the value of s,

the higher the sensitivity). One important point should be noted here, namely that the sensitivity as defined above does not tell the whole story. In some configurations, the mutual coupling between the source and the receiver (the induced signal in the receiver) is so low that the measured signal would be practically drowned in ambient noise.

Figures 26 through 29 show the sensitivity in a similar section, when the source is a 300m long grounded dipole (marked Tx), perpendicular to the section. The receiver (Rx) is as before a horizontal coil measuring dBz/dt. Figures 30 through 33 show the sensitivity in the case when the source is a grounded dipole and the receiver is also a grounded dipole. Both the dipoles are perpendicular to the section and the receiver is measuring the electric field component parallel to the transmitter.

The figures show that right after the source turn-off, the sensitivity is confined to shallow depths, but as time passes, the sensitivity extends to greater depths. This reflects the fundamental property of the TEM-method that the depth of exploration increases with time after the source turn-off.

Figures 22 through 25 show that, except at very early times, the sensitivity is low underneath both the source and receiver loops. Figures 26 through 29 show that the sensitivity is considerably higher under the source, when the source is a dipole instead of a loop, and the sensitivity is low under the receiver loop. This shows that loops have the general property of being relatively insensitive to resistivity variations right under the loop, and this applies to both sources and receivers. A loop, either as transmitter or receiver, has the highest sensitivity on a cone, extending with time downwards and outwards from the loop.

Figures 26 through 33 show that, opposite to the loops, the grounded dipoles have highest sensitivity under the dipole and this applies to both transmitter and receiver dipoles. At late times the sensitivity is relatively uniform at depth underneath and in between the grounded dipole source and receiver. In the case of horizontal loop source and receiver, the sensitivity is, at late times, highest in between the loops (see figure 25), but it is considerably lower than in the case of grounded dipoles (see figure 33). In the case of dipole source and a loop receiver, the sensitivity at at depth (at late times) is highest in between the source and receiver, and an order of magnitude higher than in the case of a loop source.

TEM soundings with a grounded dipole transmitter and horizontal loop receiver have been a very popular and widely used. The sounding results are commonly interpreted in terms of layered models which are taken to reflect the resistivity structure underneath the receiver. In the light of figures 26 through 29, this procedure must be considered very questionable because the sensitivity is lowest under the receiver. This procedure is only justified in the case when the earth is nearly layered and with little lateral resistivity variations. According to figures 30 through 33, such an interpretation of grounded dipole receiver data is better justified.

We have here concentrated on the cases of horizontal loop source and horizontal loop receiver, grounded dipole source and horizontal loop receiver (which by reciprocity is equivalent to the case of a loop source and dipole receiver perpendicular to the line to the

loop centre) as well as a dipole receiver parallel to the source dipole centred on the normal axis to the source dipole. The reason is that these configurations are the most commonly used and have relatively high mutual coupling between the source and receiver and hence relatively high signal to noise ratio. Many other alternative configurations have also been considered, such as measuring the horizontal components of the magnetic field (dBx/dt and dBy/dt) and the electric field perpendicular to the source dipole and at various orientations to the sources. It would be too lengthy to discuss all these alternatives in details.

The sensitivity of a given configuration of the TEM method can be thought of as the combined result of a sensitivity ascribed to the source (how strongly the source couples to a given region) and how strong a signal the excitation generates in the receiver (how strongly the induced currents in a given region couple to the receiver). A horizontal loop (either as a source or receiver) has highest sensitivity on a cone propagating downwards and outwards from the loop with increasing time. A grounded dipole has highest sensitivity in an elongated region under the dipole which propagates downwards and outwards with time. The sensitivity of a dipole has, however, in a sense, an orientation which is predicted by the current distribution under the dipole, when acting as a source. A receiver dipole oriented nearly perpendicular to the currents generated by the source can have high intrinsic sensitivity as defined by equation (1), but that can be of little importance because it has a very low signal to noise ratio.

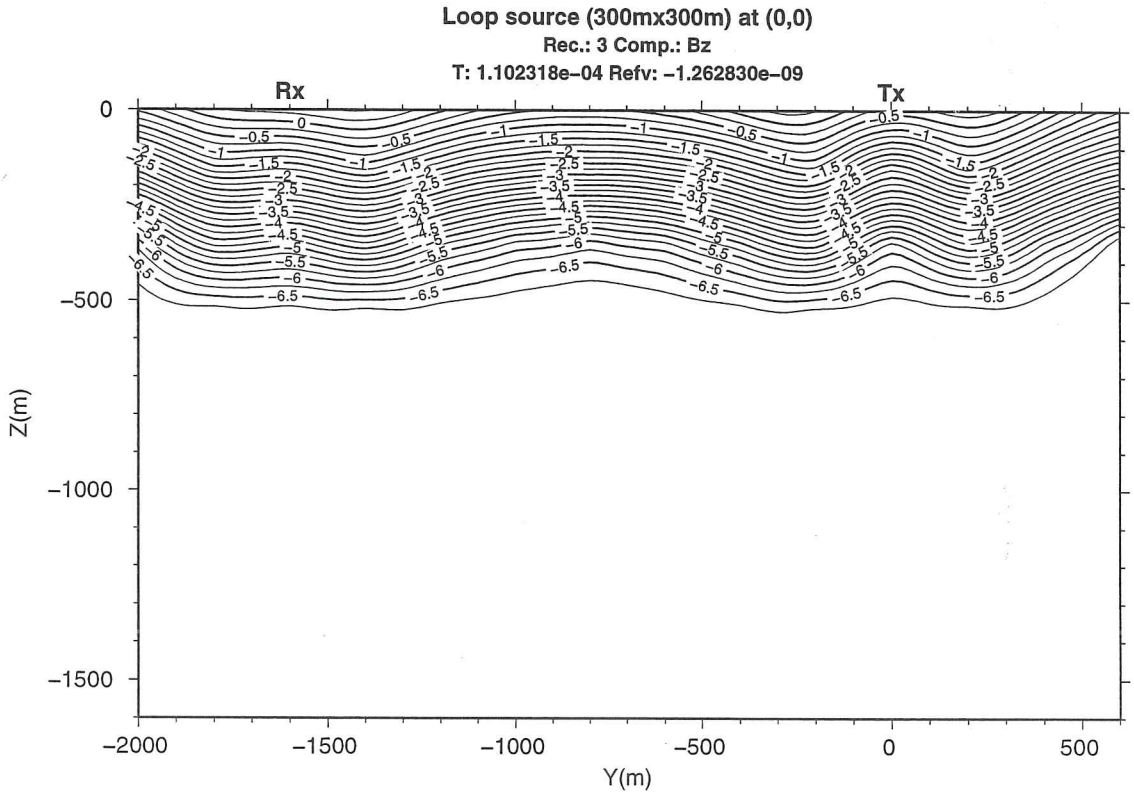

Figure-22. Intrinsic sensitivity for transmitter loop (Tx) and horizontal coil (dBz/dt, at Rx) at 0.11ms after current turn-off (Tx-Rx distance 1.6km).

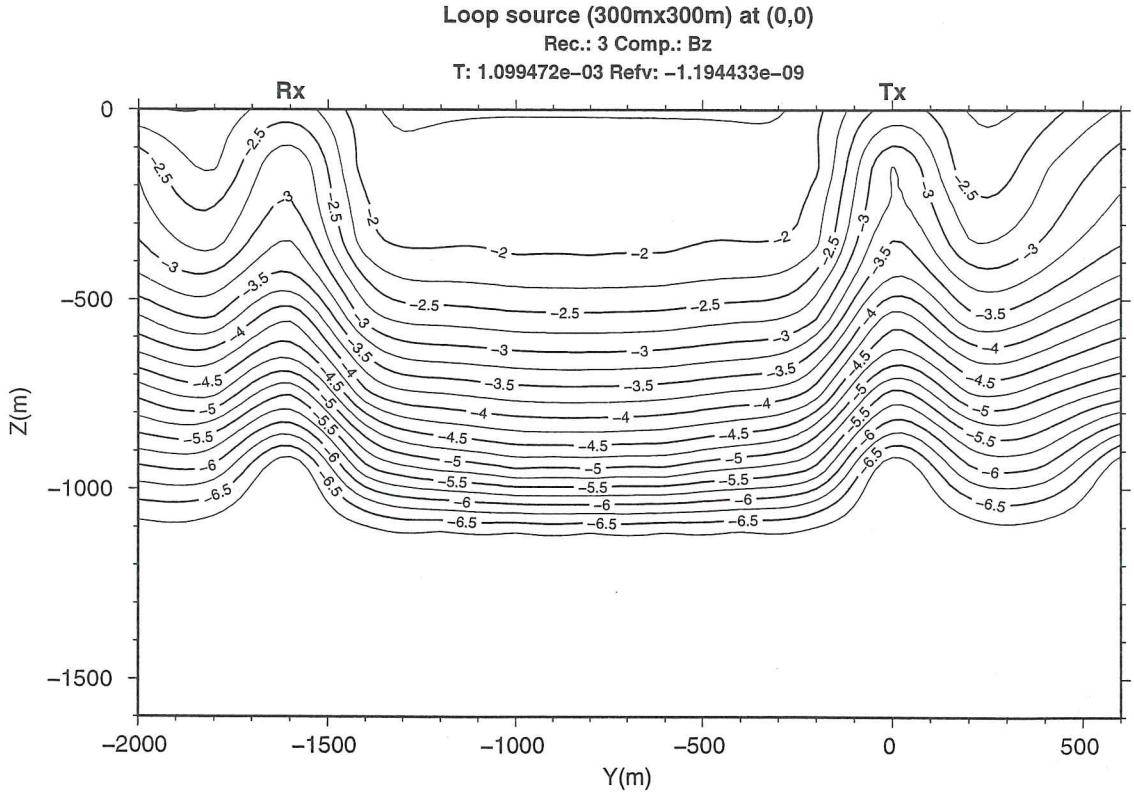

Figure-23. Intrinsic sensitivity for transmitter loop (Tx) and horizontal coil (dBz/dt, at Rx) at 1.1ms after current turn-off (Tx-Rx distance 1.6km).

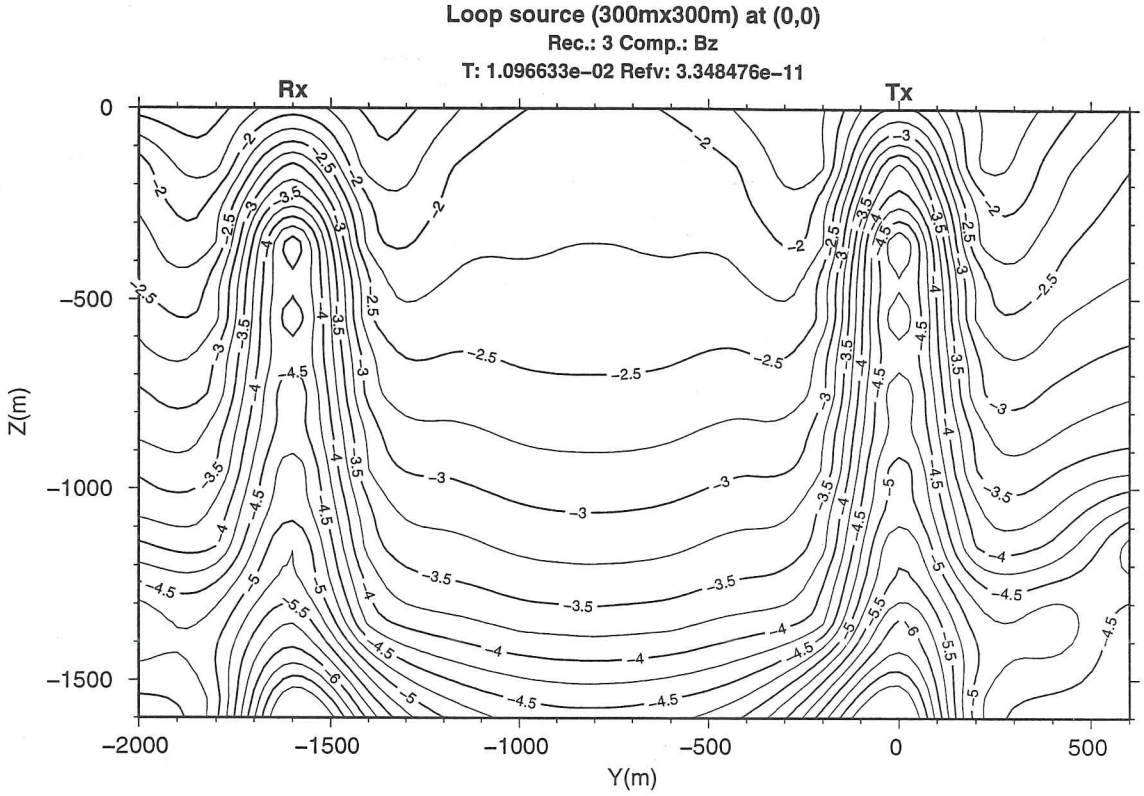

Figure-24. Intrinsic sensitivity for transmitter loop (Tx) and horizontal coil (dBz/dt, at Rx) at 11ms after current turn-off (Tx-Rx distance 1.6km).

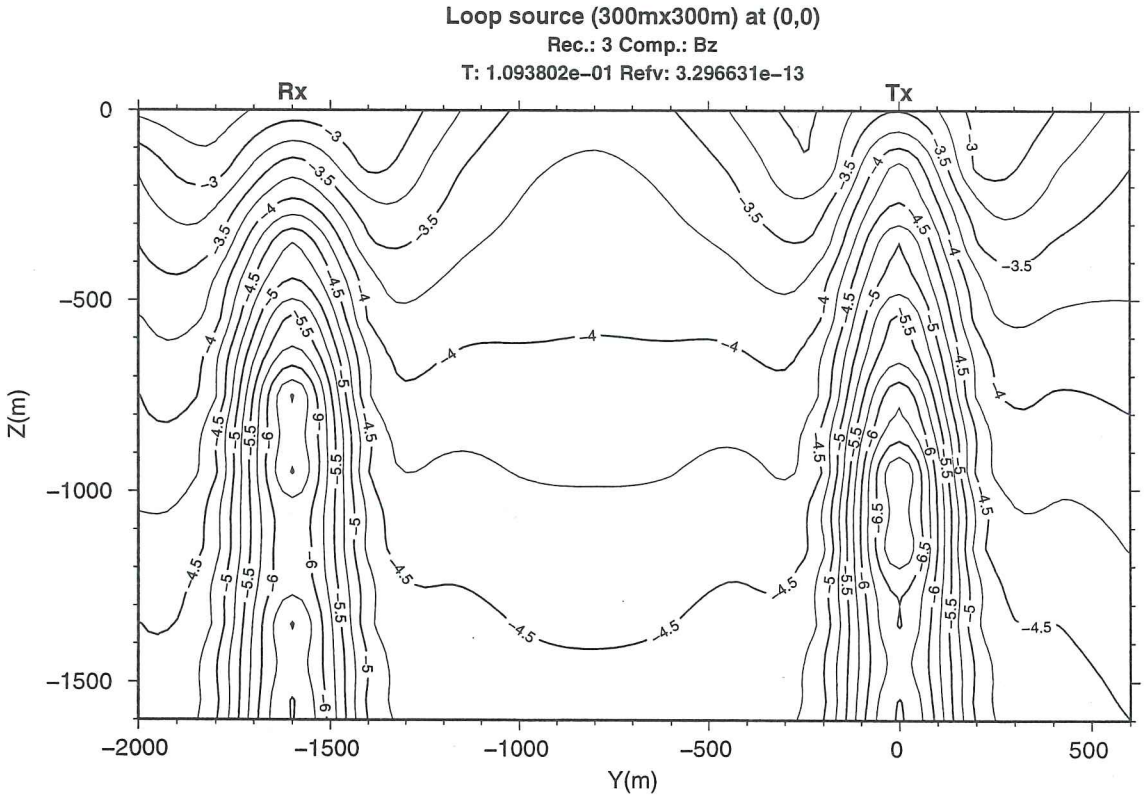

Figure-25. Intrinsic sensitivity for transmitter loop (Tx) and horizontal coil (dBz/dt, at Rx) at 110ms after current turn-off (Tx-Rx distance 1.6km).

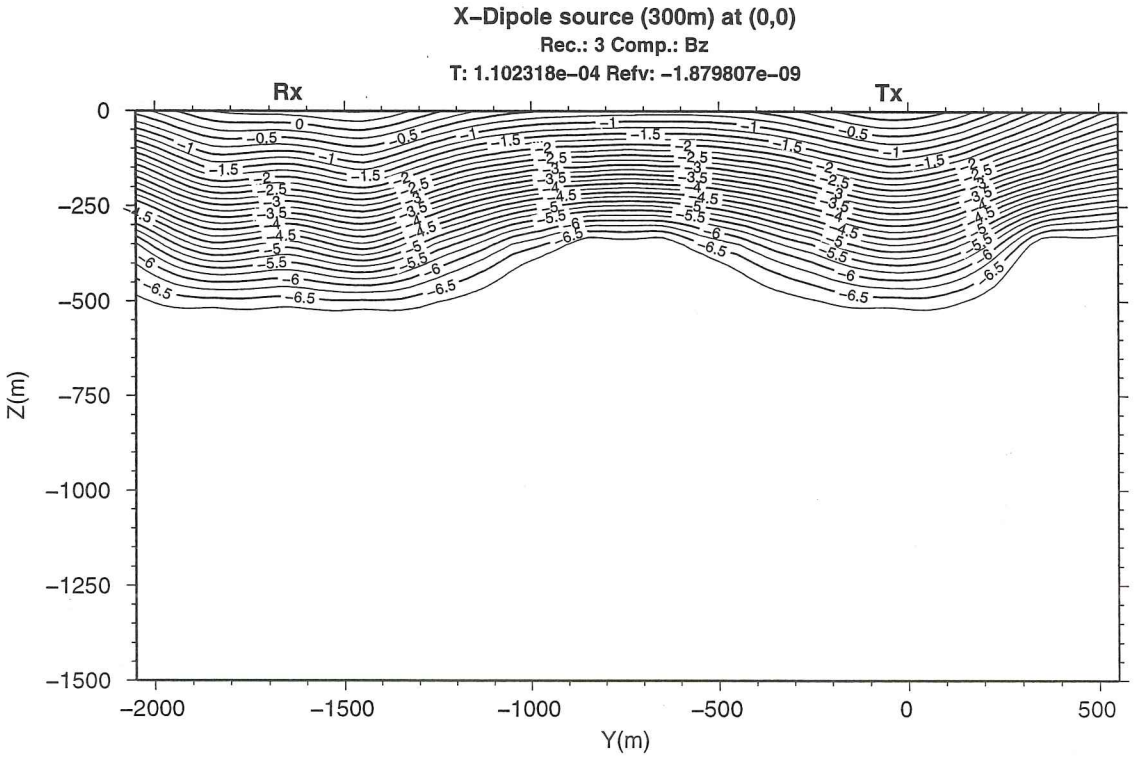

Figure-26. Intrinsic sensitivity for transmitter dipole (Tx), perpendicular to the section, and horizontal coil (Rx) at 0.11ms after current turn-off (Tx-Rx distance 1.6km).

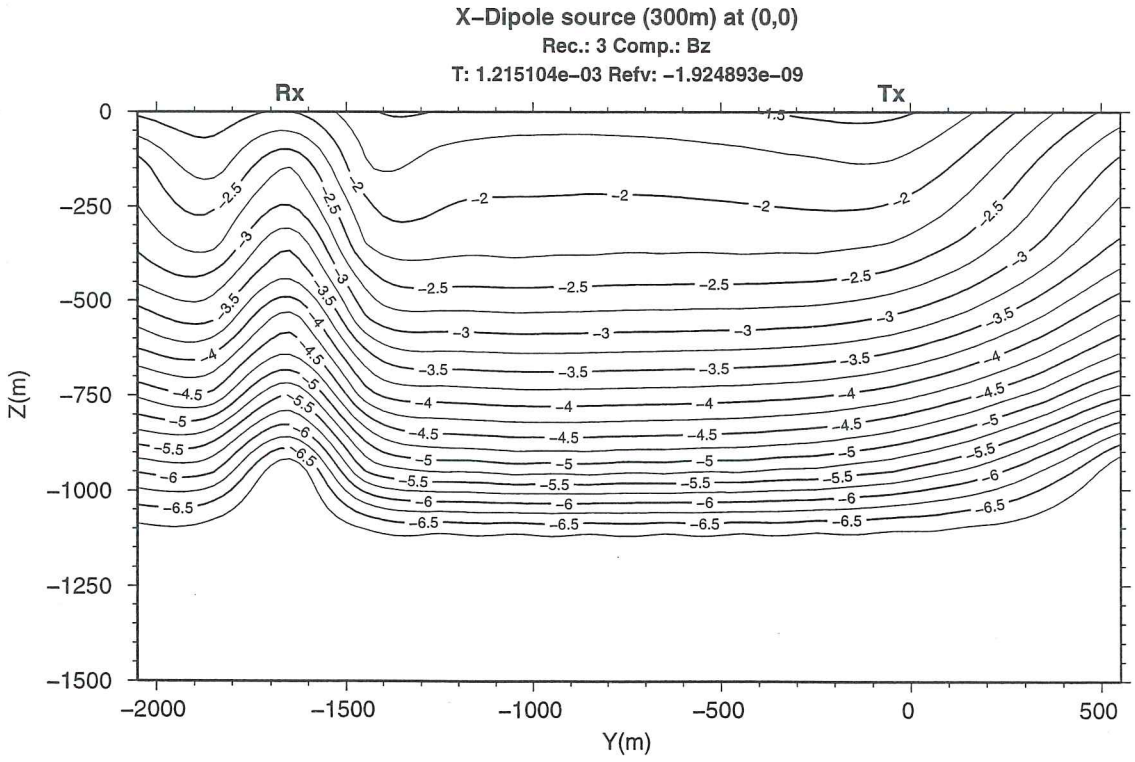

Figure-27. Intrinsic sensitivity for transmitter dipole (Tx), perpendicular to the section, and horizontal coil (Rx) at 1.1ms after current turn-off (Tx-Rx distance 1.6km).

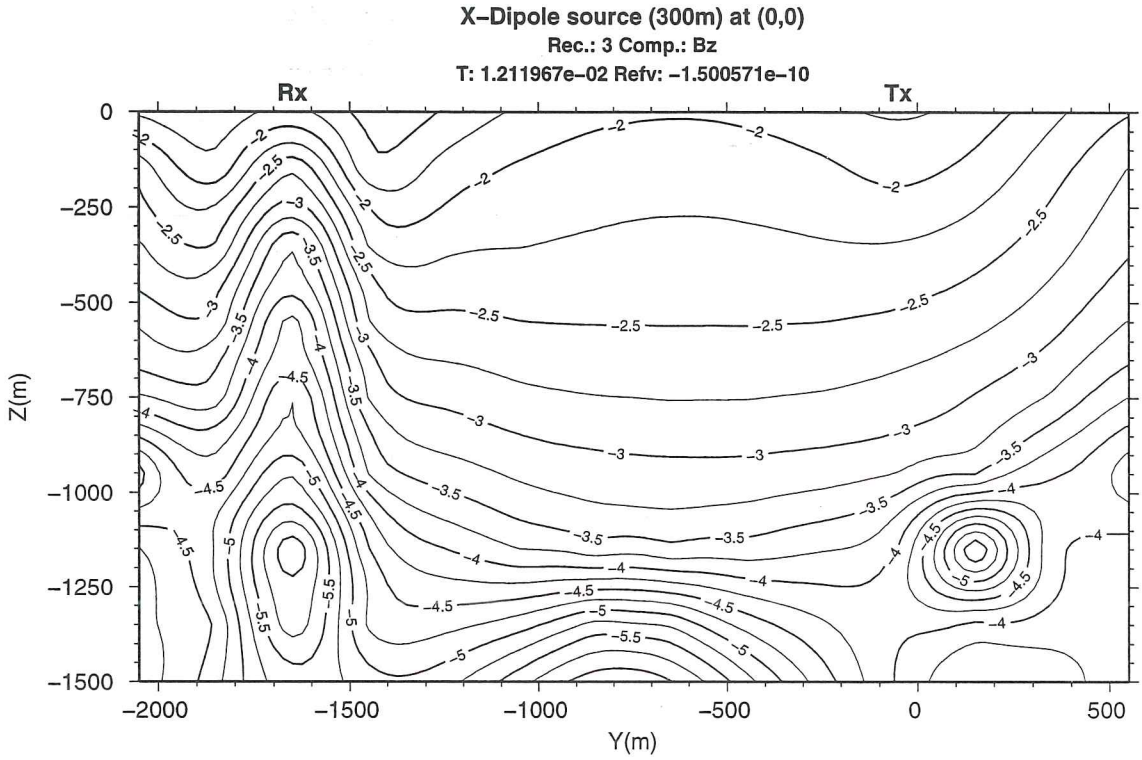

Figure-28. Intrinsic sensitivity for transmitter dipole (Tx), perpendicular to the section, and horizontal coil (Rx) at 11ms after current turn-off (Tx-Rx distance 1.6km).

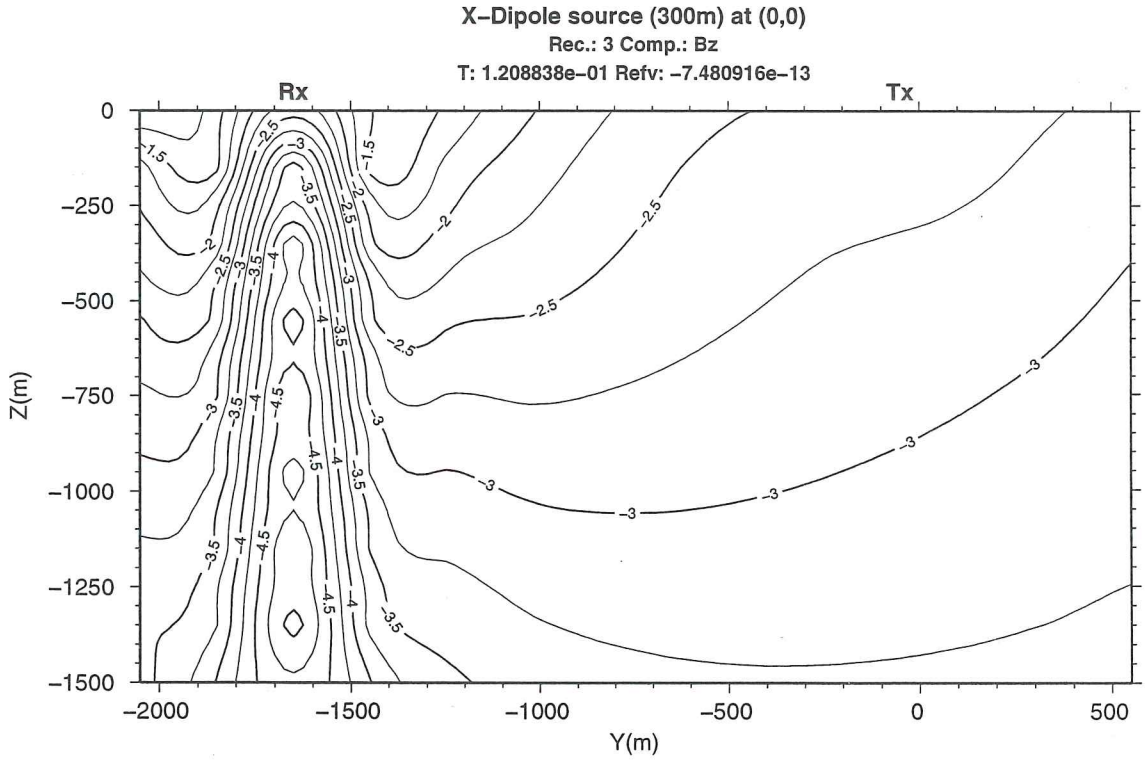

Figure-29. Intrinsic sensitivity for transmitter dipole (Tx), perpendicular to the section, and horizontal coil (Rx) at 110ms after current turn-off (Tx-Rx distance 1.6km).

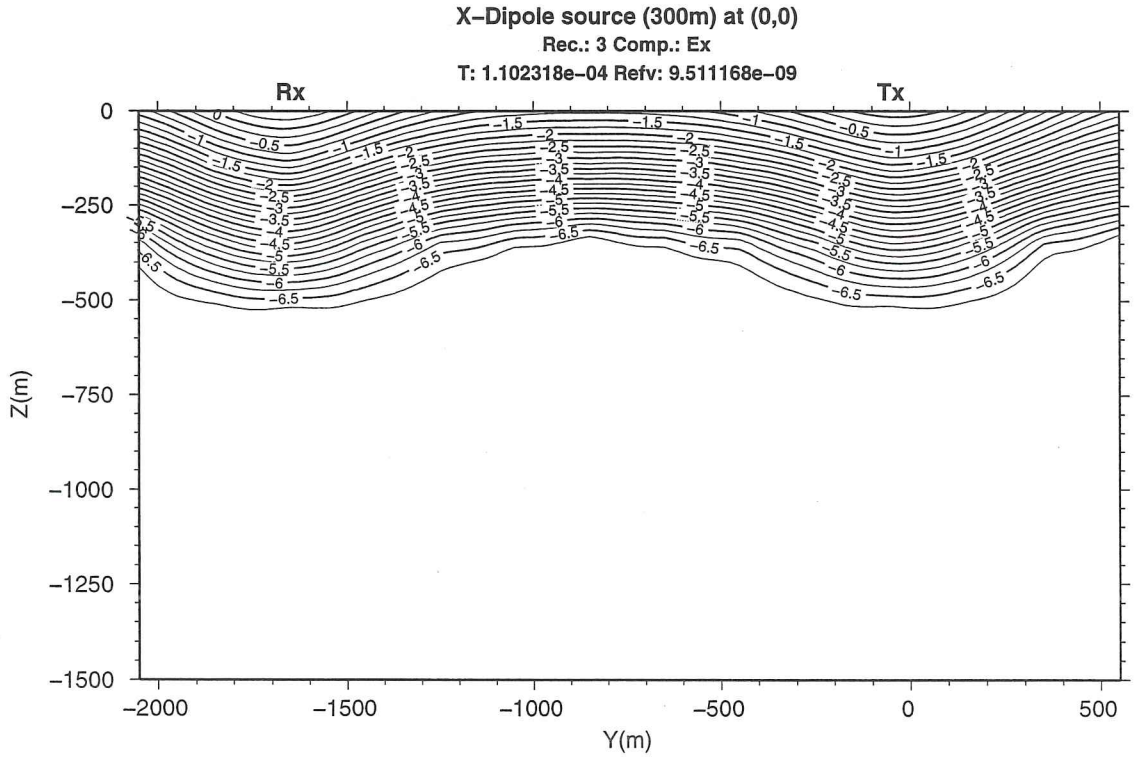

Figure-30. Intrinsic sensitivity for transmitter dipole (Tx), perpendicular to the section, and grounded dipole (Ex, at Rx) at 0.11ms after current turn-off (Tx-Rx distance 1.6km).

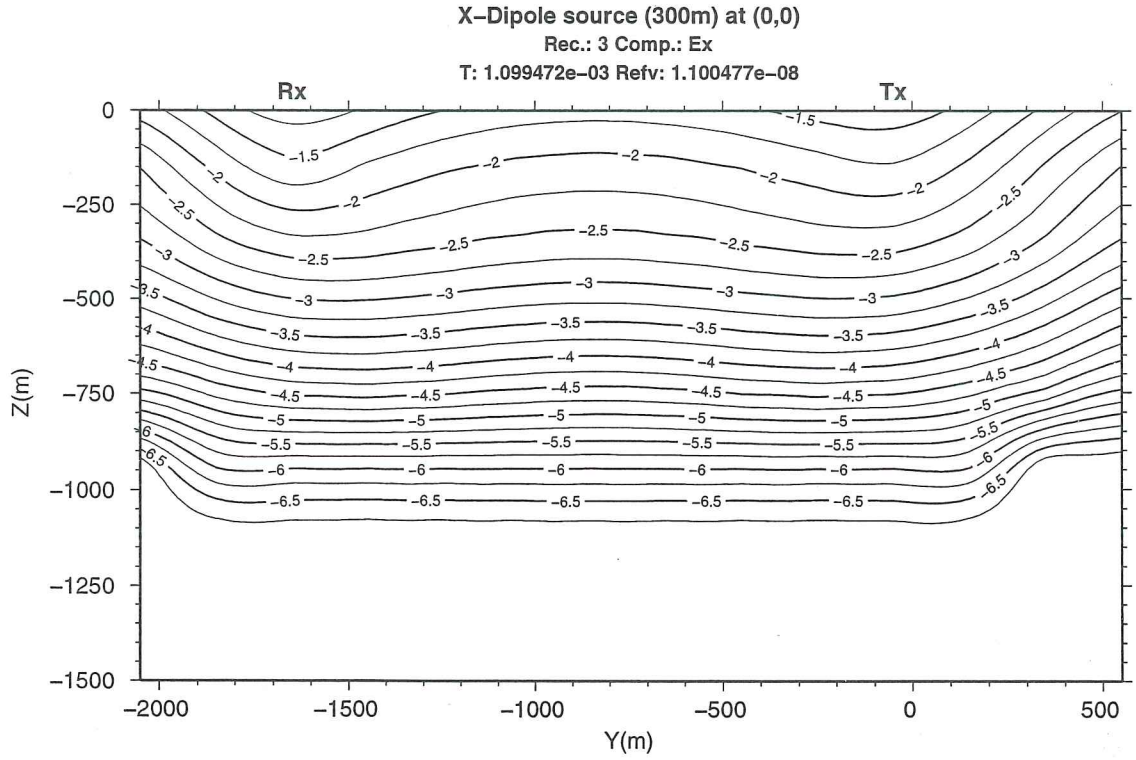

Figure-31. Intrinsic sensitivity for transmitter dipole (Tx), perpendicular to the section, and grounded dipole (Ex, at Rx) at 1.1ms after current turn-off (Tx-Rx distance 1.6km).

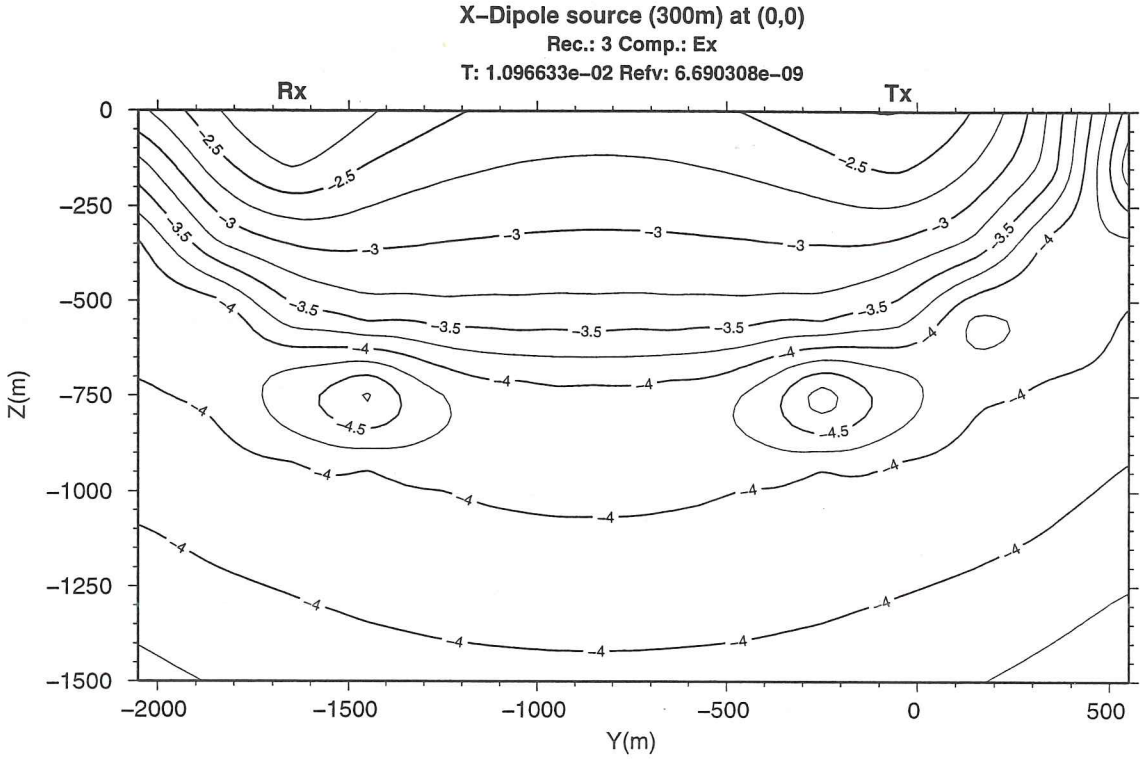

Figure-32. Intrinsic sensitivity for transmitter dipole (Tx), perpendicular to the section, and grounded dipole (Ex, at Rx) at 11ms after current turn-off (Tx-Rx distance 1.6km).

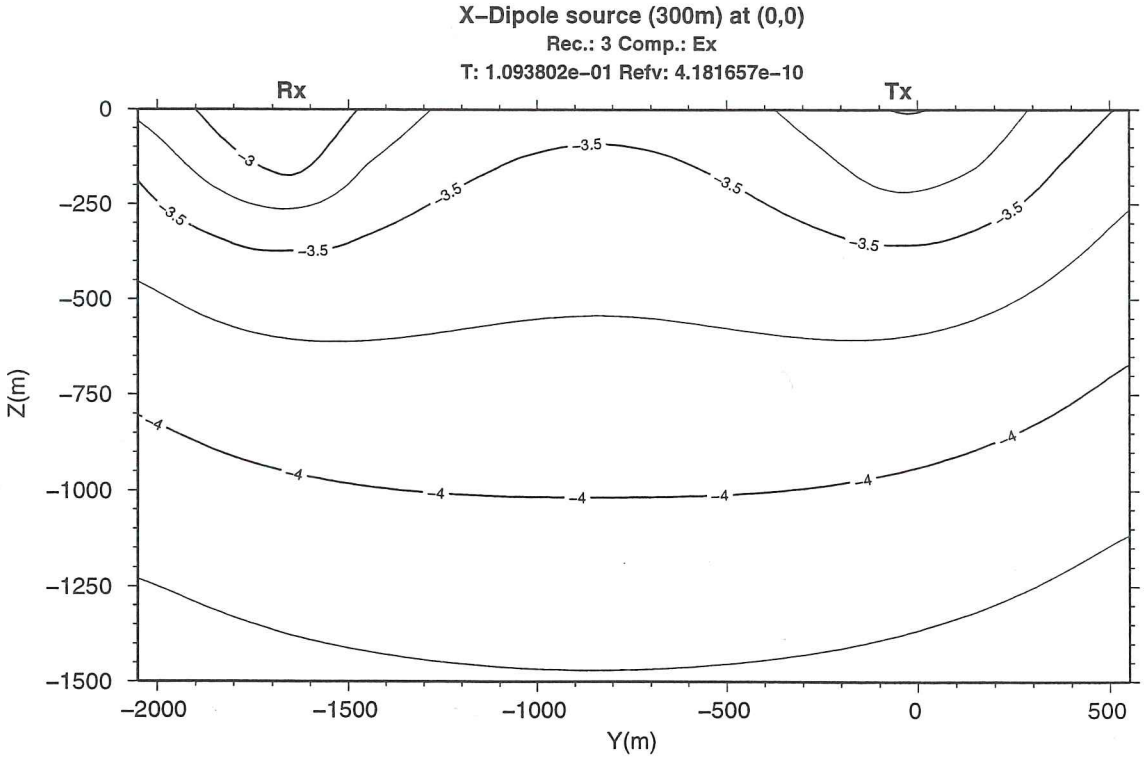

Figure-33. Intrinsic sensitivity for transmitter dipole (Tx), perpendicular to the section, and grounded dipole (Ex, at Rx) at 110ms after current turn-off (Tx-Rx distance 1.6km).

4.2.2 Sensitivity of the TEM method to the defined models

Let us now turn to the results of the sensitivity study of the TEM method for the defined test models. The main purpose of the study is to see how well the TEM method can tell if the two geothermal systems are connected by geothermal activity at depth along the volcanic zone, or not. This was done by calculating the response of pairs of models where the geothermal systems are connected and not connected and comparing the response.

The models where fitted into a regular rectangular discretization grid used by the 3D code. The grid has 59 grid planes in the horizontal directions and 35 grid nodes from the surface and downwards. The grid spacings are constant, 500m, at the centre of the models (between 41 grid planes in the horizontal directions and 26 grid planes from the surface and downwards) and then progressively increasing towards the edges. (the grid planes are shown on the horizontal and vertical sections of the models on figures 12 through 21). A coordinate system is defined for the models such that the centre at the surface is at the origin. The x-coordinates increase from front to back, perpendicular to the volcanic zone, the y-coordinates increase from left to right parallel to the volcanic zone and the z-coordinates increase with depth.

The model responses were calculated for three types of sources: Grounded 1km long dipoles, both perpendicular (in x-direction) and parallel (y-direction) to the volcanic zone and for 1kmx1km square loops. Calculations were performed for 25 different source locations, regularly spaced from the centre and 8km in the x- and y-directions, as shown on figure 34. This amounts to 75 different transmitters and is, due to symmetry, equivalent to covering the whole surface. The five components of the transient responses (dBx/dt, dBy/dt, dBz/dt, Ex, and Ey) were calculated at 81 receiver sites (numbered from 0 to 80) covering an area of 16kmx16km, as shown on figure 35. (The responses are therefore calculated for 25x3x81 = 6075 source-receiver location and type combinations and 25x3x81x5 = 30375 source-receiver-component combinations).

An example of calculated responses is shown in figure 36. The figure shows the calculated values of dBz/dt in receivers 36 to 41 on a profile across the volcanic zone in-between the two geothermal systems (for location of receivers 36 to 41, see figure 35). The source is a 1kmx1km rectangular loop on the axes of the volcanic zone and at equal distances from the two geothermal systems (the centre of the loop is at x=0 and y=0). The vertical axes on figure 36 show the logarithm of dBz/dt in V/m^2 (the induced voltage of a horizontal loop of area 1 m^2), and the horizontal axes show the logarithm of time in seconds after the source current of 1 Ampere is abruptly turned off. The broken lines show the response in the case when the geothermal systems, extending down to the depth of 6km, are not connected and the solid lines show the response when the systems are connected by a low-resistivity ridge with the top at the depth of 4km and extending down to 6km (see figures 16 and 17). By the naming conventions used for the test models, this model pair is called 2C60R40.

At first glance, figure 36 seems to indicate that there is not very much difference in the responses for time values smaller than 100ms, but for t bigger than 100ms, some difference is seen and increasing as the receiver site gets closer to the axes of the

volcanic zone. It is, however, somewhat misleading to look at the responses on log scale because the response is decaying quite fast with time. In order for the differences to measurable, the responses must be above the noise level as well as their difference. In order to estimate if the simulated measurements are able to detect whether the systems are connected or not, on has to evaluate the differences in the responses by taking expected noise into account.

There are basically two ways to increase the signal to noise ratio, namely by increasing the signal by increasing the source strength and by applying noise rejection in the data recording. There are practical limitations to how long dipoles and large loops can be used and in this study it is assumed that dipoles are not longer than 1km and loops no bigger than 1kmx1km. The source current can be kept as high as possible and in the following study it will be assumed that the source current is 20 Amperes for dipole sources and 40 Amperes for loops (this is about the maximum that is practically attainable). Increasing the the source current by a factor of 40, will increase the responses on figure 36, and the signal to noise ratio by a factor of 40.

Various noise rejection procedures are available, such as different stacking procedures (simple stacking, selective stacking, robust mean estimation) and noise compensation by remote reference. In the present sensitivity study, the recorded natural signal data, described in section 3, will be used to to estimate expected noise. As is seen on figures 4, 5 and 6, the natural signal seems to be fairly well described as normally distributed. We will therefore assume that the natural signal is an incoherent noise in the TEM measurements having a normal distribution with zero mean, but with standard deviation depending on frequency and which field component is measured.

We are looking for deep structures which manifest them selves in the transients at times considerably later than 1ms after the source turn-off, which means that the data will be low-pass filtered below 1000 Hz in the data recording and processing. The transients are further more assumed to be recorded from time zero and up to about 1s, so the the relevant frequency band for the noise is assumed to be form 1Hz and up towards 1000Hz. From figures 7 through 11, it is seen that in this frequency range, the standard deviations for the electric fields and the time derivatives of the magnetic fields can be assumed be lower than $\sigma_E = 1.0 \cdot 10^{-6}$ V/m and $\sigma_B = 0.5 \cdot 10^{-9}$ V/m^2 respectively.

In this sensitivity study we assume simple stacking of N = 1000 transients for noise reduction. It is therefore assumed that such a measuring process would lead to a mean values and standard errors given as:

$$\overline{V}(t) = I \cdot v(t) \ , \ \delta = \frac{\sigma}{\sqrt{N}} \qquad (2)$$

where I is the transmitted current, v(t) is the calculated response at time t, σ is the standard deviation of the noise (assumed to be the same for all time gates of the measured transient) and N is the number of stacked values. The task is now to quantify how significantly the mean values, $V_u(t)$ for unconnected systems and $V_c(t)$ for connected systems differ.

Probability theory and statistics lends us the tool for doing this (see eg. Mendenhall, et al., 1981). If the two mean values $\overline{V}_c(t)$ and $\overline{V}_u(t)$ are obtained from sampling N values from two normal distributions with the same standard deviation σ, then the significance of their difference can be quantified by the Student's t-test. To do so we calculate the so-called "pooled standard error", which in this case turns out to be:

$$\delta_P = \left[\frac{(N-1)\sigma_u^2 + (N-1)\sigma_c^2}{2N-2} \cdot \frac{2}{N} \right]^{1/2} = \sqrt{2}\,\delta \qquad (3)$$

and then calculate the t-test variable:

$$t = \frac{\overline{V}_u(t) - \overline{V}_c(t)}{\delta_P} \qquad (4)$$

The Student's t-distribution of the test variable t, with 2N - 2 degrees of freedom, then gives the significance, s(t), of the difference in $\overline{V}_u(t)$ and $\overline{V}_c(t)$, i.e. the probability that the two distributions have different means.

By using this procedure and the above listed values for the transmitted current, standard deviation of the noise, the stacking number (N = 1000), and the calculated transients, the significance, s(t), of the difference between the response of connected and non-connected models, can be calculated for different times after the source turn-off.

Figure 37 shows the results of such calculations for the transients on figure 36 (the source is a 1kmx1km loop and the current is I = 40 Ampere; the recorded signal is dBz/dt and the standard deviation is $\sigma = 0.5 \cdot 10^{-9}$ V/m^2). The vertical axes show the probability (in the range of 0 to 1) that the two transient values are significantly different and the horizontal axes show the logarithm of time in milli-seconds. The figure shows that the significance of the differences is very small for receivers 36 and 37, furthest away from the volcanic zone and the transmitter. It increases as the receiver gets closer to the axis of the volcanic zone. It is also seen that significance varies very much with the delay time. It is low at early times because at early times the ridge is below the depth of exploration. Even though figure 36 shows the biggest fractional difference in the transients at late times, the significance of this difference is very small because the transient is practically drowned in noise. The highest significance, about 75%, is seen at about 50ms for transmitter 40, which is at the axis of the volcanic zone and inside the source loop.

It is instructive to look at the significance in the difference in the response curves for connected and non-connected models at different times, like on figure 37. It would, however, take a lot of such drawings to get an overview of the sensitivity of different measurement setups. We would therefore like to have one number, S, quantifying the significance of the difference for each pair of connected and non-connected response curves. The simplest way to do this is to take the average of the significance over a given time interval. We will here define S as the integral of the significance form time zero and up to one second:

$$S = \int_0^1 s(t)dt \qquad (5)$$

The average sensitivity, S, is dependent on the model pair, the type and location of the source, and the receiver location and the measured component. The ability, of a given source and measured component, to detect whether the systems are connected or not, can now be contoured on the model surface. This gives both an overview over the sensitivity of different source receiver combinations and also shows where on the surface the anomalies are manifested. We will in the following use this presentation of the results of the model calculations to investigate the sensitivity of different TEM-measurements configurations.

There is no room here to display and discuss the results for all the tested models. We will concentrate on two model pairs. In the first pair the two geothermal systems extend down to the depth of 6km and are either connected by a low resistivity ridge with the top of the crest of the ridge at the depth of 4km and extending down to the depth of 6km. The second model pair has the geothermal systems extending down to the depth of 4.5km and either connected by a low resistivity ridge with the top at 3km depth and extending down to 4.5km or not connected. By the naming conventions used for the test models, these two model pairs are called 2C60R40 and 2C45R30, respectively, and the contour plots that follow and pertain to these model pairs are marked with these names. We will display results for different transmitter types and locations and contour the sensitivity of a given measured component at the surface. The source location is shown by solid squares for loop sources and solid lines for x- and y-oriented dipoles. The contours show iso-lines of the significance (sensitivity) as defined in equation (5).

Figures 38 through 42 show the sensitivity of dBz/dt, dBx/dt, dBy/dt, Ex, and Ey, respectively. for a ridge at 4km depth (model pair 2C60R40) when the source is a loop over the centre of the ridge. The average sensitivity of Bz is highest (about 10%) for a receiver inside the source loop, and decreases towards zero away form the ridge. Both Bx and Ey show similar pattern which is natural because the dBx/dt signal is due to time variation in currents in the y-direction, which are the result of variations in Ey. They have two maxima, offset in x-direction on each side of the ridge, and a minimum along the axis of the ridge. Because the source is a loop and due to symmetry, there is no Ey component on the y-axis, neither for connected nor unconnected systems, and hence the minimum in sensitivity. Similarly By and Ex the same pattern with two maxima, but now offset in the y-direction along the ridge, and a minimum along the x-axis. The reason for the minima is that same as before.

The sensitivities for the electric fields are a little higher than those of the horizontal components of the magnetic fields. The highest average sensitivity values, about 10%. are seen for dBz/dt inside the source loop. The significance curve (as a function of time) for this receiver (receiver 40) is shown on figure 37. It shows much higher significance (as high as 75%) in a limited time range but the average significance is rather low.

Figures 43 through 47 show the sensitivity of the five field components for the model 2C60R40, in the case when the source is a loop, offset 8km from the axis of the volcanic

zone. The sensitivities are vanishingly small, except for Bx an Ey, showing that the biggest effect of the ridge is to deflect the current distribution parallel to the volcanic zone towards the conducting ridge. An important point to note is that the anomalies appear mainly over the ridge, and are not pulled away from it, by the source. Here again the sensitivity for the electric field is higher than for the magnetic field and the sensitivity of the electric field Ey is even higher than the highest sensitivity seen in the case when the loop is above the centre of the ridge. This can be understood in the light of the discussion of the intrinsic sensitivities in section 4.1.1, where it was found that the sensitivity is low under loops.

Figures 48 through 52 show the sensitivity for the model pair 2C60R40 when the transmitter is a grounded 1km long grounded dipole at the centre of the volcanic zone and oriented parallel to the ridge (y-direction). The vertical component of the magnetic field shows two symmetric maxima with average significance of about 12%, offset by about 4km from the axis, and a distinctive minimum along the axis of the volcanic zone. This is to be expected because, if the dipole is in a plane of symmetry for the resistivity distribution, then the vertical component of the magnetic field is very small near the axis of the dipole and the signal to noise ratio is therefore very low. The sensitivity of By and Ex is very low, especially in between the geothermal systems, but slightly increasing towards the systems. The other two horizontal components are, on the other hand very sensitive to the presence of the ridge. The Magnetic field perpendicular to the volcanic zone (and the ridge) has the average significance as high as 21% close to the source and the electric field parallel to the volcanic zone (Ey) has a still higher average significance, up to 35%.

Figure 53 shows the calculated transient curves of Ex, for receivers 36 to 41 (on a profile along the central normal to the dipole, from the edge of model and over the volcanic zone) and figure 54 shows calculated significance at different delay times. The difference in the response curves does not look too impressive but due to the strong signal, the difference is very significant, even with 100% certainty over a considerable portion of some of the curves.

Figures 55 through 59 show the sensitivity in he case of an y-oriented dipole offset by 8km from the axis of the volcanic zone and at equal distances to the geothermal systems. In this case the Bz is relatively insensitive to the presence of the ridge and By and Ex are, as before, almost completely insensitive. Bx and Ey show on the other hand considerable sensitivity. Bx shows a maximum of about 11% average significance, slightly shifted from the ridge and towards the transmitter. Ey has a maximum of about 23% at the same place, so as before, the electric field seems to be more sensitive than the magnetic field.

The discussion above summarises the results of the sensitivity study for the case when the geothermal systems are connected by a low-resistivity ridge at the depth of 4km. We will not go through a detailed discussion of the cases when the systems are connected by a ridge at shallower depth, but only give three examples and concentrate on the most sensitive configurations. Figures 60, 61, 62 and 63 show examples of the sensitivity when the geothermal systems are connected by a low-resistivity ridge at the depth of 3km and extending down to 4.5km depth (model pair 2C45R30).

Figure 60 shows the case when the source is a 1km dipole above the centre of the ridge and parallel to the volcanic zone and the receiver measures the the electric field Ey, parallel to the transmitter. The figure shows that the average significance is high over the whole survey area and with maximum of 50% at the source. Figure 61 shows the sensitivity of Ey when the dipole is offset by 8km from the axis of the volcanic zone. The sensitivity is about a factor of two lower than on figure 60, but still relatively high, with a maximum of about 28% over the centre of the ridge.

We have up to now only shown examples of loop sources and dipoles parallel to the volcanic zone. Figures 62 and 63 show the sensitivity when the source is an 1km x-oriented dipole, perpendicular to the volcanic zone, and the measured signals are Ex and Ey respectively. The figures show that the Ey component, perpendicular to the source, is insensitive to the ridge. The Ex component, parallel to the source, has on the other hand high sensitivity. This confirms that, in the case of dipole sources, the electric field parallel to to the source dipole is the most sensitive component. Comparison of figure 62 and figure 61 shows, however, that for a source dipole perpendicular to the ridge, the sensitivity is somewhat lower, and with the maximum slightly more pulled towards the source, than for a source dipole parallel to the ridge.

The above results show that, for realistic resistivity contrasts and under realistic noise conditions, the TEM method is capable of detecting a ridge of geothermal activity connecting the geothermal systems at least to the depth of 4km. The various source-receiver combinations and locations show considerably different sensitivity. It is found that grounded dipoles couple more strongly to the ridge and result in higher sensitivity than loop sources. It is also found that the horizontal magnetic field perpendicular to the source dipole, and the electric field parallel to the dipole have much higher sensitivity than the other components. The electric field parallel to the dipole is the most diagnostic one. The relatively low sensitivity of the vertical component of the magnetic field is interesting in the light of the fact that TEM measurement configurations which record this component have been very popular and widely used.

The higher sensitivity of the electric field, as compared to the horizontal magnetic field, can be counteracted by static shifts in the electric field. Static shifts are caused by lateral and vertical variations at, or close to, the surface. Such inhomogeneities can distort and shift the response curves of nearby recording stations relative to each other. This can be considered as a geological noise and has not been included in the present study. The magnetic field is much less affected by near surface inhomogeneities. This may mean, when geological noise is taken into account, that the horizontal magnetic field will be more robust and sensitive than the electric field. Whether this is the case, will depend on the surface conditions in the survey area.

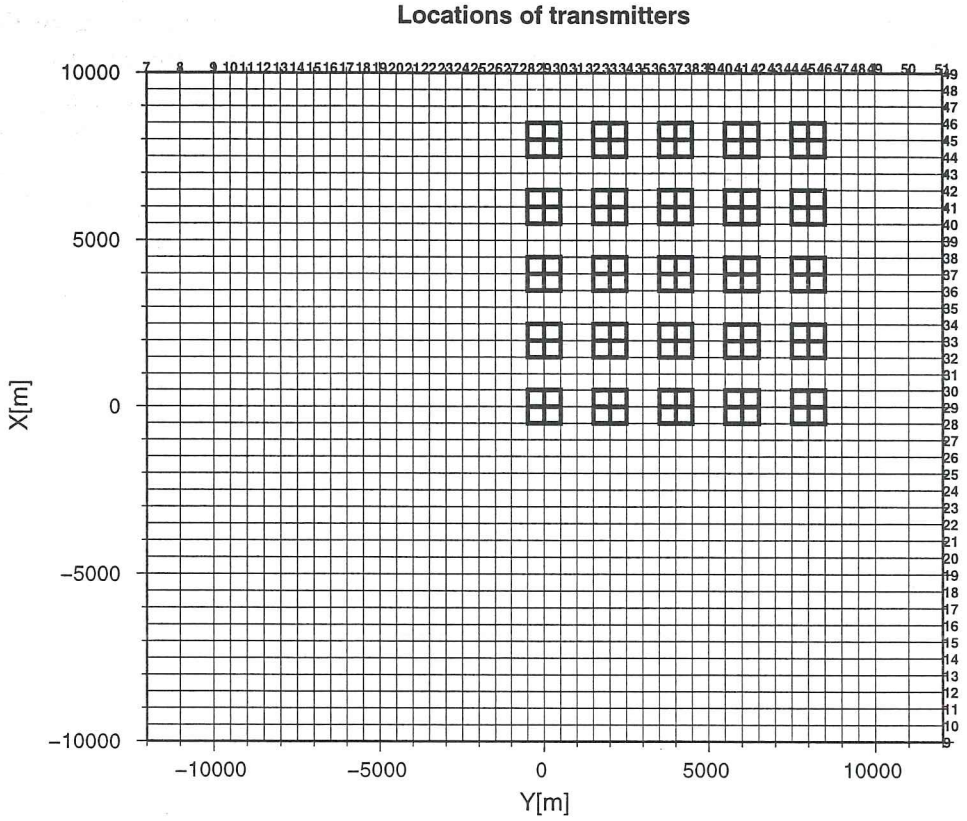

Figure-34. Locations of TEM transmitters (loops and dipoles).

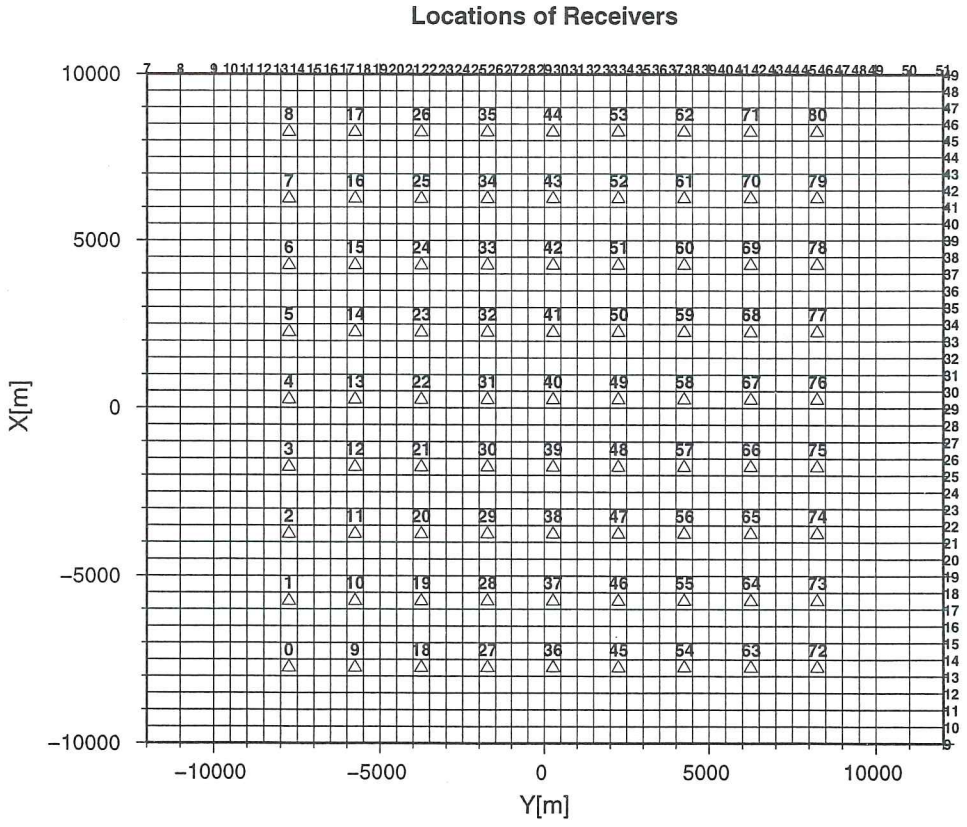

Figure-35. Locations and numbering of TEM receivers.

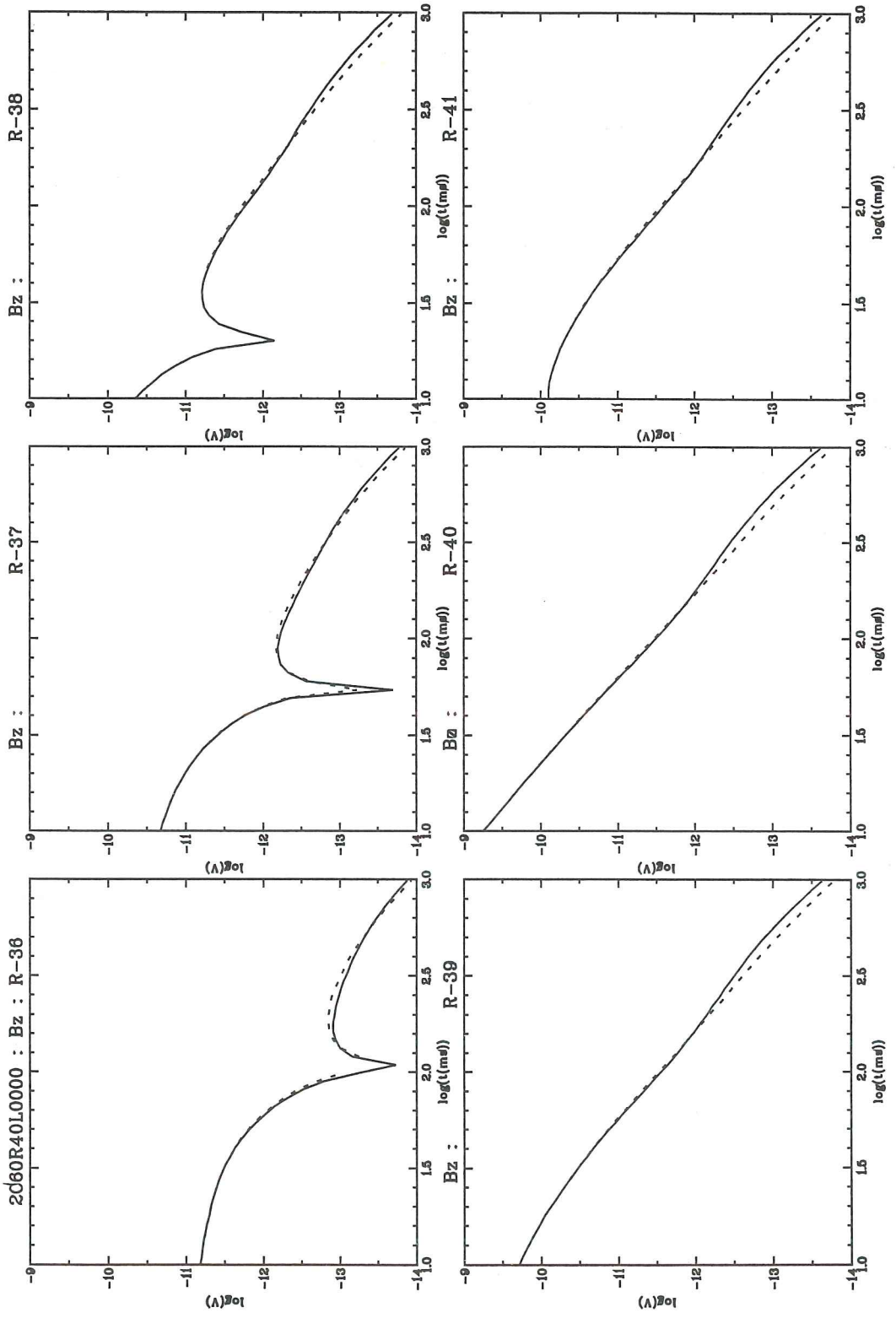

Figure-36. Calculated dBz/dt responses for non-connected (dashed lines) and connected (solid lines) geothermal systems at 4km depth (see model on fig.-15). The source is a 1km x 1km loop on the axis of the volcanic zone, centrally between the systems. The receivers (36 through 41) are on a profile perpendicular to the volcanic zone (see fig.-35).

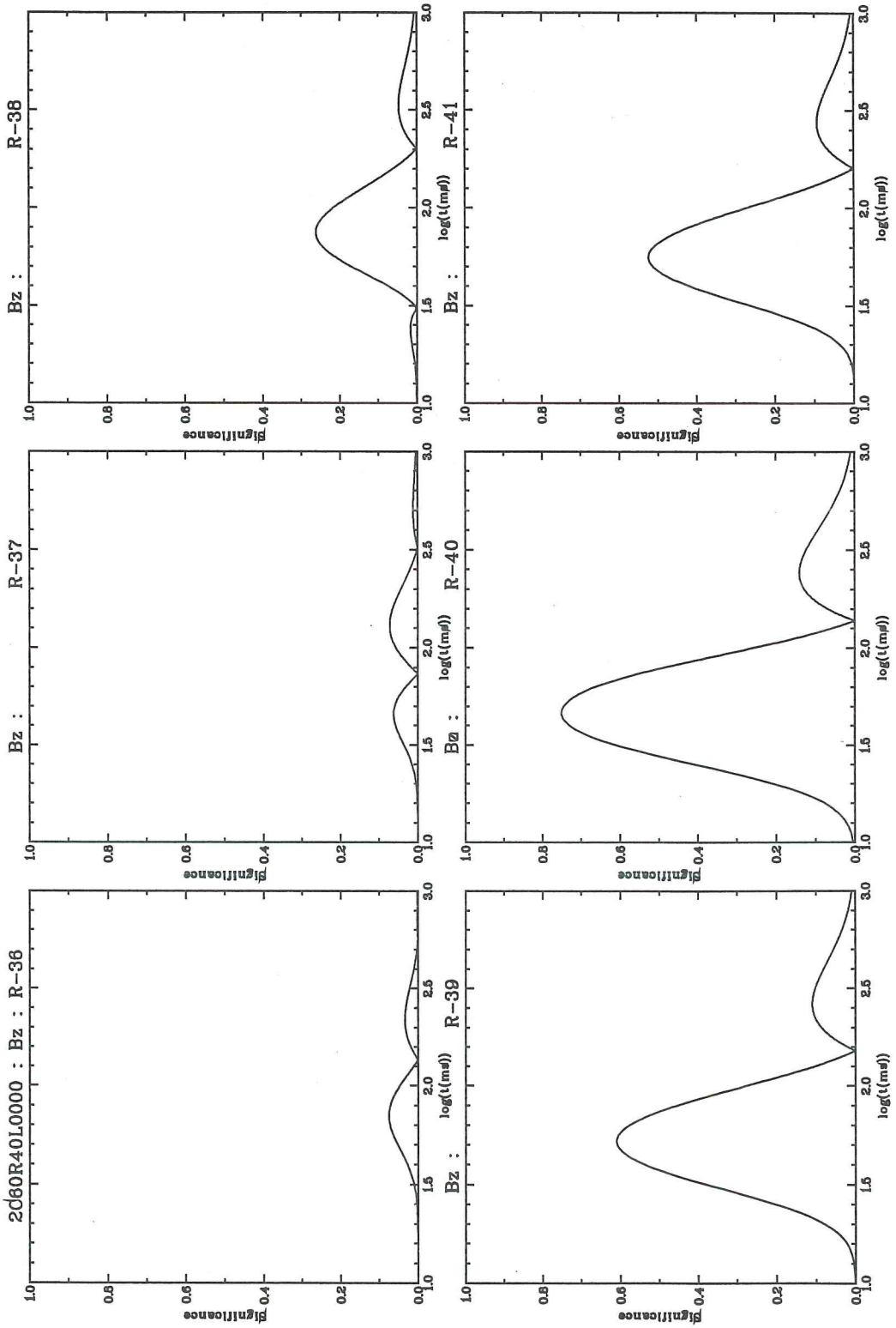

Figure-37. The significance of the difference in the "connected" and "non-connected" responses on fig.-36, at different times after the source turn-off.

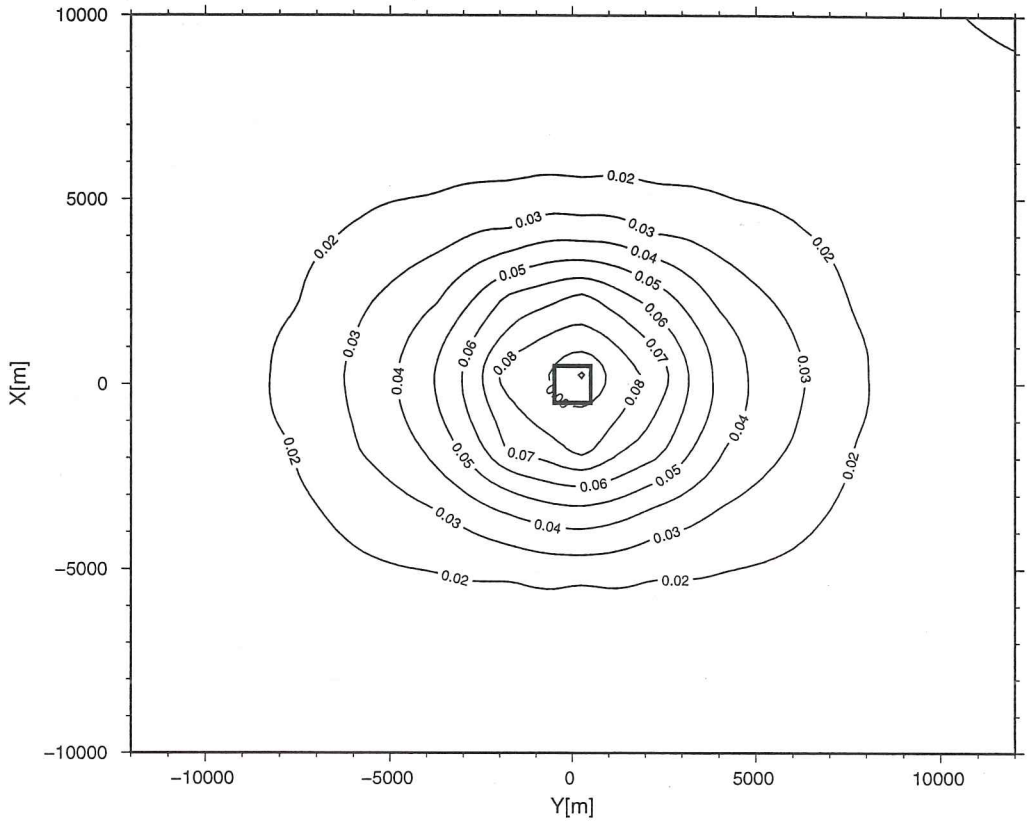

Figure-38. Spatial distribution of integrated significance of difference in **dBz/dt** of a loop source (solid square) for non-connected and systems connected at 4km depth.

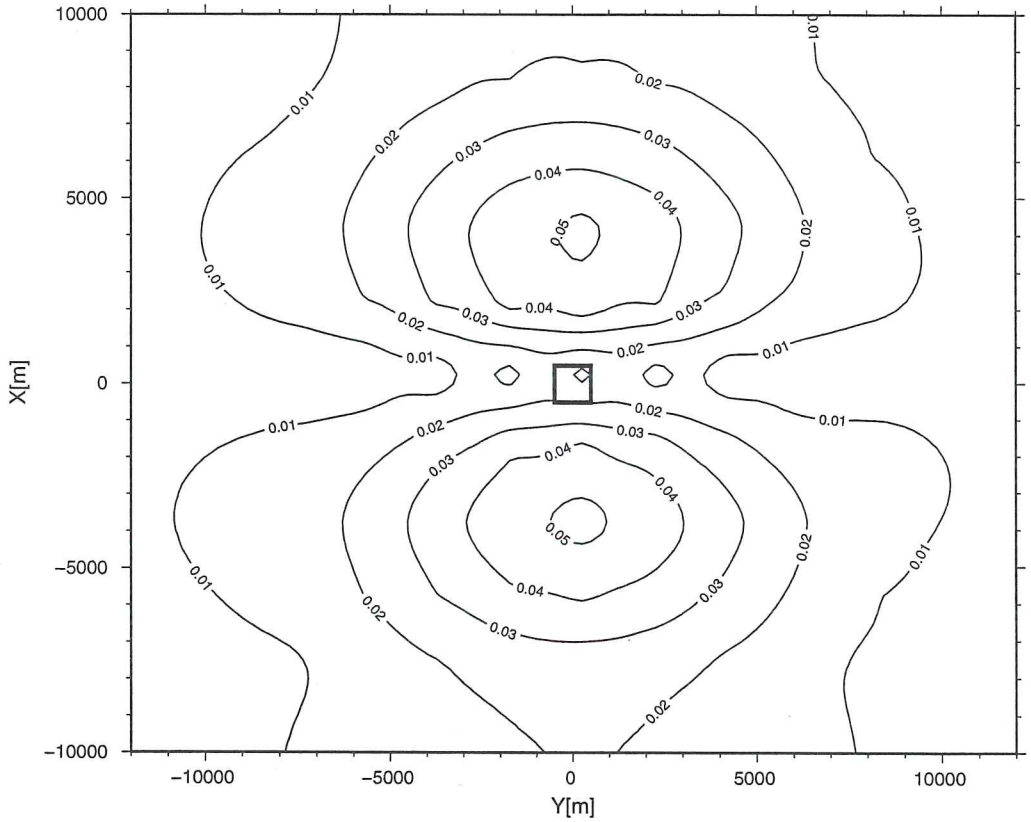

Figure-39. Spatial distribution of integrated significance of difference in **dBx/dt** of a loop source (solid square) for non-connected and systems connected at 4km depth.

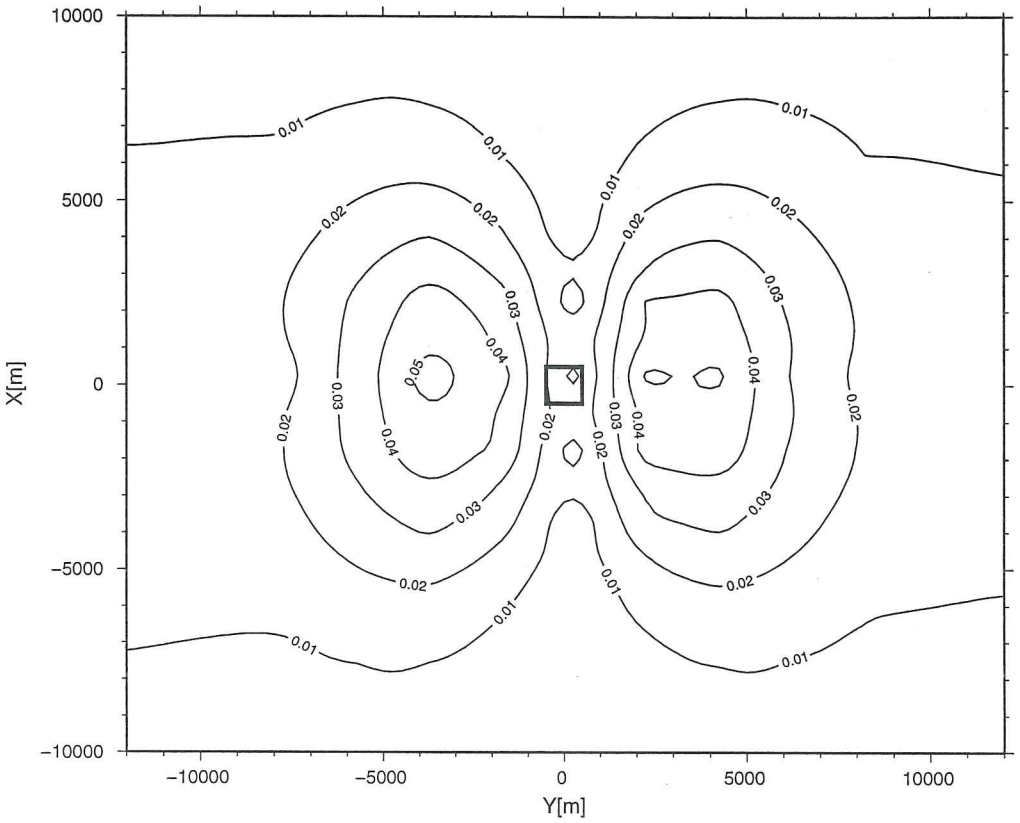

Figure-40. Spatial distribution of integrated significance of difference in **dBy/dt** of a loop source (solid square) for non-connected and systems connected at 4km depth.

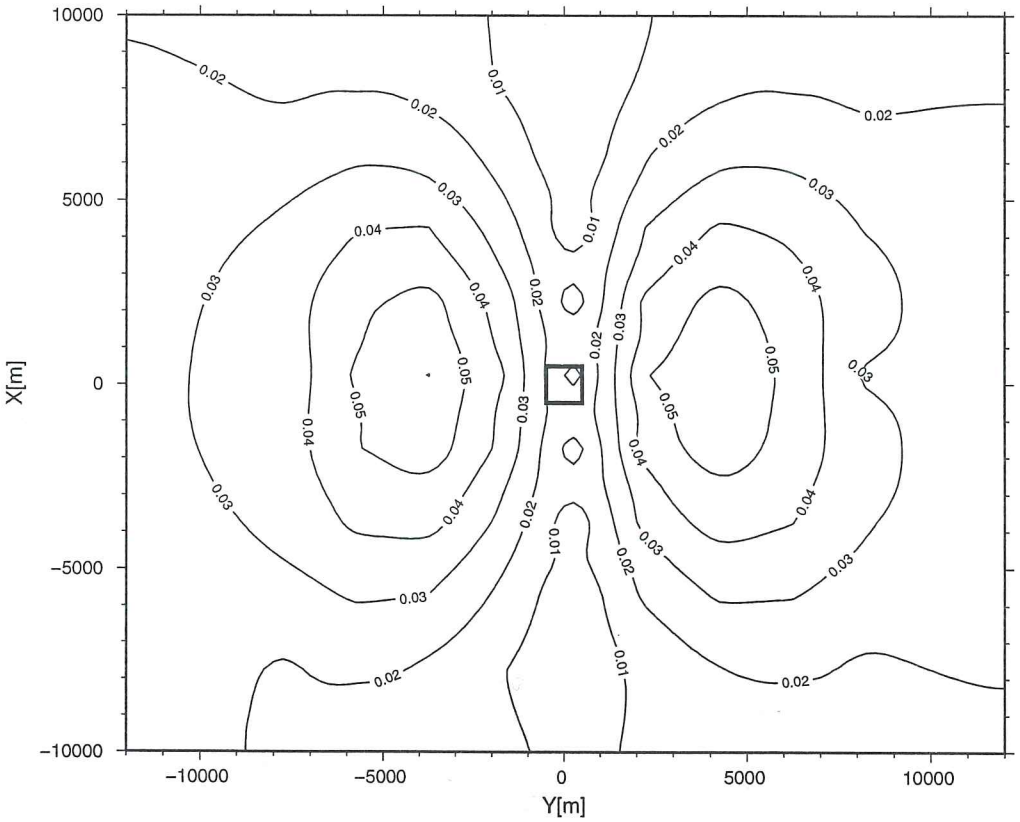

Figure-41. Spatial distribution of integrated significance of difference in **Ex** of a loop source (solid square) for non-connected and systems connected at 4km depth.

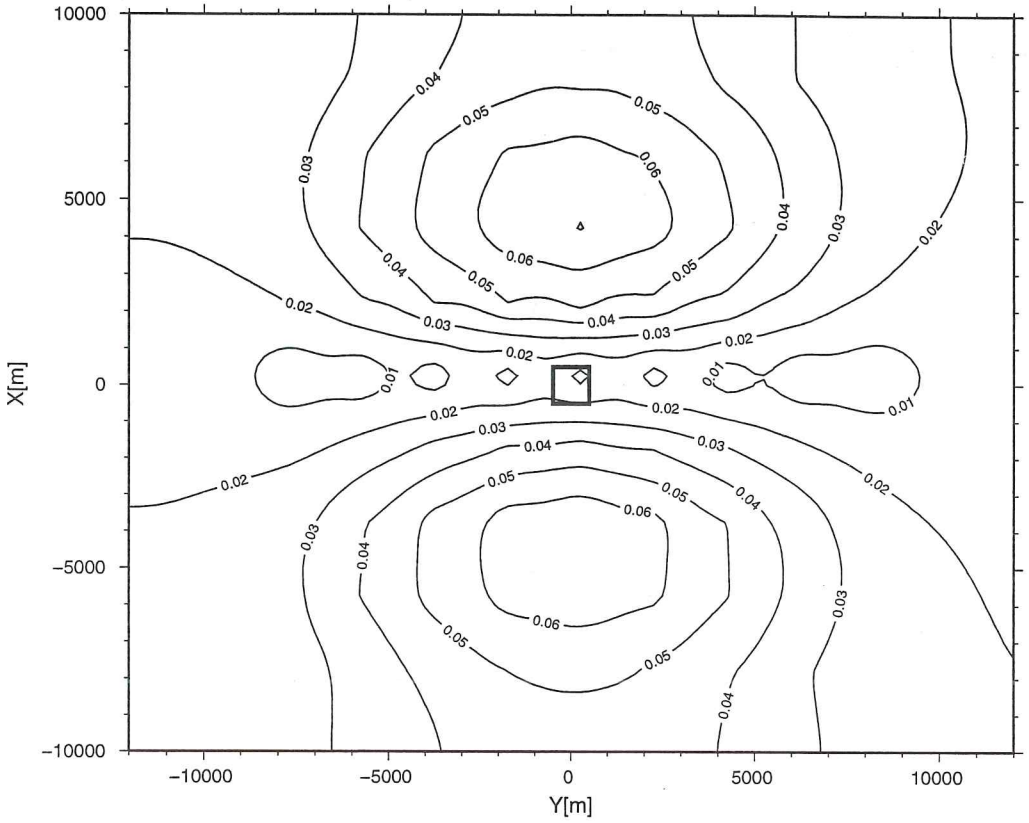

Figure-42. Spatial distribution of integrated significance of difference in **Ey** of a loop source (solid square) for non-connected and systems connected at 4km depth.

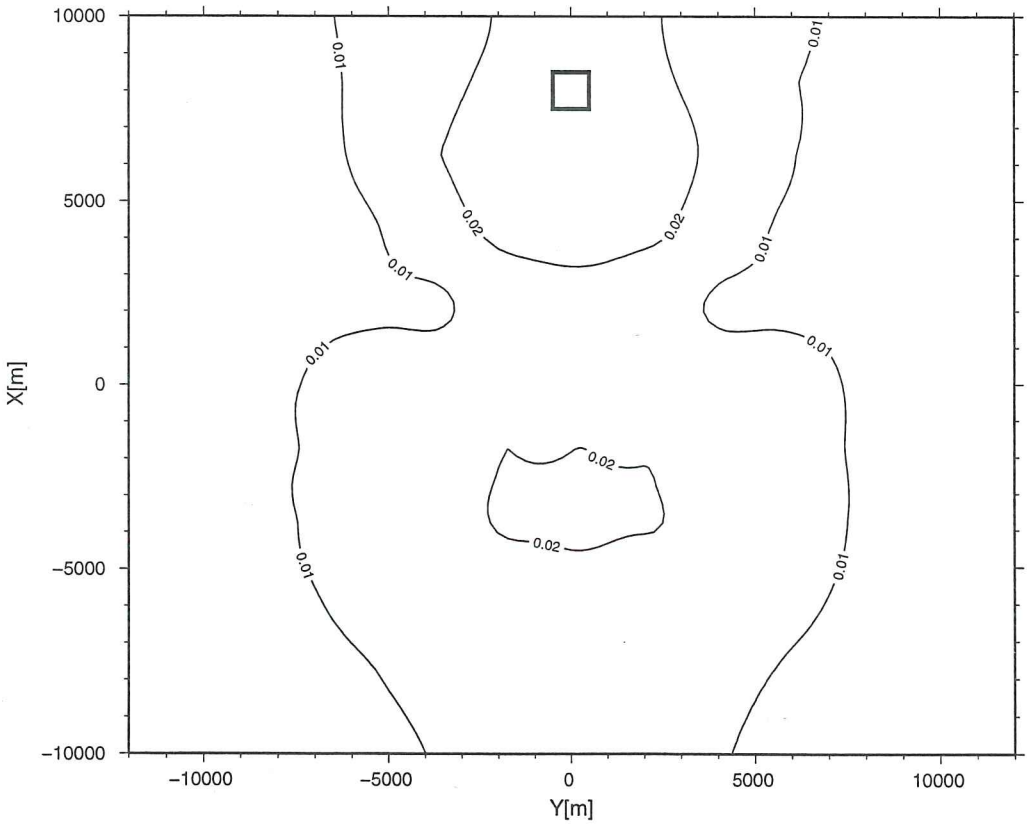

Figure-43. Spatial distribution of integrated significance of difference in **dBz/dt** of a loop source, 8km off axis, for non-connected and systems connected at 4km depth.

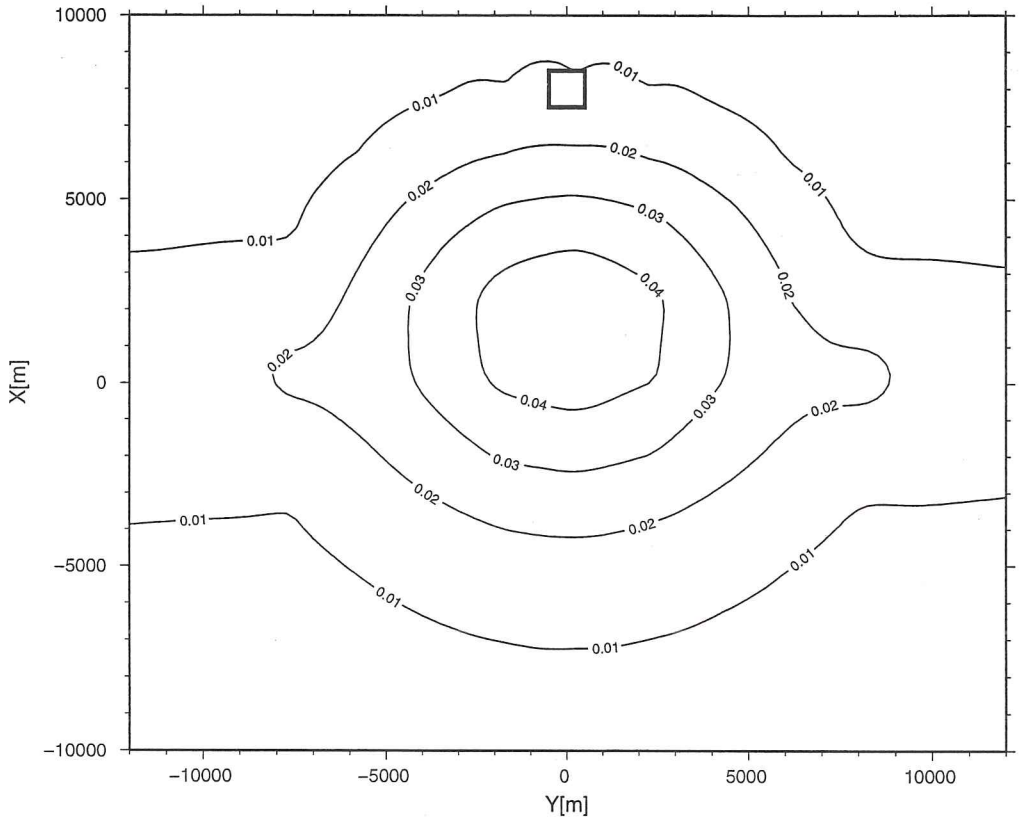

Figure-44. Spatial distribution of integrated significance of difference in **dBx/dt** of a loop source, 8km off axis, for non-connected and systems connected at 4km depth.

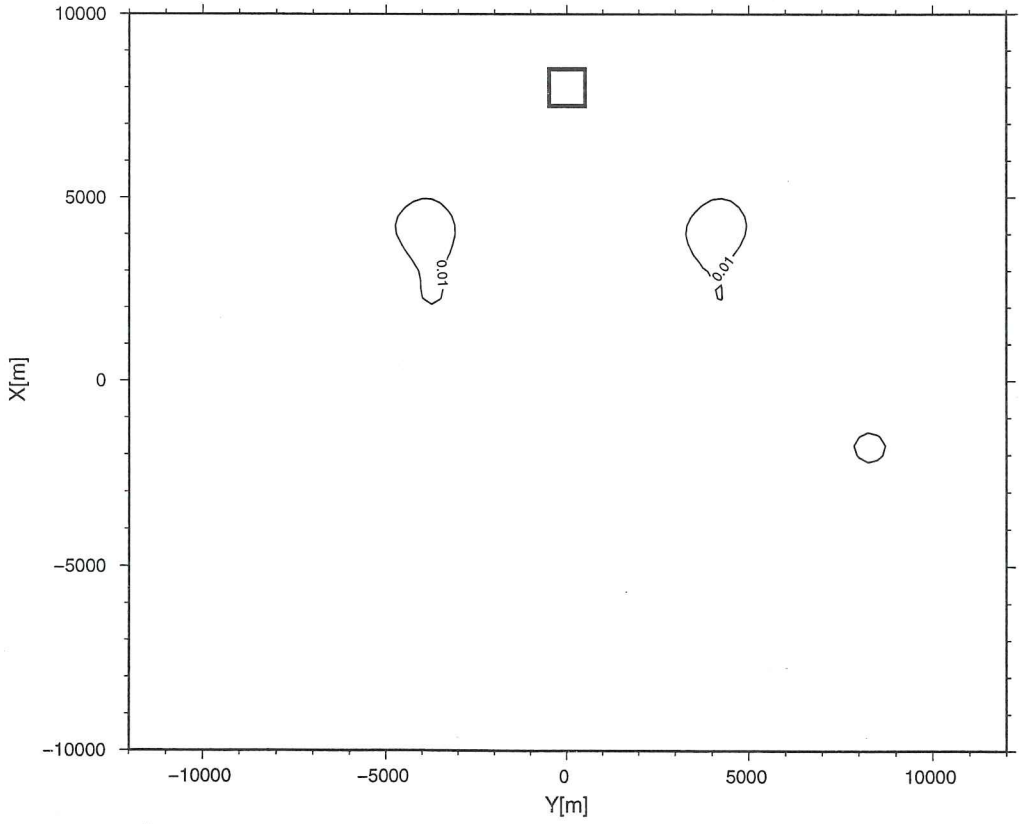

Figure-45. Spatial distribution of integrated significance of difference in **dBy/dt** of a loop source, 8km off axis, for non-connected and systems connected at 4km depth.

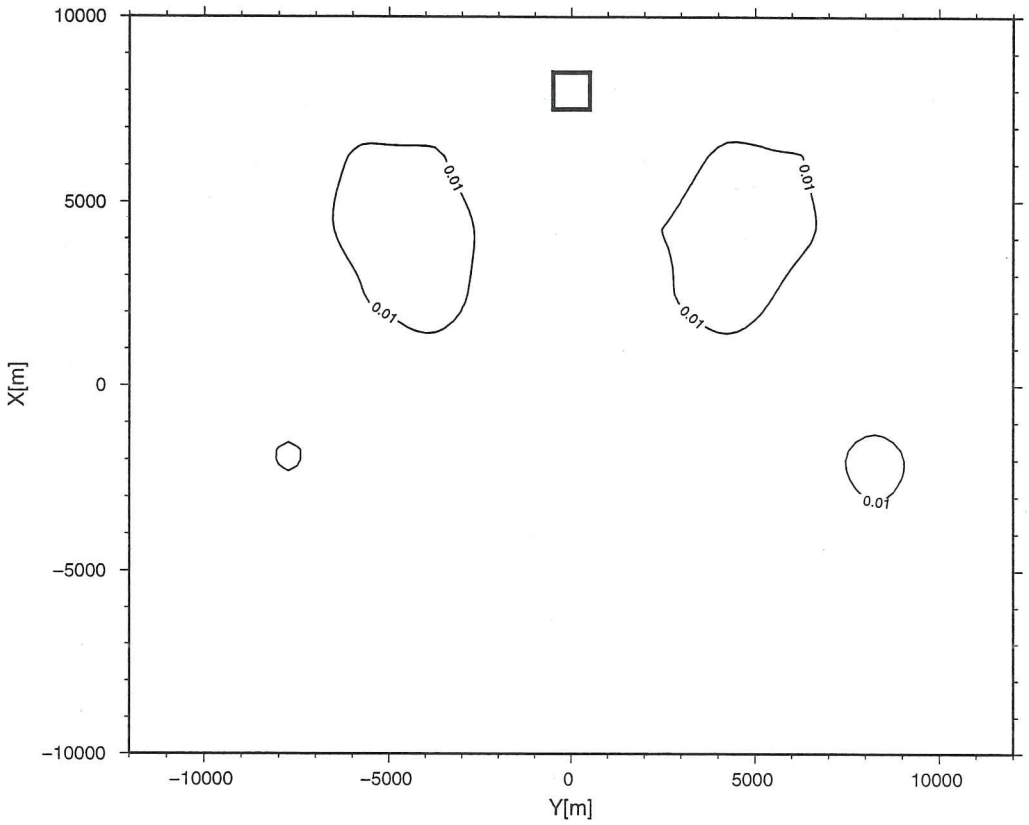

Figure-46. Spatial distribution of integrated significance of difference in **Ex** of a loop source, 8km off axis, for non-connected and systems connected at 4km depth.

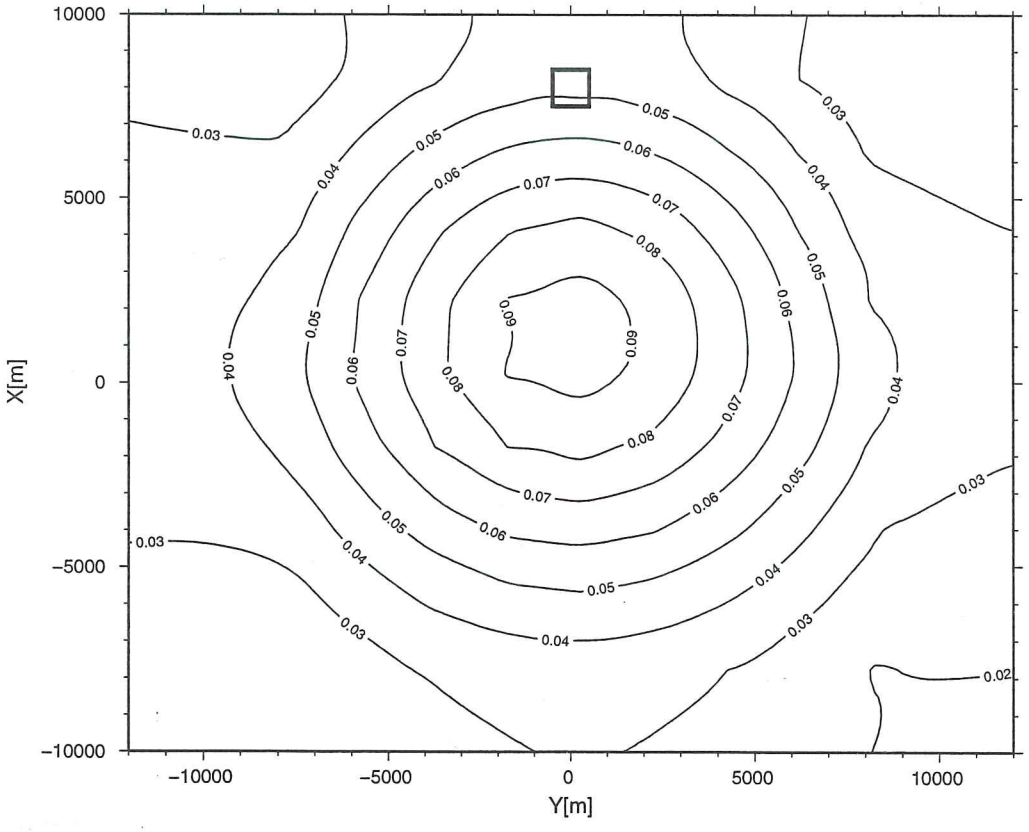

Figure-47. Spatial distribution of integrated significance of difference in **Ey** of a loop source, 8km off axis, for non-connected and systems connected at 4km depth.

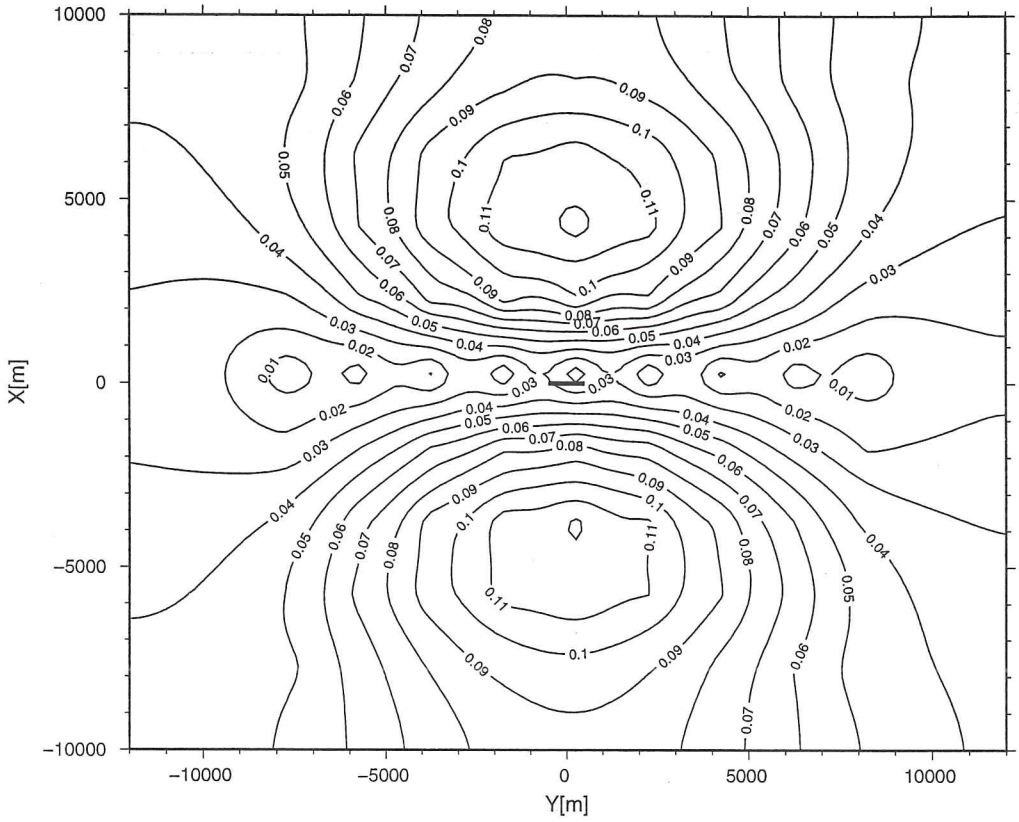

Figure-48. Spatial distribution of integrated significance of difference in **dBz/dt** of a y-dipole source on axis (solid line) for non-connected and systems connected at 4km depth.

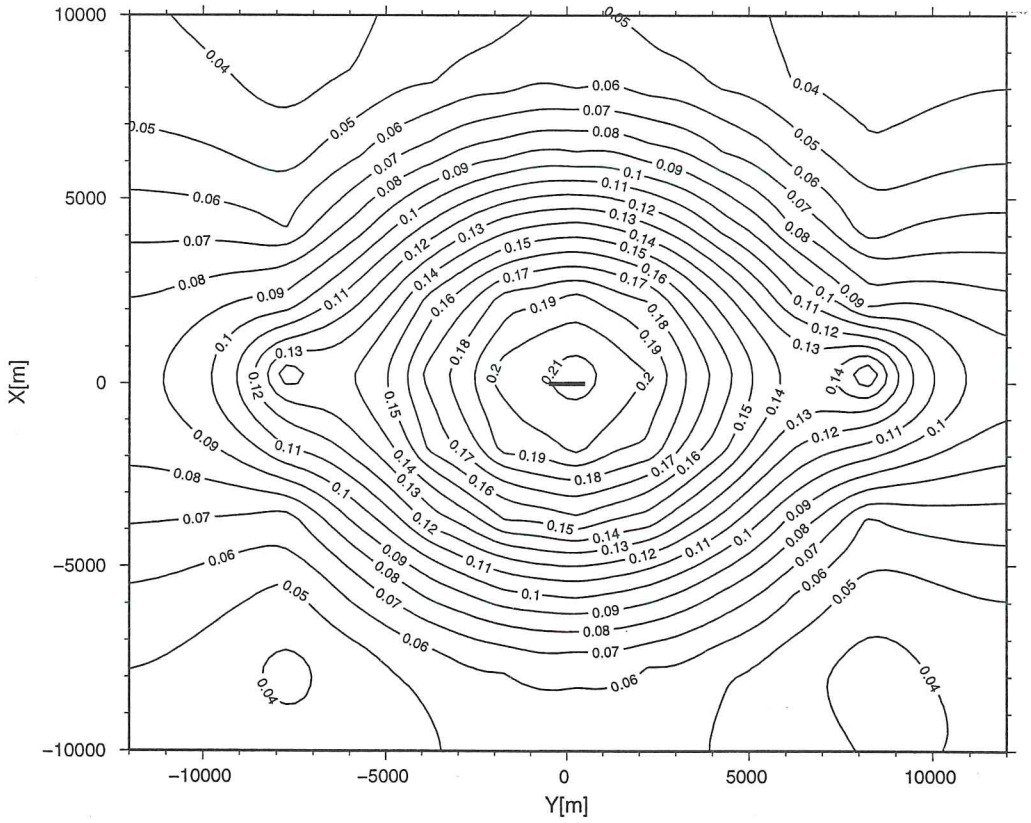

Figure-49. Spatial distribution of integrated significance of difference in **dBx/dt** of a y-dipole source on axis (solid line) for non-connected and systems connected at 4km depth.

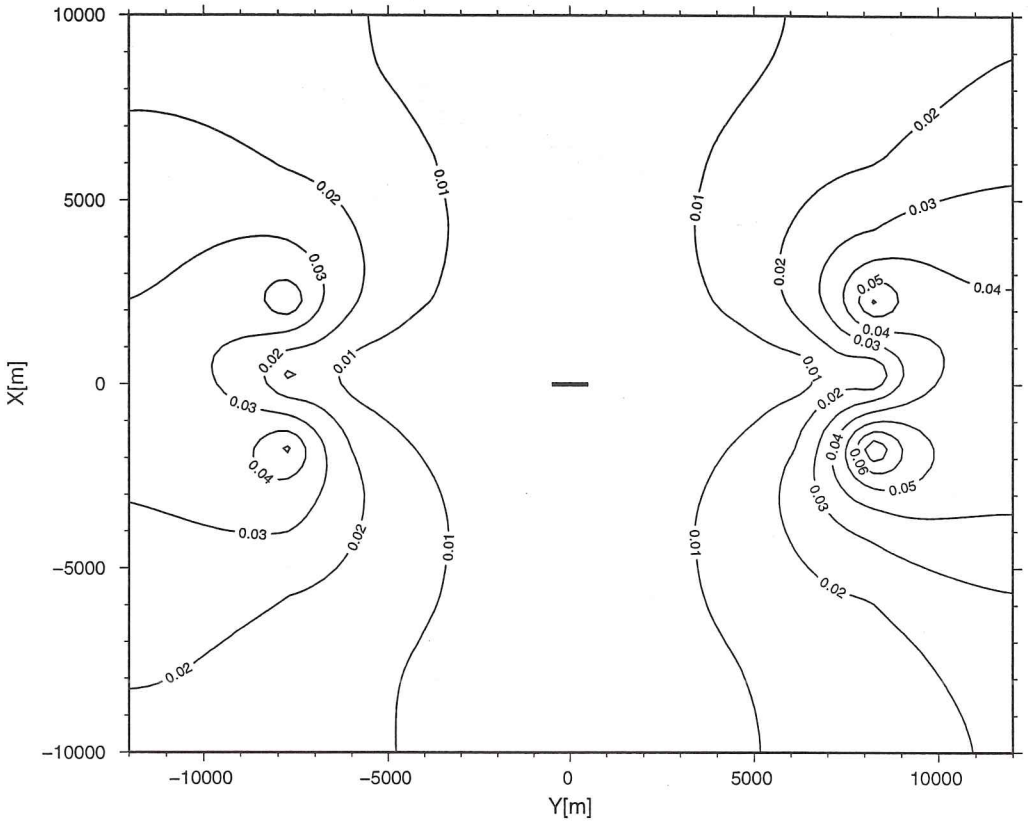

Figure-50. Spatial distribution of integrated significance of difference in **dBy/dt** of a y-dipole source on axis (solid line) for non-connected and systems connected at 4km depth.

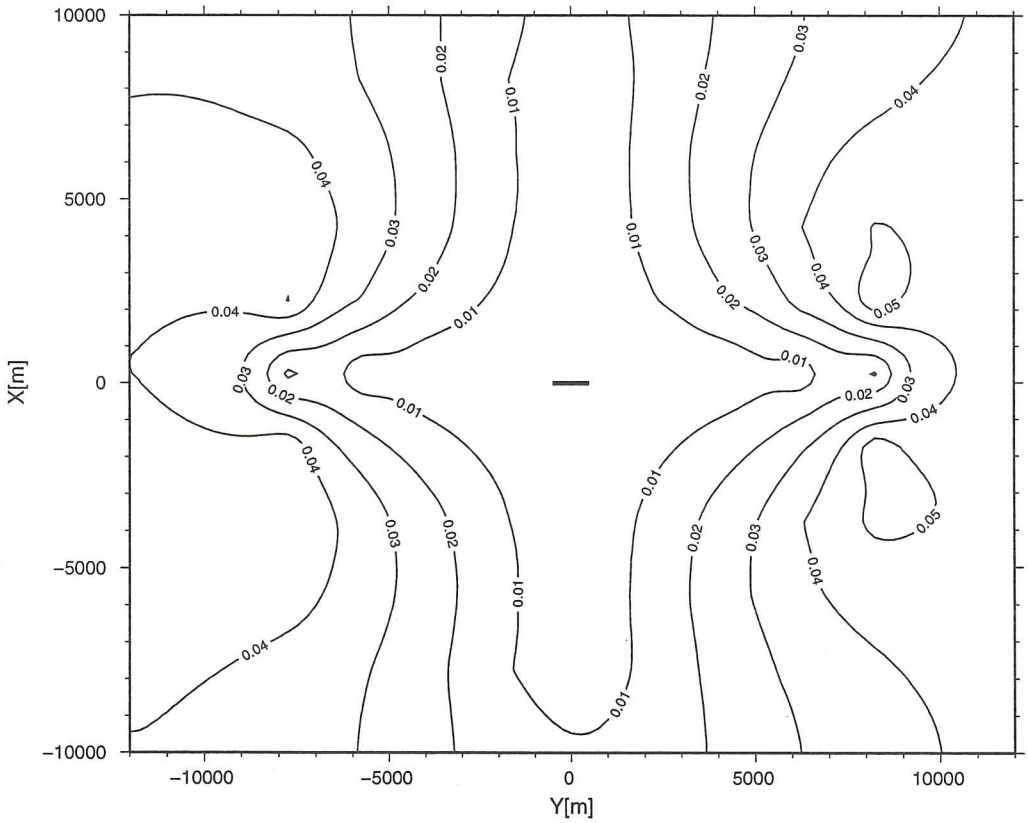

Figure-51. Spatial distribution of integrated significance of difference in **Ex** of a y-dipole source on axis for (solid line) non-connected and systems connected at 4km depth.

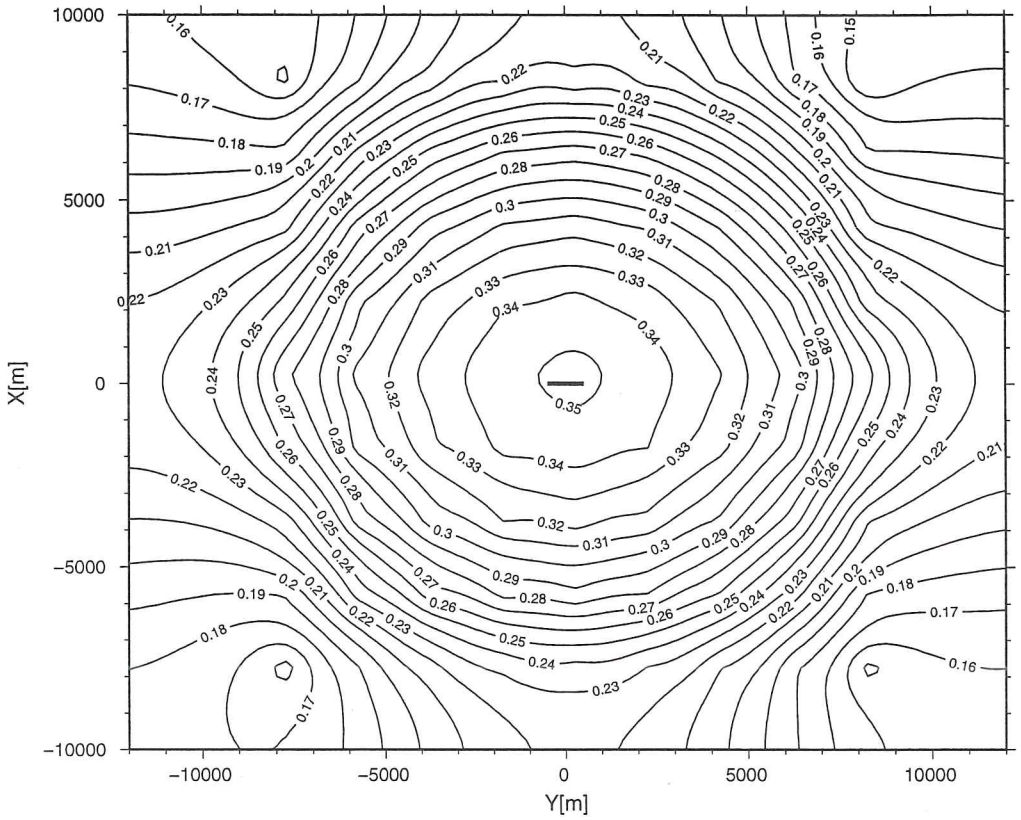

Figure-52. Spatial distribution of integrated significance of difference in **Ey** of a y-dipole source on axis (solid line) for non-connected and systems connected at 4km depth.

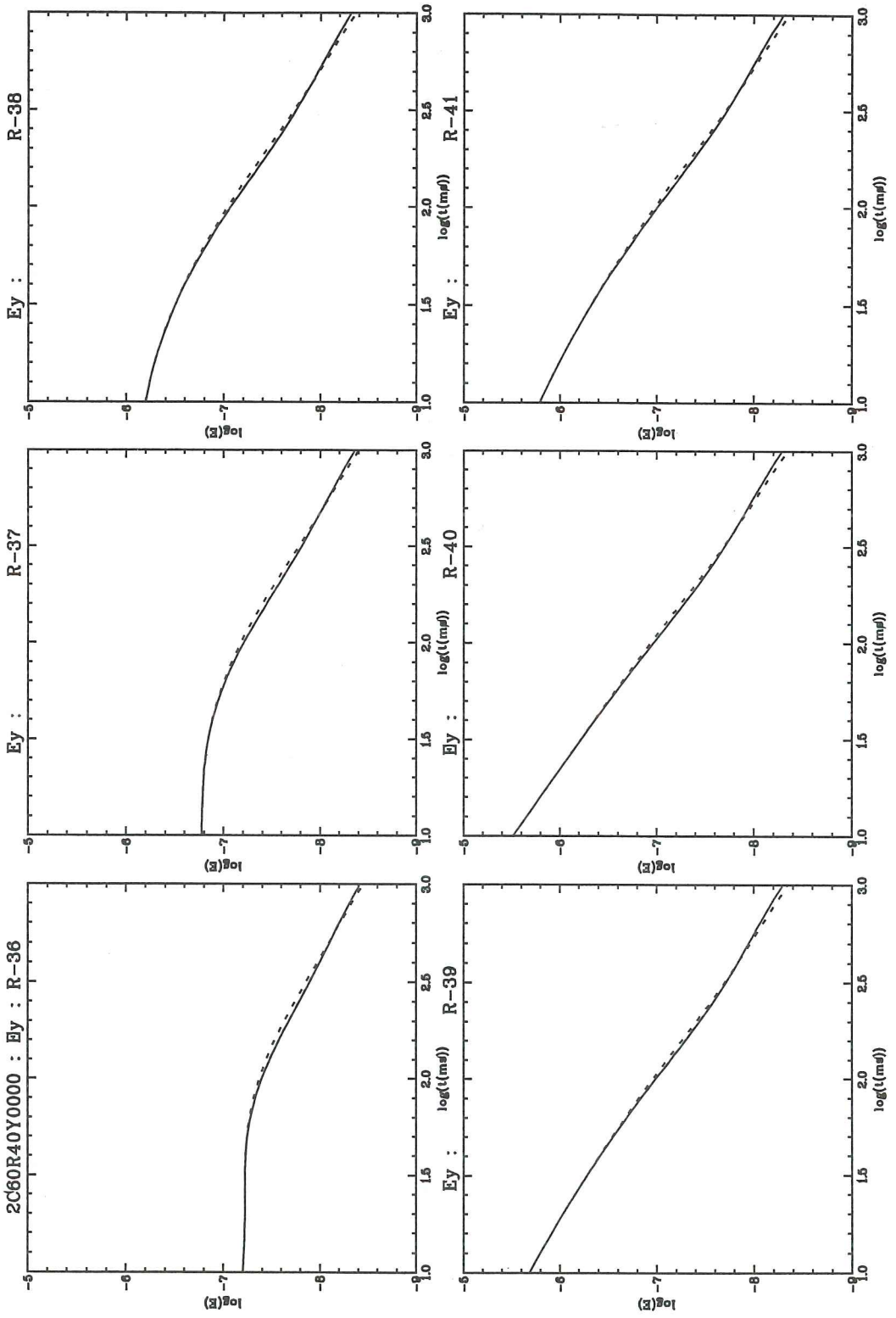

Figure-53. Calculated Ey responses for non-connected (dashed lines) and connected (solid lines) geothermal systems at 4km depth (see model on fig.-15). The source is a 1km grounded dipole along the axis of the volcanic zone, centrally between the systems. The receivers (36 through 41) are on a profile perpendicular to the volcanic zone (see fig.-35).

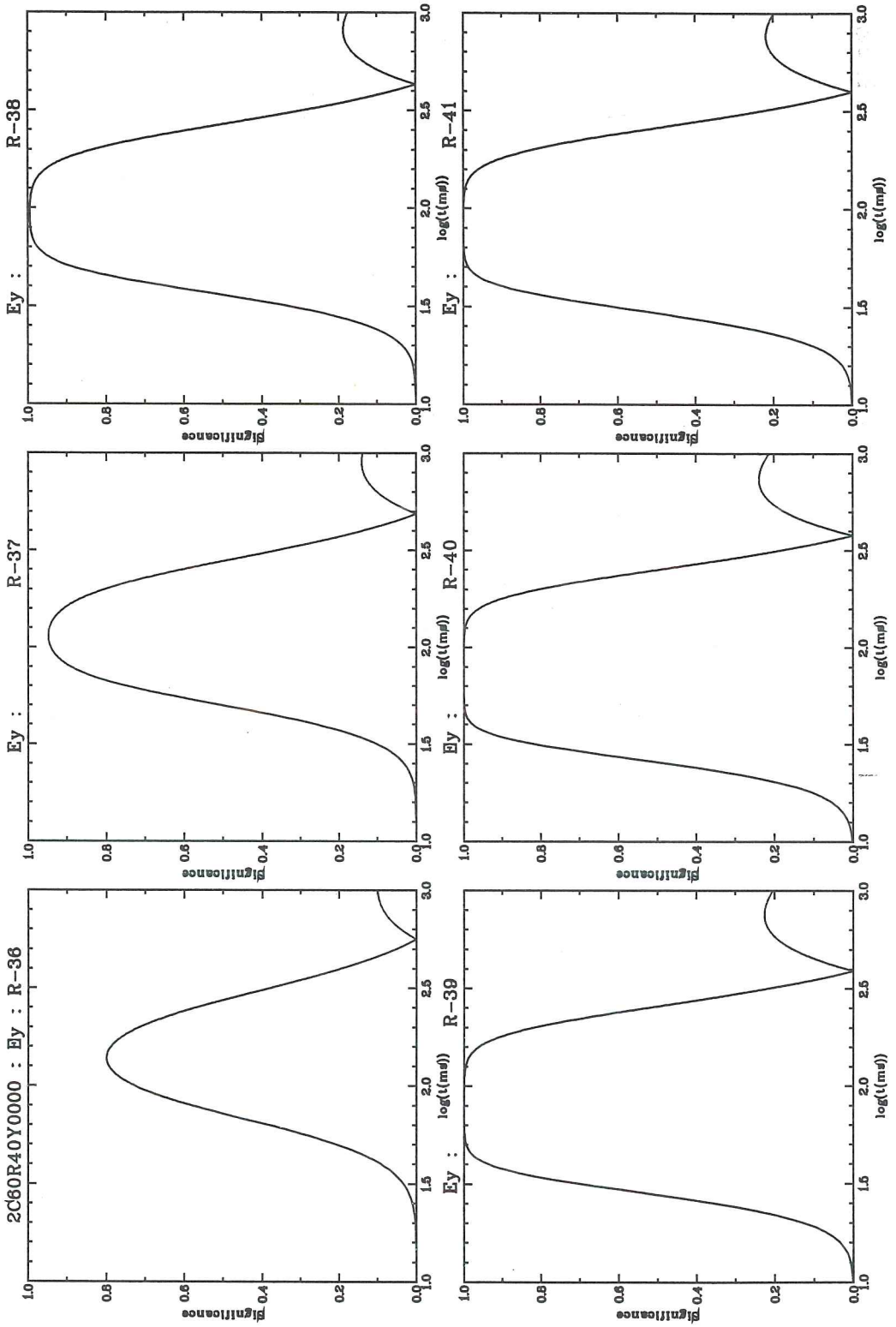

Figure-54. The significance of the difference in the "connected" and "non-connected" responses on fig.-53, at different times after the source turn-off.

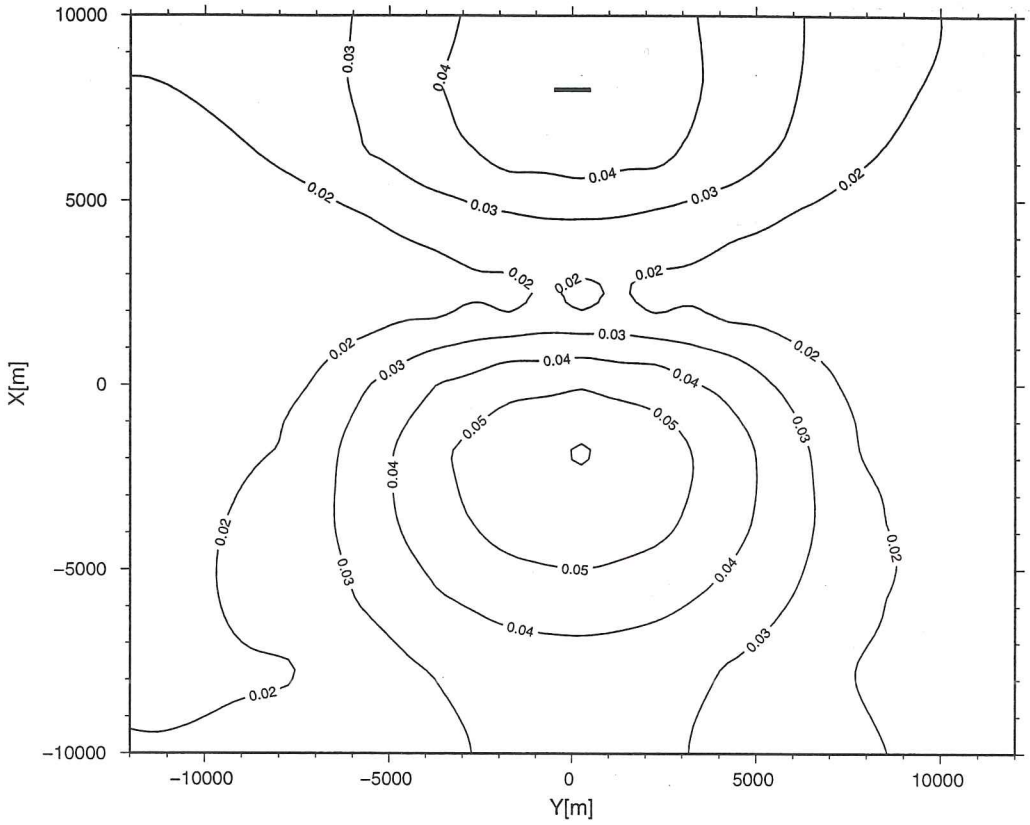

Figure-55. Spatial distribution of integrated significance of difference in **dBz/dt** of a y-dipole source 8km off axis (solid line) for non-connected and systems connected at 4km depth.

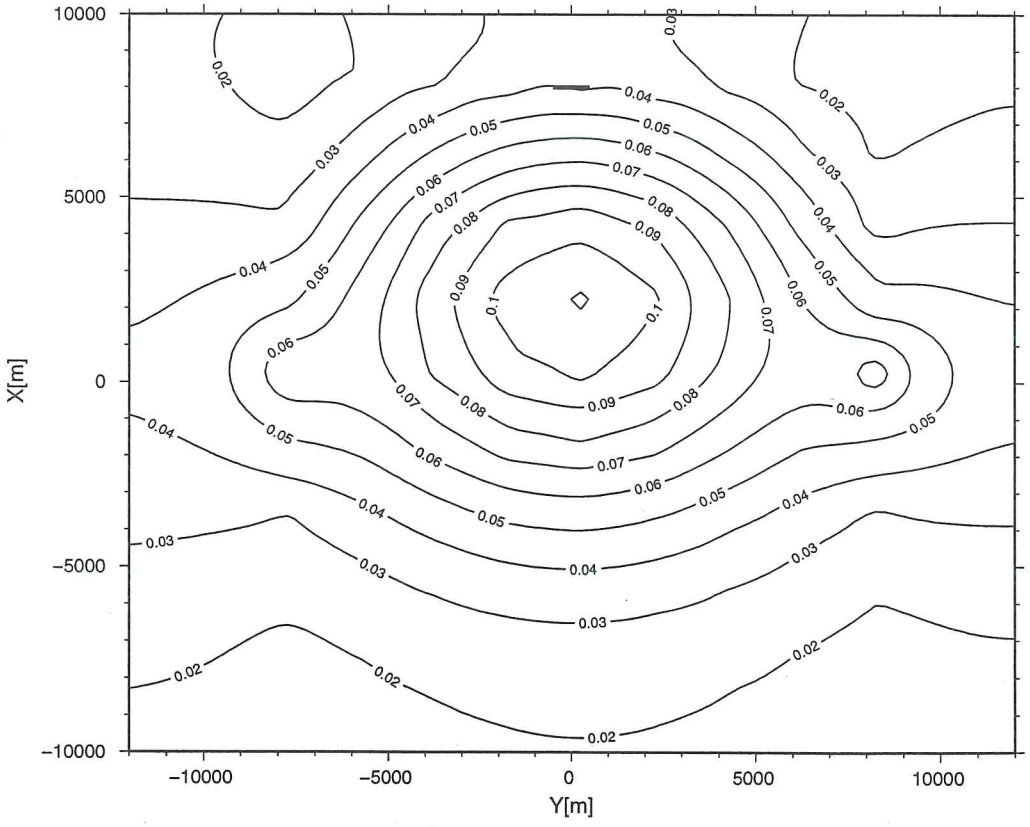

Figure-56. Spatial distribution of integrated significance of difference in **dBx/dt** of a y-dipole source 8km off axis (solid line) for non-connected and systems connected at 4km depth.

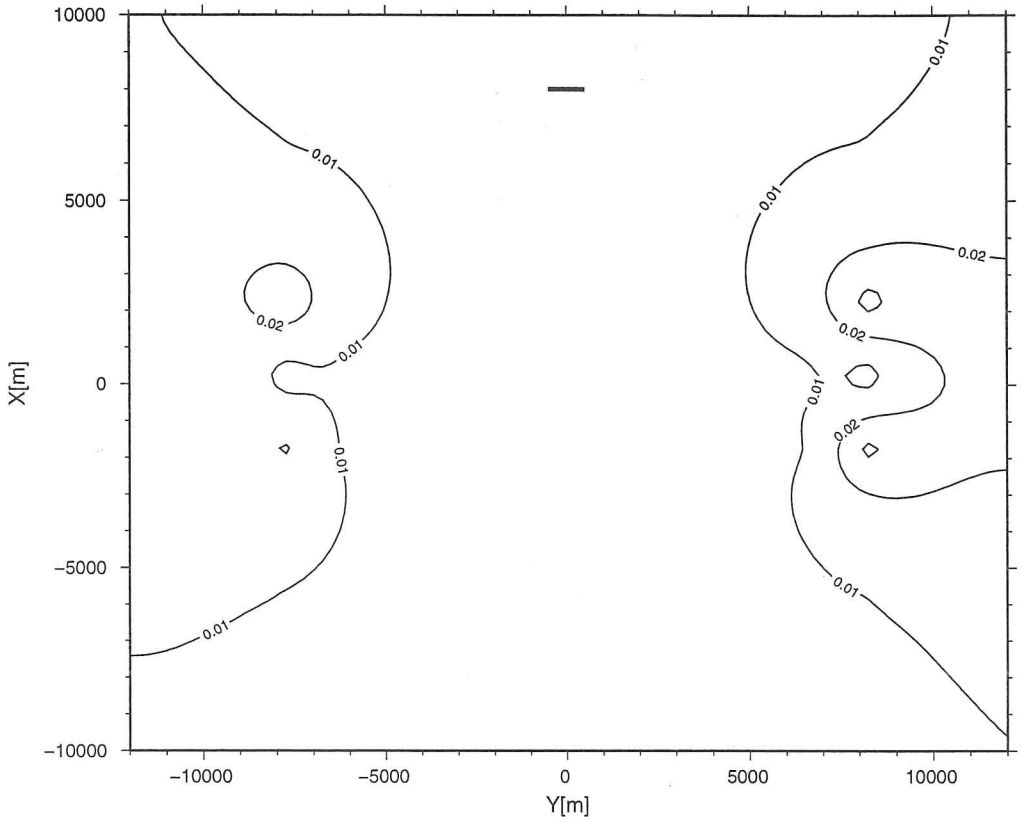

Figure-57. Spatial distribution of integrated significance of difference in **dBy/dt** of a y-dipole source 8km off axis for non-connected and systems connected at 4km depth.

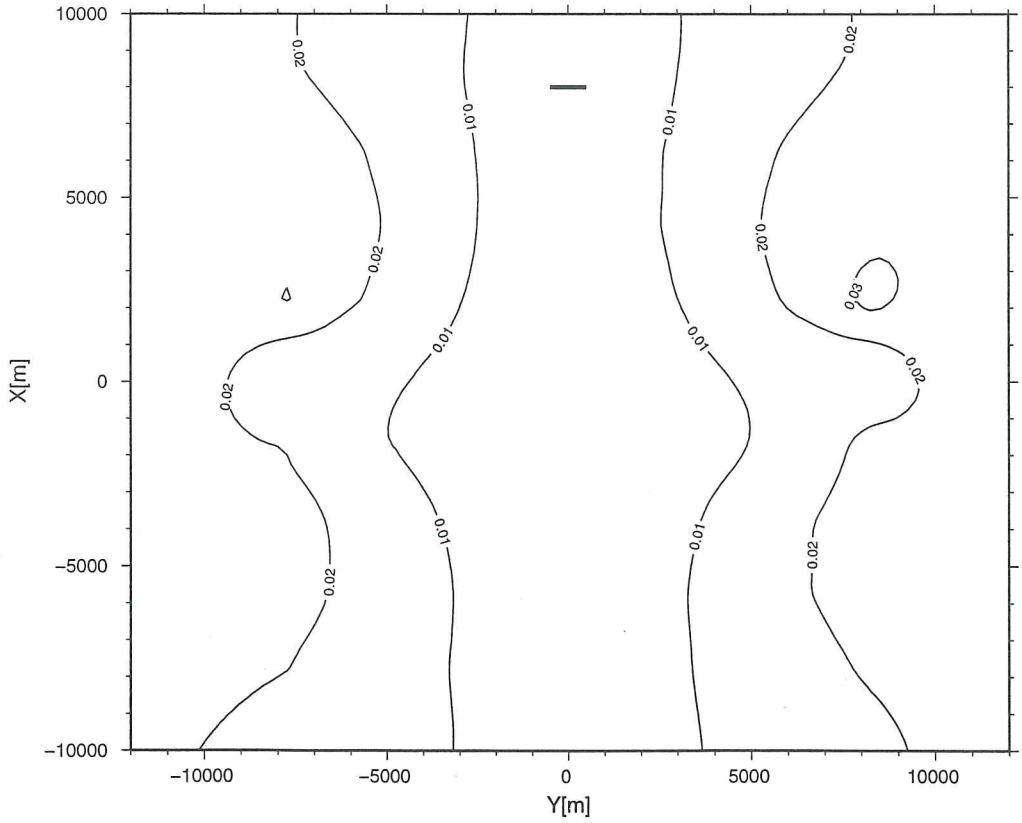

Figure-58. Spatial distribution of integrated significance of difference in **Ex** of a y-dipole source 8km off axis for non-connected and systems connected at 4km depth.

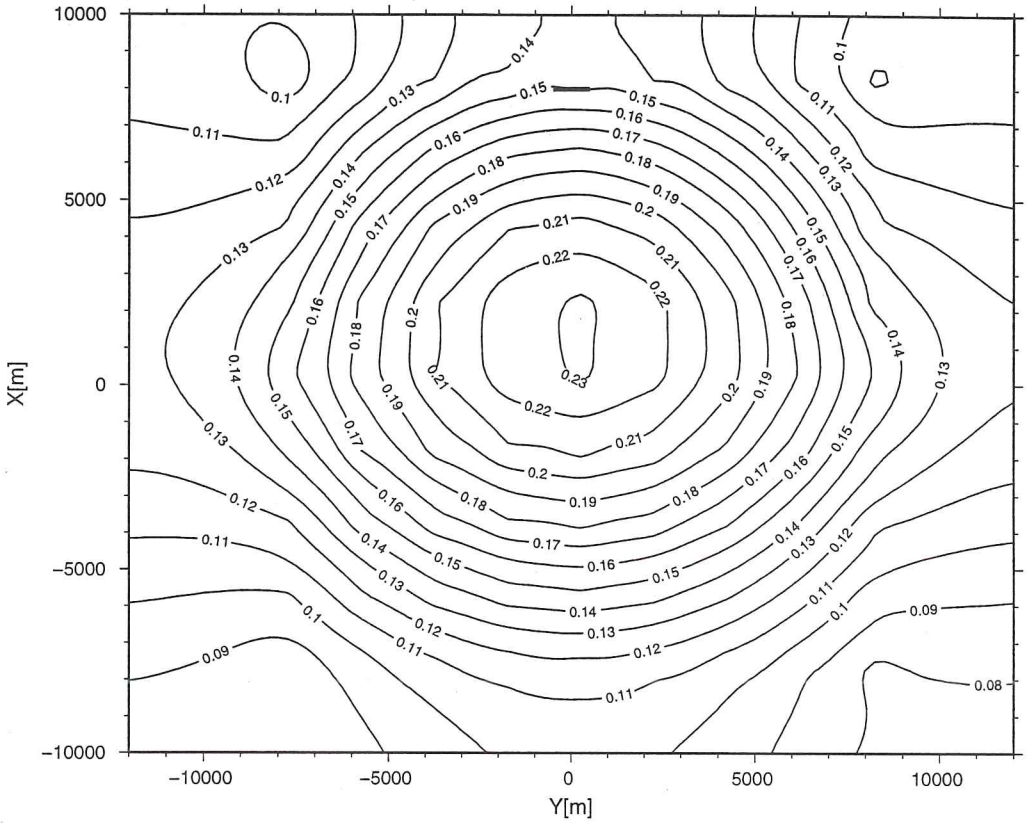

Figure-59. Spatial distribution of integrated significance of difference in **Ey** of a y-dipole source 8km off axis for non-connected and systems connected at 4km depth.

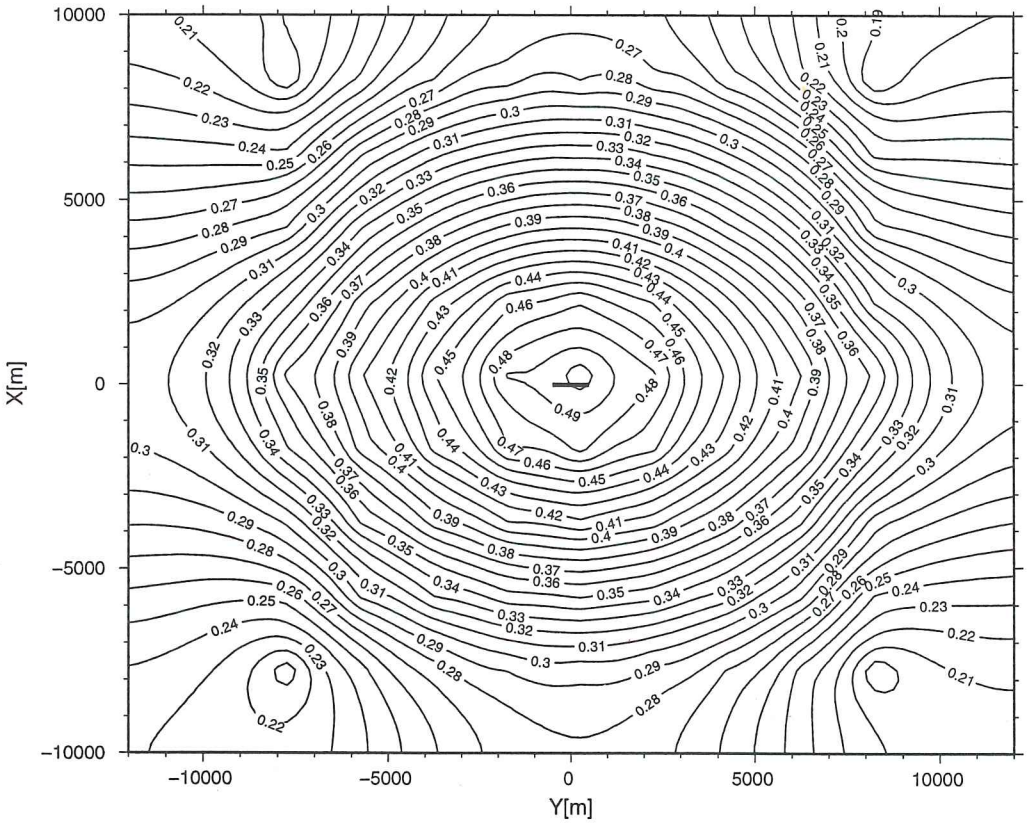

Figure-60. Spatial distribution of integrated significance of difference in **Ey** of a y-dipole source on axis for non-connected and systems connected at 3km depth.

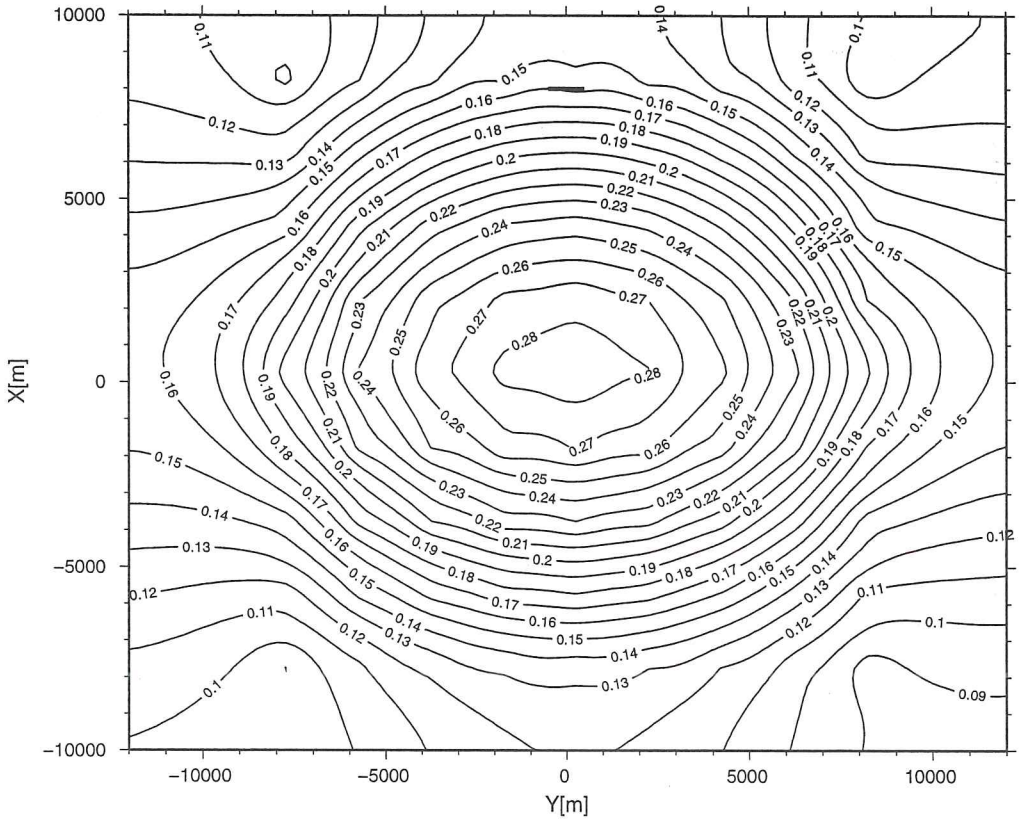

Figure-61. Spatial distribution of integrated significance of difference in **Ey** of a y-dipole source 8km off axis for non-connected and systems connected at 3km depth.

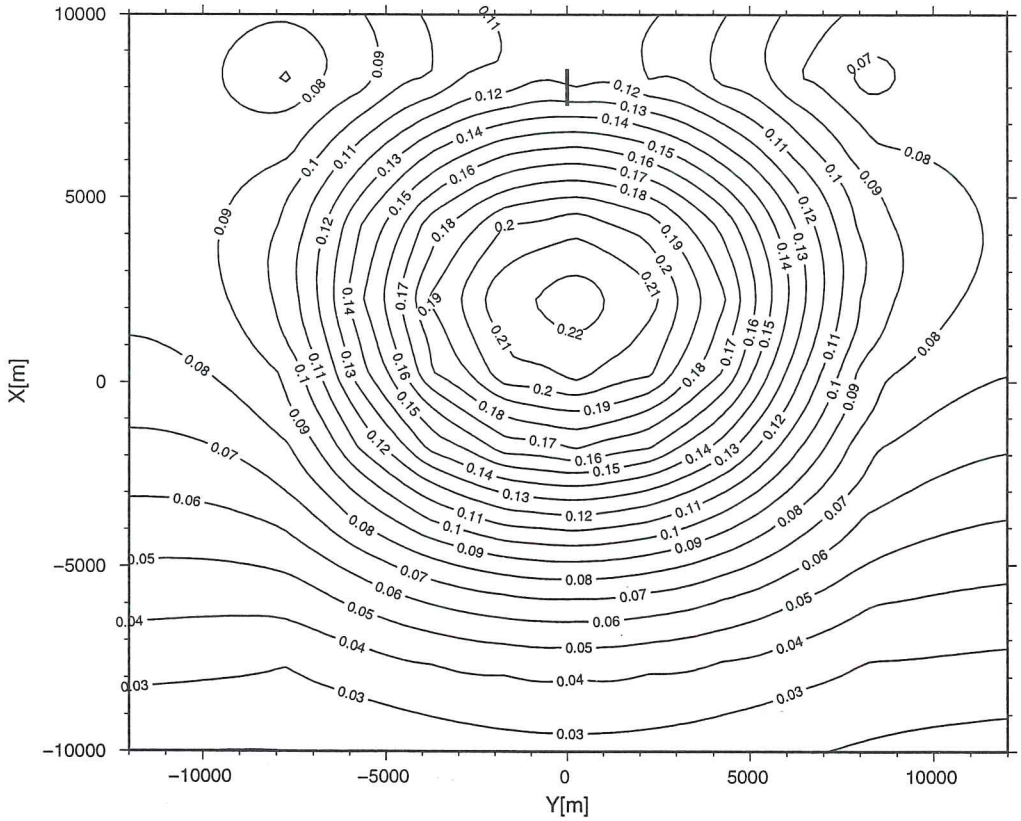

Figure-62. Spatial distribution of integrated significance of difference in **Ex** of a x-dipole source 8km of axis for non-connected and systems connected at 3km depth.

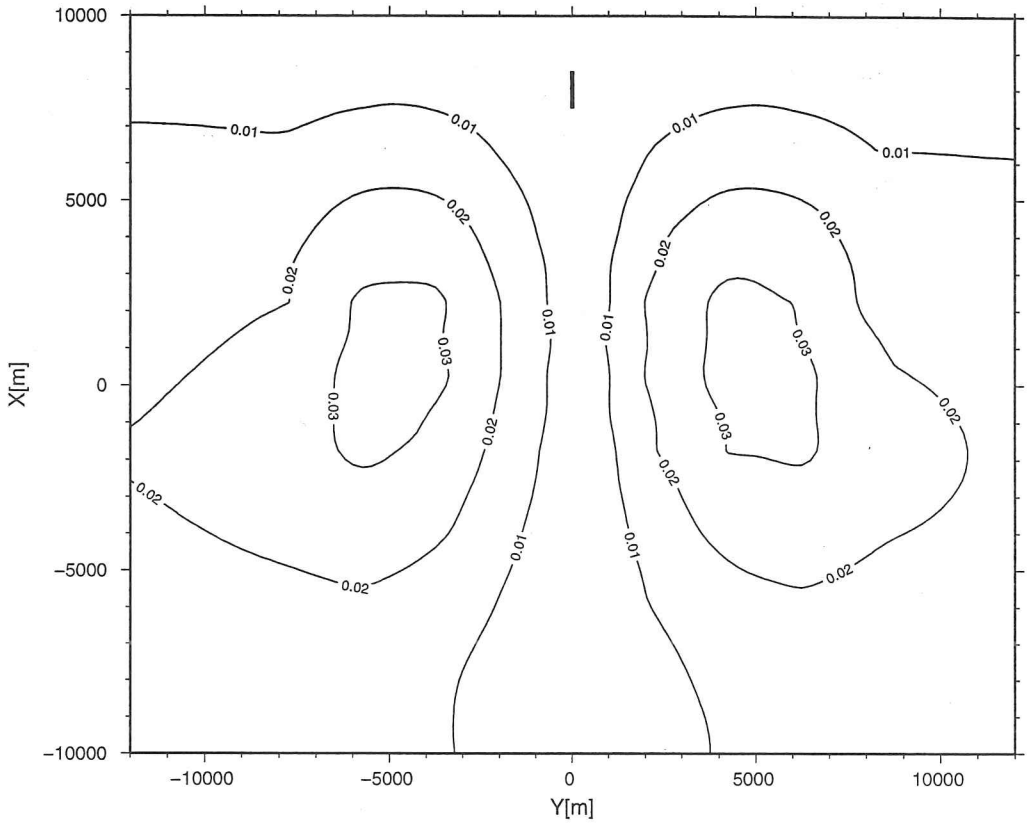

Figure-63. Spatial distribution of integrated significance of difference in **Ex** of a x-dipole source 8km of axis for non-connected and systems connected at 3km depth.

4.2.3 Sensitivity of the MT method to the defined models

The fundamental difference between TEM methods and MT is that, in the former, the electro-magnetic field in the earth is produced by a controlled source, but in the MT, the source field is the time varying earths electro-magnetic field. In MT, it is assumed that the source field can be considered as superposition of plane waves of different frequencies and polarisation. The source field therefore excites the whole earth, where as in the TEM method the source field produces strong excitations close to the source and decreasing away from it. This means that in the TEM method, the sensitivity is dependent on the geometry of the source (source type) and the receiver type as well as their orientation and separation. A study of the intrinsic sensitivity of different TEM measurement setups is of help for field survey design and understanding of the measured responses. In standard MT all the five field components (Bx, By, Bz, Ex and Ey) are measured and the sensitivity to resistivity variations at a given place in the earth is mainly dependent on the distance to the receiver and hence no separate study was made of the intrinsic sensitivity of the MT method.

The sensitivity of the MT method to the defined test models was performed. The response of the models was calculated using the 3-D finite differences forward algorithm by Mackie and Madden (1993), and modified by Booker and Handong (1999). The MT modelling code assumes somewhat different coordinate system from the one used for the TEM modelling. Following Mackie's coordinate system definition, x is measured positive to East (to the right), y is positive to South (back to front) and z is positive downwards. This means that the x- and y-axis are interchanged between the TEM and MT models. The volcanic zone with the geothermal systems is along the x-axes (East-West) in the MT modelling but along the y-axis in the coordinate system used in the TEM modelling. The finite difference discretization grid was kept as close as possible to the one used in the TEM calculations in order to avoid possible discrepancies due to different gridding.

The response of the test models was calculated for 25 different sites in a regular grid with 4km spacings on the surface. The locations of the these sites are the same as the even numbered sites of every other receiver line perpendicular to the volcanic zone on figure 35. The receiver sites will here be identified by the same numbers as for the TEM (sites 0, 2, 4, 6, 8, 18, 20, 22, 24, 26, 36, 38, 40, 42, 44, 54, 56, 58, 60, 62, 72, 74, 76, 78 and 80 on figure 35). To compare the response of the different models the calculated field values in the frequency range of 1000 Hz to 0.1 Hz were converted to apparent resistivities and phases as well as magnetic transfer functions.

Figures 64 through 69 show the apparent resistivities (rho_a) and phases for two model pairs, that is for the models where the geothermal systems extend to the depth of 3km and and are either connected by a ridge with top at 2km and extending down to 3km or not connected (model pair 2C30R20 in the naming convention for the models) and the models where the geothermal systems extend to the depth of 6km and and are either connected by a ridge in the depth range of 4km to 6km or not connected (model pair 2C60R40). The figures show the calculated results for three of the TEM receiver locations ie. 04, 20 and 40 (for location see figure 35).

The transfer functions are presented as apparent resistivities and phases for all of the four elements of the impedance tensor (values for the non-connected case are red and black for the connected). The strongest changes when connecting the two geothermal systems are found for site 40, above the ridge in the middle, between the systems. For this location a comparison between responses for the model pair 2C30R20 (figure 66) shows clear differences in rho_a and especially in the phases for the XY- and YX-components (off-diagonal elements of the impedance tensor) between 0.1 seconds and 10 seconds (the XY-components are calculated from the ratio of the electric field parallel to the volcanic zone and the magnetic field perpendicular to it; the YX-components are calculated from the ratio of the electric field perpendicular to the volcanic zone and the magnetic field parallel to it). The rho_a values for the XX- and YY-components (diagonal elements of the impedance tensor) are at least six decades smaller then those of the off-diagonal elements. Thus the subsurface resistivity structure is seen as two-dimensional.

For sites 04 and 20 (figures 64 and 65) which are closer to one of the systems, the 3-D effects become stronger. This causes a rising of the XX- and YY-rho_a values of four to five decades. They are, however, still some decades lower then those of the XY- and YX-components. At these receiver locations, the difference between the apparent resistivities and phases from the off-diagonal elements for models with and without a connection is much smaller than for site 40.

Similar effects to those described above are found when comparing the responses for the model pair 2C60R40 (see figures 67 to 69). Because of the larger lateral and vertical extension of the geothermal systems and due to grater depth to the ridge, the differences are smaller than for the 2C30R20 model pair, and they are shifted slightly to longer periods. At receiver site 04 the model response is nearly identical for connected and non-connected model. The difference is, as in the case of the model pair 2C30R20, biggest at site 40 and is most pronounced in the phase.

On figures 70 to 73, the real parts of the magnetic transfer functions (the coefficients relating the vertical component of the magnetic field to its horizontal components) are shown as induction arrows for all the 25 sites for which the response was calculated. The convention is such that the arrows should point away from a good conductor. The induction arrows are presented for the two model pair 2C60R40 and for the periods 0.2 seconds and 2.0 seconds (5 and 0.5Hz). For 0.2 seconds (figures 70 and 72), the induction arrows are nearly identical for all the four models. The penetration depth at 0.2 seconds does not suffice to see any differences between the models.

The strongest changes are seen at the period of 2.0 seconds and for the model pair 2C30R20 (figure 71). Both the length and direction of the arrows at nearly all the sites, show a clear dependency on whether the systems are connected by the conductor at depth or not. The results for the model pair 2C60R40 also show some consistent differences in the induction arrows for 2.0 seconds (see figure 73). The difference is, however, smaller because the large geothermal systems cause strong effects themselves and the effect of the connection is relatively small.

The model studies show, that it should be possible to see, by MT soundings, whether the two geothermal systems are connected at depth or not. For all models considered, differences were found in the transfer functions, both in apparent resistivity and phase curves as well as for induction arrows. The strength of the differences is dependent on the sounding site location. The largest difference in apparent resistivity and phase is seen right above the connecting ridge, in between the geothermal systems. The differences decrease near the systems and also with increasing distance from the assumed connection. But, in contrast to the apparent resistivities and phases, the strongest differences for the induction arrows are found outside the volcanic zone. As the geothermal systems extend deeper and their base size increases, the response of the systems them selves tends to mask the response of a connecting ridge.

A study of the significance of the differences in the responses of connected and non-connected models is more difficult for the MT method than fore the TEM method, because the natural signal is the primary signal for the MT. Such a study can only be performed systematically for large set of MT soundings and has not been performed in this study. An estimate of the uncertainty in the apparent resistivity and phase values, based on existing MT data from Iceland, indicates that, for long periods, the uncertainty in the apparent resistivity is at least about a factor of two and that the uncertainty in the phase is about +/- 5 degrees. This means that the differences for connections at the depth of 4km are hardly detectable in practice by MT.

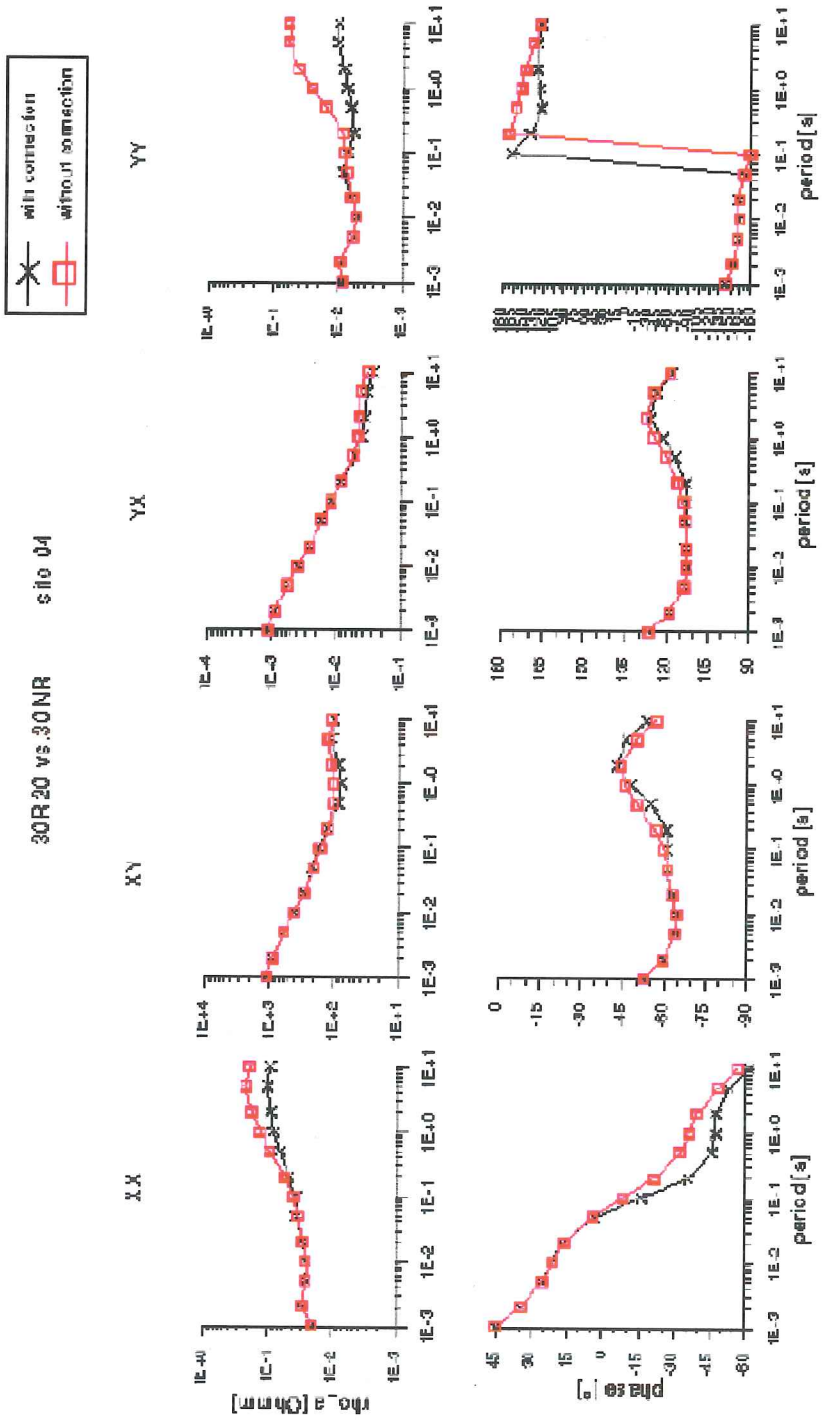

Figure-64. Calculated apparent resistivities and phases for an MT-sounding at site 04 (see fig.-35) for non-connected systems (red) and systems connected at 2km depth (black).

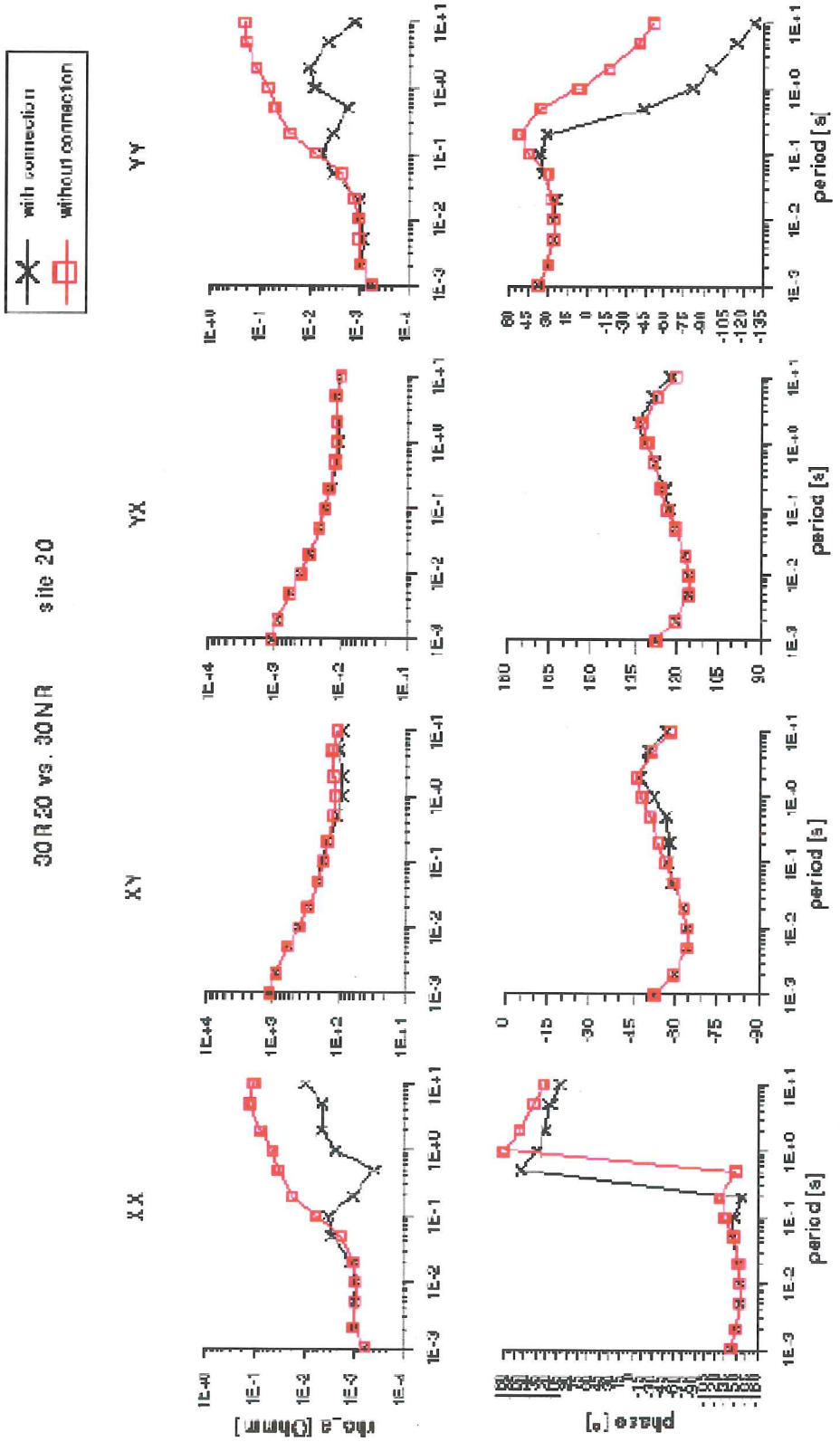

Figure-65. Calculated apparent resistivities and phases for an MT-sounding at site 20 (see fig.-35) for non-connected systems (red) and systems connected at 2km depth (black).

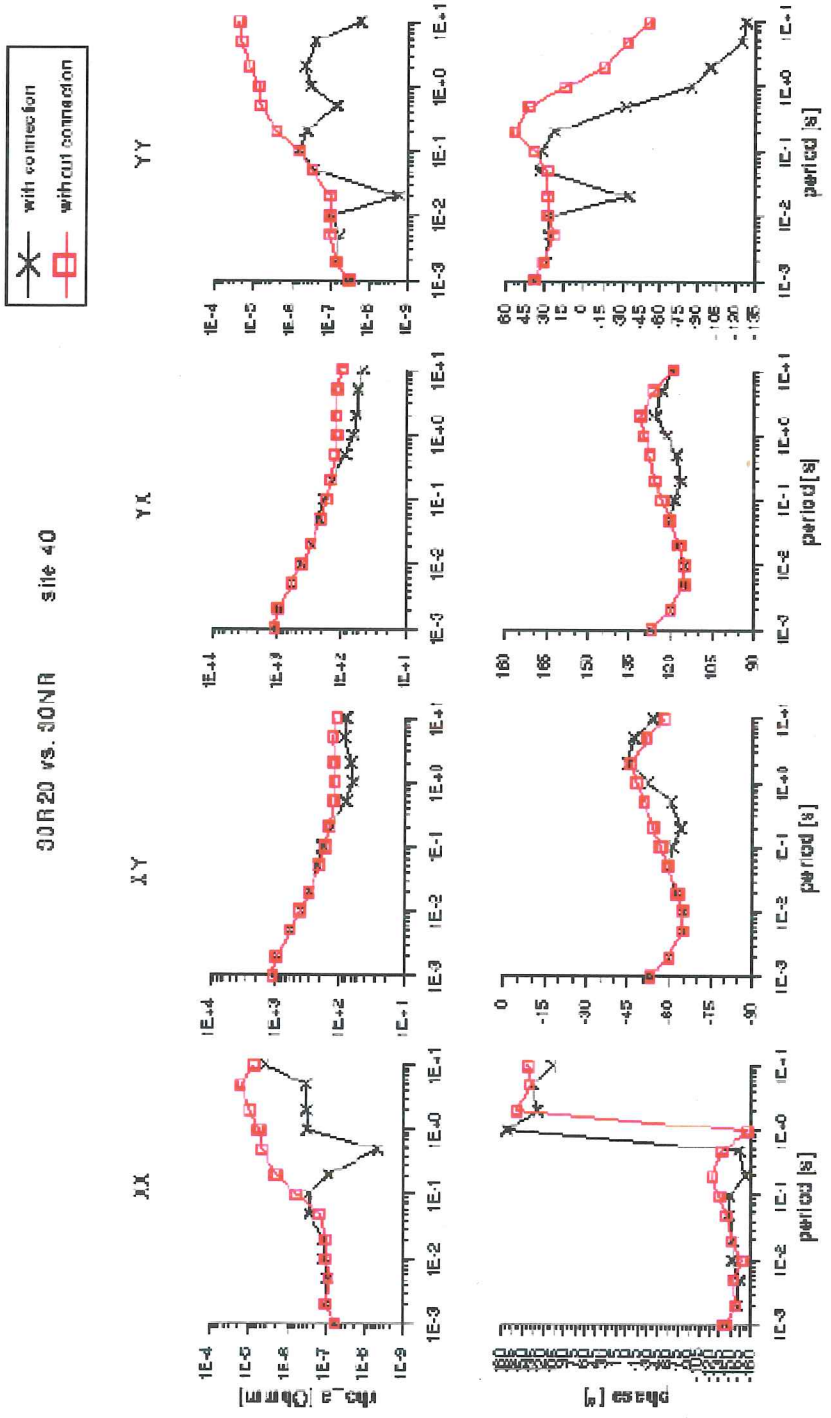

Figure-66. Calculated apparent resistivities and phases for an MT-sounding at site 40 (see fig.-35) for non-connected systems (red) and systems connected at 2km depth (black).

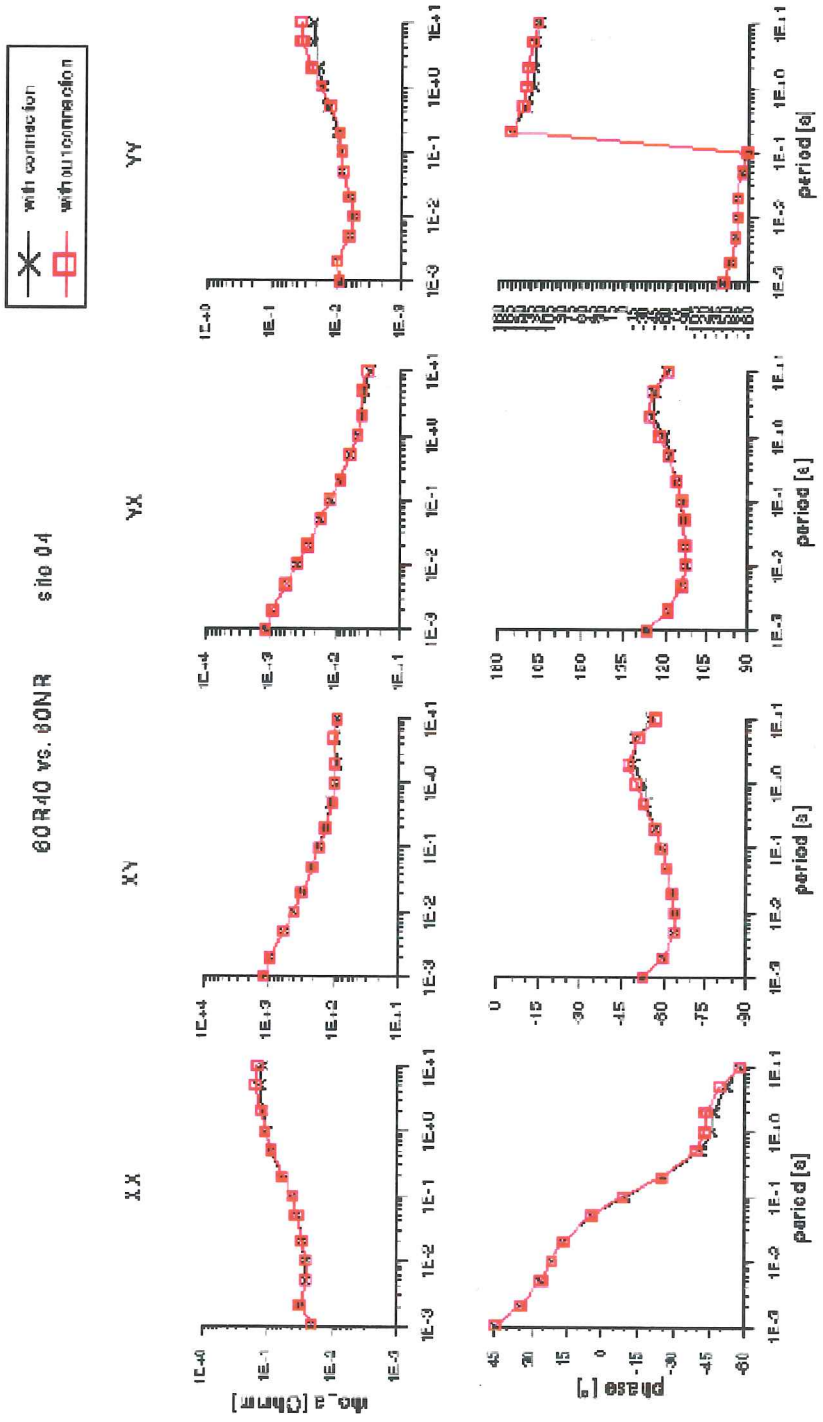

Figure-67. Calculated apparent resistivities and phases for an MT-sounding at site 04 (see fig.-35) for non-connected systems (red) and systems connected at 4km depth (black).

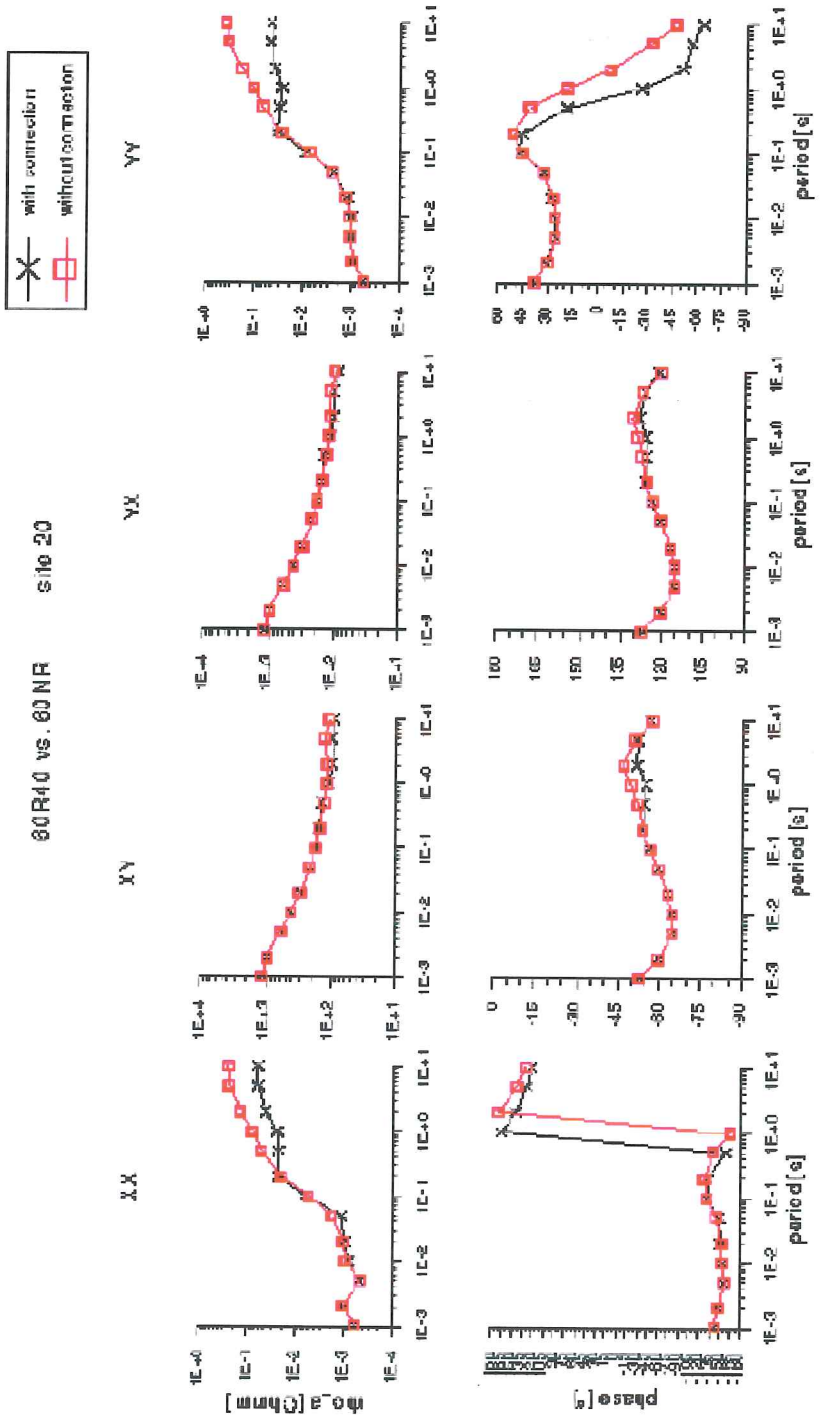

Figure-68. Calculated apparent resistivities and phases for an MT-sounding at site 20 (see fig.-35) for non-connected systems (red) and systems connected at 4km depth (black).

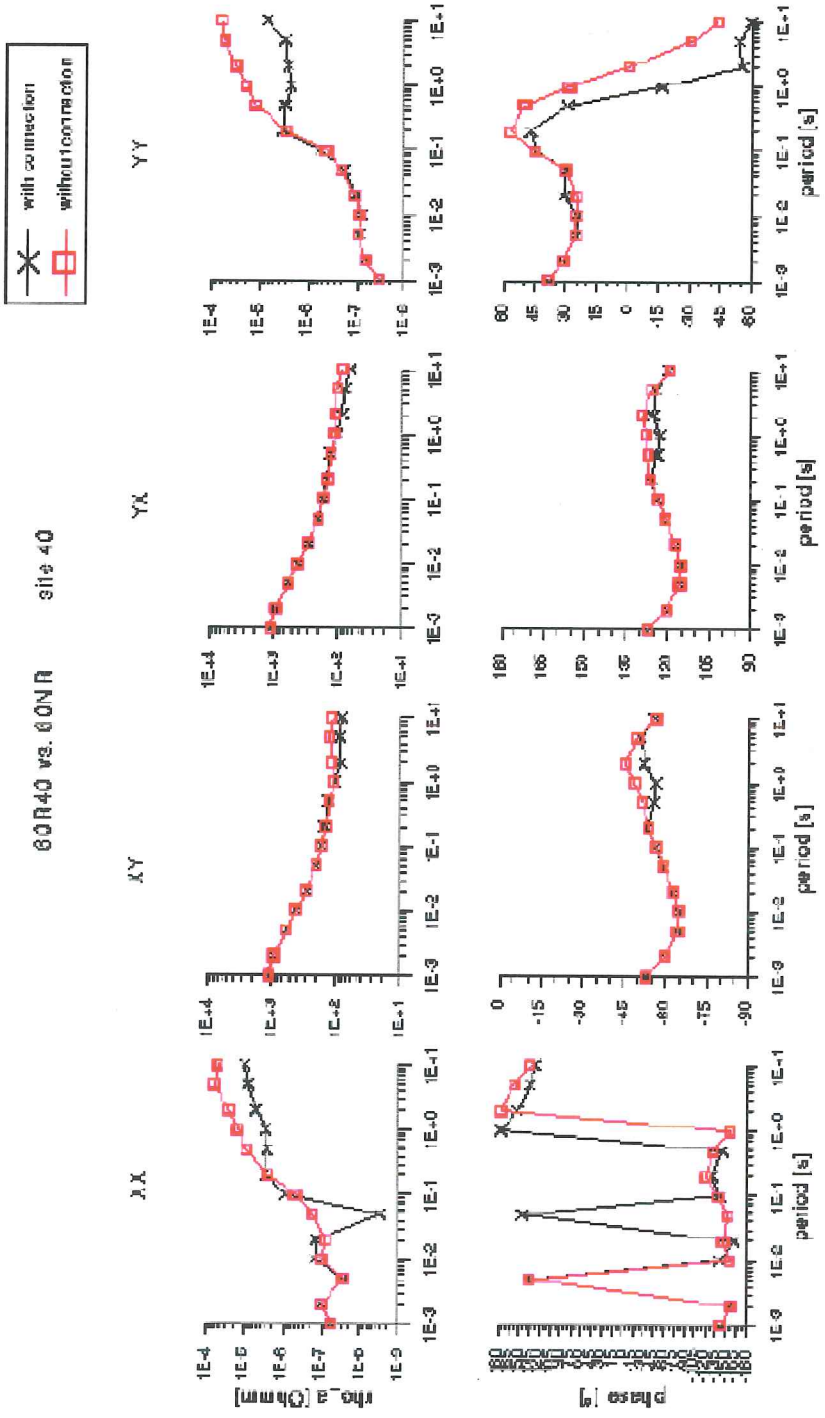

Figure-69. Calculated apparent resistivities and phases for an MT-sounding at site 40 (see fig.-35) for non-connected systems (red) and systems connected at 4km depth (black).

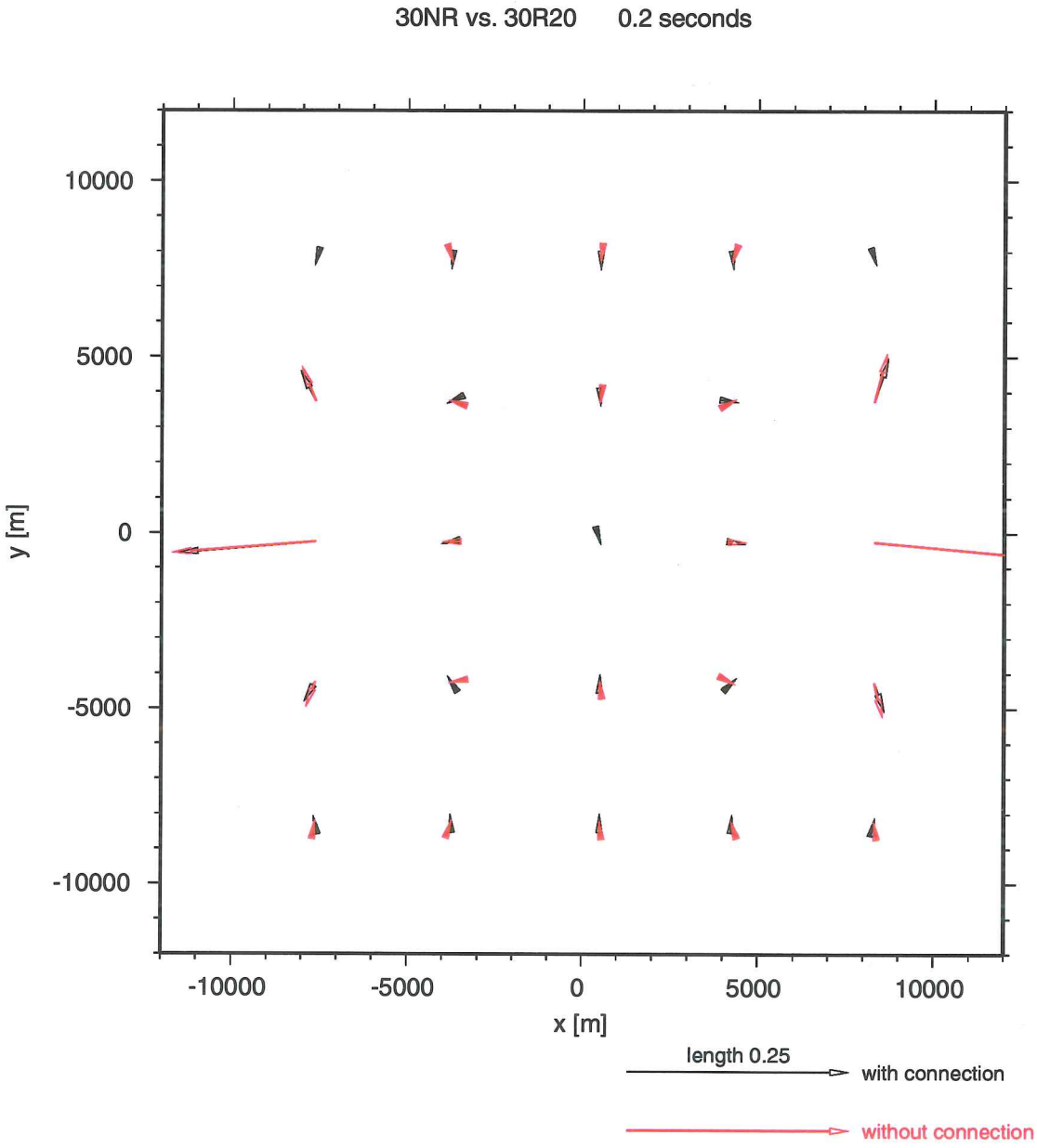

Figure-70. Spatial distribution of the real part of magnetic transfer functions at the period of 0.2sec. for non-connected systems (red) and systems connected at the depth of 2km (black).

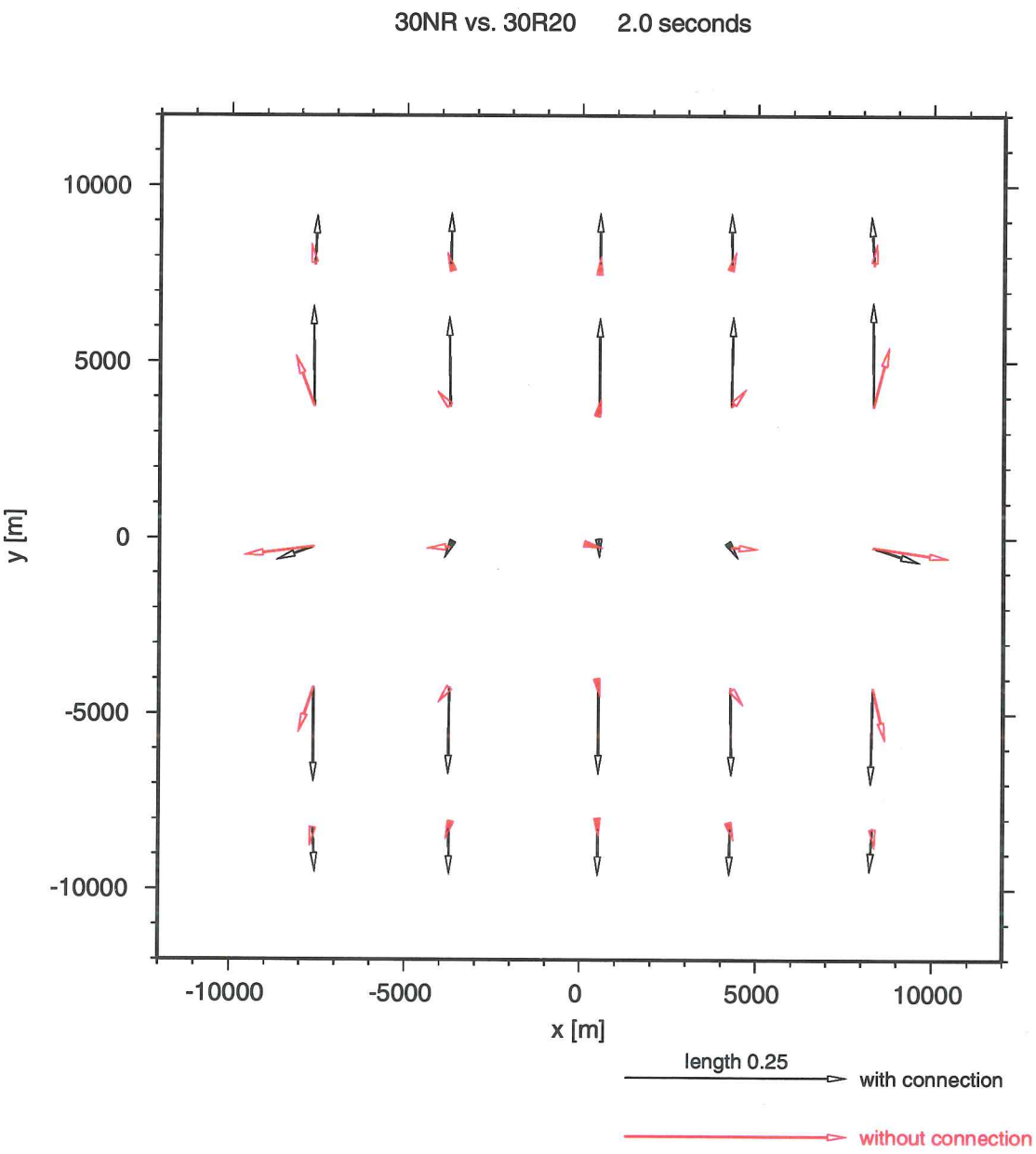

Figure-71. Spatial distribution of the real part of magnetic transfer functions at the period of 2.0sec. for non-connected systems (red) and systems connected at the depth of 2km (black).

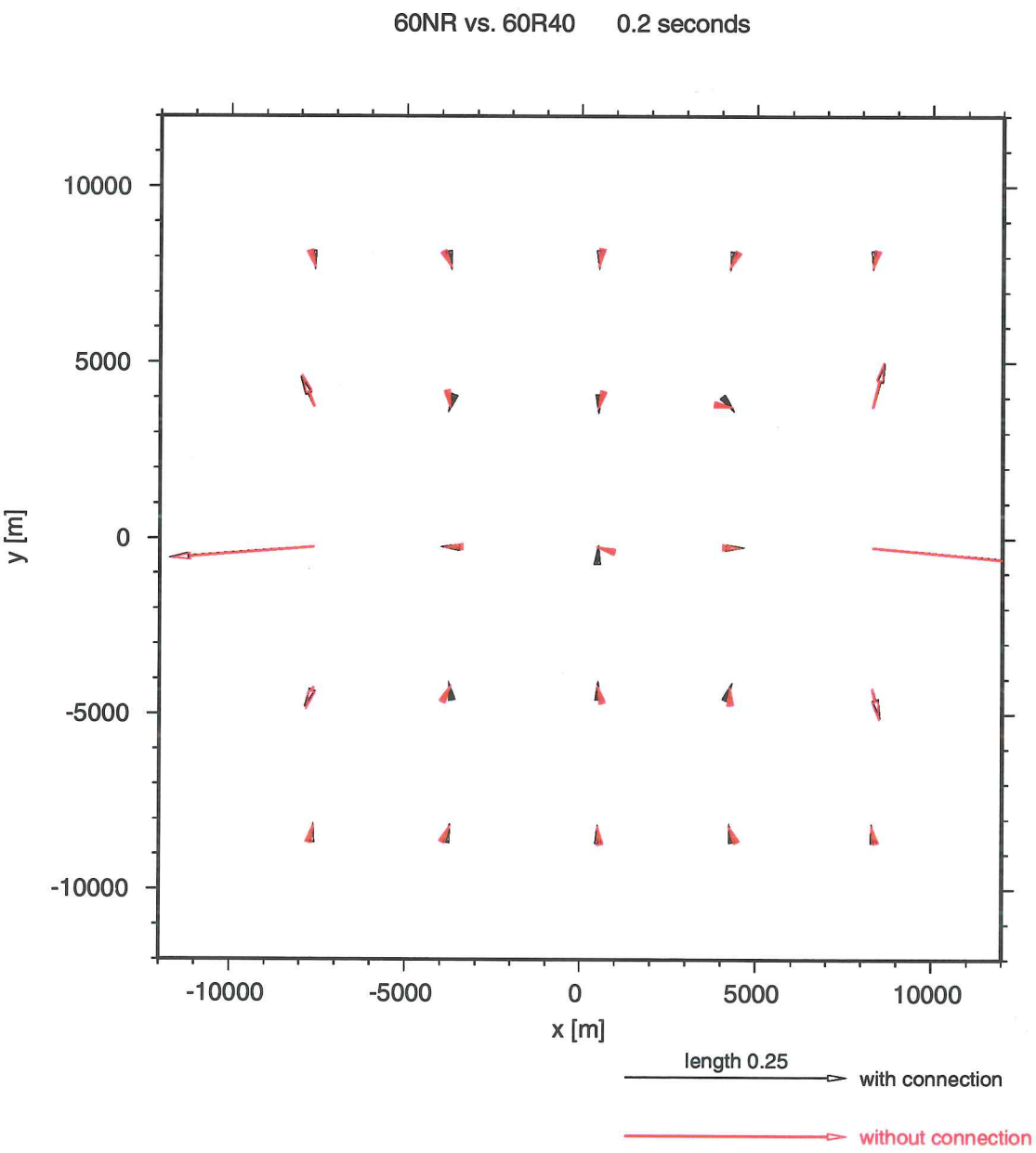

Figure-72. Spatial distribution of the real part of magnetic transfer functions at the period of 0.2sec. for non-connected systems (red) and systems connected at the depth of 4km (black).

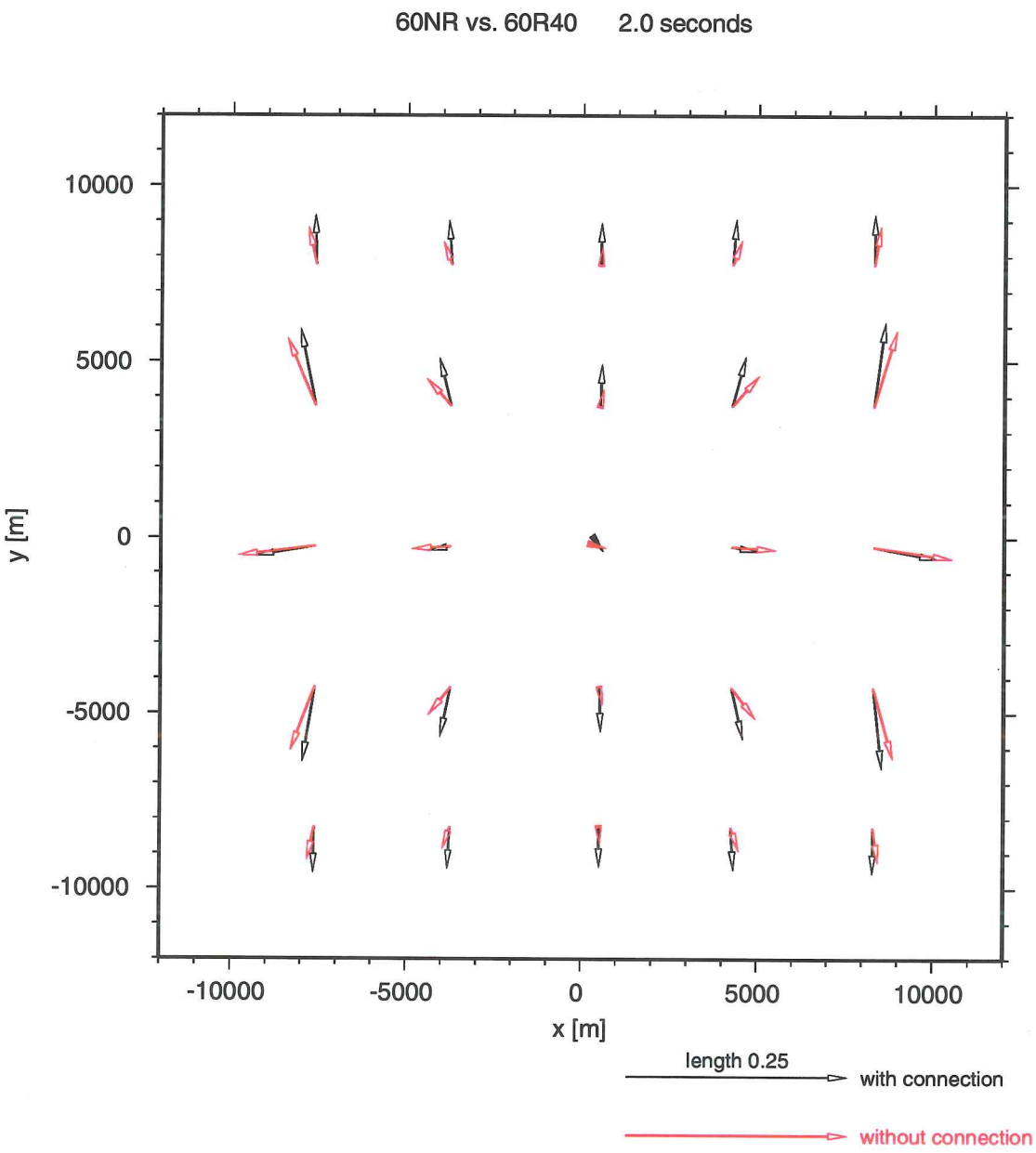

Figure-73. Spatial distribution of the real part of magnetic transfer functions at the period of 2.0sec. for non-connected systems (red) and systems connected at the depth of 4km (black).

5. SUMMARY AND CONCLUSIONS

The first phase of the Deep Geothermal Prospecting project has been successfully completed. Prior to this study, it was an open question whether the natural variations in the earth's electro-magnetic field are strong enough in Iceland to allow the use of MT measurements to study the resistivity structure in the uppermost kilometres of the crust. Test measurements of the natural electro-magnetic field confirmed that there is enough energy in the high-frequency part of the spectrum to allow the use of MT soundings.

The test measurements were also used for statistical analysis of the field variations. Statistically the recorded signals seem to be fairly well described as normal distributed around a zero mean but with standard deviations that vary the field components in question and frequency.

A fairly comprehensive study of the intrinsic sensitivity of different TEM measurement configurations has been performed. The main findings of this study were that the sensitivity is low for localised resistivity variations directly under loops, both as sources receivers. The combination of a dipole source and dipole receiver, oriented parallel to the source dipole, seems to have the highest intrinsic sensitivity.

A set of likely models simulating two hypothetical geothermal systems in a volcanic zone were defined. They come in pairs where the systems are either connected by geothermal activity at various depth, along the volcanic zone, or not connected. Forward 3D codes were used to calculate the response of the models and the response for connected systems compared to that of non-connected systems. This was done both for various configurations of TEM soundings and for classical MT.

The observed standard deviations of the recorded natural fields were used as uncertainties for calculated model responses for the TEM method. Statistical methods were then used to estimate the significance of the difference in the responses of connected and non-connected models in order to determine the sensitivity for geothermal activity at depth inbetween the geothermal systems. The main findings are that the TEM-method is capable of detecting geothermal activity at least to the depth of 4km. It was found that a grounded dipole transmitter, parallel to the volcanic zone, and a receiver measuring the electric field parallel to the transmitter dipole, is the most sensitive TEM configuration. The sensitivity is highest in between the geothermal systems, above the connecting geothermal activity at depth, and the maximum response is only slightly shifted towards the source.

Model calculations for the MT-soundings showed that stations in the middle of the volcanic zone, above the connecting geothermal activity at depth, show the highest sensitivity in apparent resistivity and phase (which are derived from the horizontal fields). The anomaly seems to be more clear in the phase than in the apparent resistivities. The magnetic transfer functions (induction arrows, derived from the vertical component of the magnetic field) show, on the other hand, the strongest indication of the presence of a connection at stations to the sides of the volcanic zone. No study has been made of the significance of the difference in the MT response for connected and non-connected models. The anomaly due to the connection decreases, as is to be expected,

with increasing depth and it is not known whether the response of a connection at 4km depth is detectable in practice.

The overall conclusions are that both TEM and MT are capable of detecting geothermal activity, if present, inbetween shallow geothermal systems in the volcanic zones of Iceland. The TEM seems to be able to identify the associated low-resistivity anomaly, at least down to the depth of 4km, but it is more uncertain how deep MT can detect it. There is a reason to believe that the TEM has a better resolution for such an anomaly, superimposed on the anomaly of the geothermal systems. The controlled source field is more localised than the wide spread plane wave source field for MT. The controlled source can be aimed to illuminate the volume of interest, but the MT source field illuminates the much bigger volume and the measured response consequently contains responses of surrounding resistivity anomalies.

6. REFERENCES

Árnason, K., 1999: *Consistent Discreitzation of Electromagnetic Fields and Transient Modelling*; in: Three-Dimensional Electromagnetics, Ed. Michael Oristaglio and Brian Spies, Geopys. devel. series: v7, SEG, pp. 103-118.

Árnason, K., Karlsdóttir, R.,Eysteinsson, H., Flovenz, Ó.G. and Guðlaugsson, s.Þ., 2000: *The resistivity structure of high-temperature geothermal systems in Iceland*. Proc. of the WGC2000.

Mackie, R.L. and Madden, T.R., 1993: *Three-dimensional magnetotelluric modelling and inversion.* Proc. IEEE., 77, pp. 318-333.

Mendenhall, W., Scheaffer, R.L. and Wackerly, D.D., 1981: *Mathematical Statistics with Applications*, second edition. Duxbury Press, Boston, Masschusetts. 686 p.